REPORT CDOT-2020-07 March 2020

PERFORMANCE OF A GRS-IBS BRIDGE ABUTMENT: COLORADO CASE STUDY

APPLIED RESEARCH & INNOVATION BRANCH

Dr. Nien-Yin Chang, P.E., Principal Investigator;
Dr. Hien Manh Nghiem; Co-Principal Investigator,
and Dr. Kevin Lee, P.E., Co-Investigators
Center for Geotechnical Engineering Science
Department of Civil Engineering
College of Engineering and Applied Science
University of Colorado Denver

COLORADO
Department of Transportation

The contents of this report reflect the views of the authors, who are responsible for the facts and accuracy of the data presented herein. The contents do not necessarily reflect the official views of the Colorado Department of Transportation or the Federal Highway Administration. This report does not constitute a standard, specification, or regulation. The use of the information contained in the report is at the sole discretion of the designer.

Technical Report Documentation Page

1. Report No.	2. Government Accession No.	3. Recipient's Catalog No.
CDOT-2020-07		

4. Title and Subtitle	5. Report Date
Performance of a GRS-IBS Bridge Abutment:Colorado Study	March 2020
	6. Performing Organization Code

7. Author(s)	8. Performing Organization Report No.
Dr. Nien-Yin Chang, P.E., Dr. Hien Manh Nghiem, Dr. Kevin Lee, P.E.	UCD-CGES-2015-01

9. Performing Organization Name and Address	10. Work Unit No. (TRAIS)
University of Colorado Denver Campus Box 113, P. O. Box 173364, Denver, Colorado 80217	11. Contract or Grant No. 214.08

12. Sponsoring Agency Name and Address	13. Type of Report and Period Covered
Colorado Department of Transportation - Research 4201 E. Arkansas Ave. Denver, CO 80222	Final
	14. Sponsoring Agency Code

15. Supplementary Notes
Prepared in cooperation with the US Department of Transportation, Federal Highway Administration

The replacement of the CDOT Region 1 Twin Bridge over Smith Road and Union Pacific Rail Road (UPRR) on I-70 provided an excellent opportunity for the performance evaluation of GRS (geosynthetically reinforced soils) abutment. The performance of the GRS abutment was measured using SAA (shape accel array) for lateral deformation and vertical settlement measurement, Geokon 4810 for horizontal earth pressure, 4800 for vertical earth pressure, 4420 for separation measurement between abutment and top of sheet pile wall, 4150 for strain of anchor rod, and optic fiber for geosynthetic strain measurement. Phase I covered the West-Bound portion of the Abutment #4 with sheet pile façade. Results of finite element analyses were compared to the measured performance of the SAA and Geokon devices, and excellent agreements were accomplished. Besides the delay in construction and instrument installation and web-site monitoring data presentation, the study program is judged effective. The optic fiber strain gage needs further study for its effectiveness before future use in geosynthetic strain measurement. Conventional strain gages replaced the optic fiber in Phase II East-Bound Abutment #4 study with a drastically scaled-back instrumentation program. Finite element analysis was found to an effective predictor of field abutment performance and was recommended for use prior to construction to better predict potential problems during construction, such as the significant lateral displacement of the sheet-pile wall observed during the excavation for water transport pipeline installation immediate to and along the wall front. The installation of tiebacks and prompt backfilling action prevented the excessive lateral displacement of the sheet pile wall. Subsequent finite element analyses also confirmed the potential problems the excavation caused. It is recommended not to grout the tiebacks with strain gage installation until the measurement was completed to facilitate successful tieback tension measurement. This project provides precious field performance information of GRS-IBS (Geosynthetic Reinforced Soil - Integrated Bridge System) for performance check and finite element program validation. Preconstruction finite element analysis is recommended for performance prediction.

17. Keywords	18. Distribution Statement
GRS, abutment, performance, large scale model test, geosynthetic tensile stress and strength, wide-width tension test, horizontal/ vertical earth pressure, Colorado Class 1 Crush Rock Backfill, horizontal displacement of sheet pile wall, settlement	No restrictions. This document is available to the public through the National Technical Information Service, 5825 Port Royal Road, Springfield, VA 22161.

19. Security Classif. (of this report)	20. Security Classif. (of this page)	21. No. of Pages	22. Price
Unclassified	Unclassified		

Form DOT F 1700.7 (8-72) Reproduction of completed page authorized

CONVERSION TABLE

U. S. Customary System to SI to U. S. Customary System
(multipliers are approximate)

Multiply (symbol)	by	To Get (symbol)	Multiply	by	To Get
LENGTH					
Inches (in)	25.4	millimeters (mm)	mm	0.039	in
Feet (ft)	0.305	meters (m)	m	3.28	ft
yards (yd)	10.914	meters (m)	m	1.09	yd
miles (mi)	1.61	kilometers (km)	m	0.621	mi
AREA					
square inches (in^2)	645.2	square millimeters (mm^2)	mm^2	0.0016	in^2
square feet (ft^2)	0.093	square meters (m^2)	m^2	10.764	ft^2
square yards (yd^2)	0.836	square meters (m^2)	m^2	1.195	yd^2
acres (ac)	0.405	hectares (ha)	ha	2.47	ac
square miles (mi^2)	2.59	square kilometers (km^2)	km^2	0.386	mi^2
VOLUME					
fluid ounces (fl oz)	29.57	milliliters (ml)	ml	0.034	fl oz
gallons (gal)	3.785	liters (l)	l	0.264	gal
cubic feet (ft^3)	0.028	cubic meters (m^3)	m^3	35.71	ft^3
cubic yards (yd^3)	0.765	cubic meters (m^3)	m^3	1.307	yd^3
MASS					
ounces (oz)	28.35	grams (g)	g	0.035	oz
pounds (lb)	0.454	kilograms (kg)	kg	2.202	lb
short tons (T)	0.907	megagrams (Mg)	Mg	1.103	T
		TEMPERATURE (EXACT)			
Fahrenheit (°F)	5(F-32)/9 (F-32)/1.8	Celsius (° C)	° C	1.8C+32	° F
ILLUMINATION					
foot candles (fc)	10.76	lux (lx)	lx	0.0929	fc
foot-Lamberts (fl)	3.426	candela/m (cd/m)	cd/m	0.2919	fl
FORCE AND PRESSURE OR STRESS					
poundforce (lbf)	4.45	newtons (N)	N	.225	lbf
poundforce (psi)	6.89	kilopascals (kPa)	kPa	.0145	psi

ACKNOWLEDGMENTS

GRS abutment has gained its popularity in GRS-IBS (Geosynthetic Reinforced Soil - Integrated Bridge System) bridge design and construction for its capability in avoiding bridge bump problems. The replacement of the Twin Bridge on I-70 provided an excellent opportunity to evaluate the effectiveness of GRS abutment through comprehensive instrumentation program for measurement of sheet pile wall displacements, earth pressures, tensile stresses in US4800 geosynthetic, abutment performance, including abutment displacements, tilting, and earth pressures. The joint sponsorship of this study by the Colorado Department of Transportation and the Federal Highway Administration is greatly appreciated. The close collaboration of the following partners was critical to the success of this GRS abutment performance evaluation project: all study panelists from CDOT and FHWA, CDOT bridge Branch, CDOT Construction Management Group, construction company, the Shannon and Wilson, Inc. and the Center for Geotechnical Engineering Science at the University of Colorado Denver. The team spirit of over ten students made this project an excellent learning experience.

EXECUTIVE SUMMARY

The replacement of the CDOT Region 1 Twin Bridge over Smith Road and Union Pacific Rail Road (UPRR) on I-70 provides an excellent opportunity for the performance evaluation of GRS (geosynthetically reinforced soils) abutment. The abutment, GRS backfill, sheet pile façade with anchored bulkhead, and approach and sleeper slabs are instrumented with comprehensive instrumentation program to measure performances, including horizontal and vertical earth pressures, displacements of the steel sheet pile façade, geosynthetic strains, strain of steel anchor bar, abutment-sheet pile façade separation and settlement. Phase I of this showcase study covered the performance of GRS bridge abutment of West-Bound Abutment #4 with sheet pile façade. Finite element analyses were performed with the intent to calibrate the effectiveness of the numerical analyses in assessing the performance of the GRS abutment by comparing the analysis results against the instrument measured performance.

Because of problems experienced in the geosynthetic strain measurement using optic fiber strain gauges, geosynthetic strain measurement was not successful and, therefore, the geosynthetic stress and strain comparisons were not available in this full-scale case study. However, all other field measurements were found to be in good agreement with the results of finite element analyses. Because of the unsuccessful attempt of using optic-fiber strain gauges in geosynthetic strain measurement, it was discontinued in the Phase II study of the east-bound Abutment #4 and replaced with conventional strain gauges, which was deemed successful. The delay in the delivery of field measurement data significantly slowed the comparison effort between the field performance measurement and finite element analysis results. The project of this nature full and timely collaboration of all concerned parties is most critical.

Lab experiments were successfully conducted to obtain the properties of backfill and US4800 geosynthetic. Wide width tension tests were performed to obtain the tensile force-displacement curves of the geosynthetics, new and exhumed samples. Test results were good when compared with geosynthetic properties from other sources, including the manufacturer. The average geosynthetic strength loss caused by the field compaction of Class I granular backfill of hard crushed granite ranged from 15 to 30%. Laboratory tests, including specific gravity, sieve analysis, compaction tests (both Standard and Modified) and consolidation drained triaxial compression tests were performed to characterize the backfill and also for geo-cap model parameters for finite element analysis. All tests were performed following the ASTM specifications.

IMPLEMENTATION PLAN

All study findings were submitted to CDOT for implementation in EM 074 Reinforced Soil Abutments 2012 07 at its next revision through presentations at CDOT and Show Case conference. The successful completion of the GRS Abutment #4 construction validated the CDOT GRS Abutment Design Specifications. The successful performance of steel tieback rods in deadman installation was evidenced in the prevention of gross lateral displacement of steel sheet pile façade during the excavation of the water transportation pile line trench.

TABLE OF CONTENTS

1. BACKGROUND 1

2. LITERATURE REVIEW 5

3. GRS ABUTMENT #4 CONSTRUCTION AND INSTRUMENTATION.....7

4. FIELD PERFORMANCE MEASUREMENTS OF ABUTMENT #4.....12

4.1 Horizontal and Vertical Earth Pressures along The Back of Sheet Pile Façade.....12

4.2 Sheet Pile Façade Movement.....18

4.3 Wall Top and Sill Corner Separation from Crack Meter.....20

4.4 Tie Rod Strain.....21

4.5 Geosynthetic 22

4.6 Adjust the Instrumentation Program.....25

5. COEFFICIENT OF EARTH PRESSURE AT REST 25

6. ABUTMENT PERFORMANCE DURING PIPELIINE TRENCH EXCAVATION27

7. LABORATORY TESTING OF BACKFILL AND GEOSYNTHETIC.....29

7.1 General.....29

7.2 Wide-Width (WW) Tension Tests of US4800 Geosynthetic 29

7.3 Triaxial Compression Tests on Colorado Class I Backfill of Crushed Granite.....37

7.3.1 Hydrostatic Compression Tests 37

7.3.2 Conventional Triaxial Compression Tests.....38

7.4 Oedometer and Direct Shear Tests 42

7.4.1 Device Description.....42

7.4.2 Oedometer Tests.....45

7.4.3 Direct Shear Tests.....46

7.4.4 Interface between Soil and Geosynthetic.....49

7.4.5 Index Property Tests and Density-Moisture Relationship.....51

8. FINITE ELEMENT ANALYSIS OF GRS ABUTMENT #4.....52

8.1 CDOT Finite Element Analysis Requirements for #4 Abutment 52

8.2 Finite Element Analysis Program Development.....52

8.2.1 Introduction.....52

8.2.2 Soil Model 53

8.3 Model Geometry and Boundary Conditions 58
8.4 Model Materials and Properties 59
8.5 Loadings 62
8.6 Field versus FEA Performance Comparison 63
9. SUMMARY, CONCLUSIONS AND RECOMMENDATIONS 73
9.1 Summary and Conclusions 73
9.2 Recommendations 74
REFERENCES 75
Appendix A 77
Appendix B 93

LIST OF FIGURES

Figure 1 Single-span GRS-IBS with Block Facing (Center for Innovation, FHWA) 6
Figure 2 Facing wall of the GRS Abutment #4 8
Figure 3 Plane view and cross-section of GRS Abutment #4.....9
Figure 4 Instrument layout.....10
Figure 5 Data from vertical pressure cells I1-1-VP 13
Figure 6 Data from vertical pressure cells I1-2-VP 14
Figure 7 Data from vertical pressure cells I1-3-VP 14
Figure 8 Data from vertical pressure cell I1-4F-VP 15
Figure 9 Data from vertical pressure cells I1-4M-VP and I1-4B-VP 15
Figure 10 Data from vertical pressure cell I1-5-VP.....16
Figure 11 Data from vertical pressure cells I1-6-VP and I1-7-VP 16
Figure 12 Data from horizontal pressure cells I1-1-HP and I1-2-HP 17
Figure 13 Data from horizontal pressure cells I1-3L-HP and I1-3U-HP.....17
Figure 14 Data from horizontal pressure cell I1-5-HP 18
Figure 15 Data from horizontal pressure cell I1-6-HP 18
Figure 16 Data from Sensors 19
Figure 17 Wall deflection 20
Figure 18 Gap history of sill front corner vs top of sheet pile façade (inches).....20
Figure 19 Tieback strain in micro strain 21
Figure 20 Tieback strain in micro strain I1-B-SG and I1-F-SG 21
Figure 21 Deadman and tie rod installation.....22
Figure 22 Fiber optic strain gauge field installation 23
Figure 23 Measurement of fiber optic strains 25
Figure 24 Wall height and construction time.....26
Figure 25 Wide width tension test sample preparation parts and layout 31
Figure 26 Tests of I1 new and field geosynthetic samples 31
Figure 27 Tests of I2 new and field geosynthetic samples 32
Figure 28 Tests of all new and field geosynthetic samples 33
Figure 29 Tests of geosynthetic samples in different directions.....34

Figure 30 Load-Displacement curves of geosynthetic from tension tests 37
Figure 31 Hydrostatic test 38
Figure 32 Triaxial test results 39
Figure 33 Determination of friction angle and cohesion 40
Figure 34 Mohr circle and failure line 41
Figure 35 Comparison of triaxial tests (σ_3=30 psi) 41
Figure 36 Triaxial test (σ_3=30 psi) with volume change measurement 42
Figure 37 Volume change measurement 42
Figure 38 Direct shear test device 44
Figure 39 Loading system of direct shear box 45
Figure 40 Oedometer tests 46
Figure 41 Constraint moduli 46
Figure 42 Soil sample after shearing 47
Figure 43 Shear stress and displacement curves 47
Figure 44 Vertical displacement and horizontal displacement curves 48
Figure 45 Determination of shear strengths 48
Figure 46 Backfill with geosynthetic inclusion after shearing 49
Figure 47 Shear stress and displacement curves for the backfill 50
Figure 48 Vertical displacement and horizontal displacement curves 50
Figure 49 Interface shear strengths 51
Figure 50 Nonlinear stress-strain behavior 53
Figure 51 Mohr-Coulomb failure criteria 54
Figure 52 Mohr-Coulomb failure criteria in principal stress space 55
Figure 53 Yield surface of modified hyperbolic model 56
Figure 54 Yield, cap and failure surfaces 57
Figure 55 Model geometry 59
Figure 56 Element mesh 59
Figure 57 Sheet pile dimensions 61
Figure 58 Stress-strain curve for geosynthetic 62
Figure 59 Applied load on abutment 63
Figure 60 Comparison of final lateral pressure along the back of façade at final stage 65

Figure 61 Comparison of final vertical earth pressures along the back of façade 67
Figure 62 Comparison of measurement and calculated fiber optic strains 69
Figure 63 Abutment displacement before excavation 70
Figure 64 Abutment displacement after excavating 71
Figure 65 Comparison of final wall displacements 72

LIST OF TABLES

Table 1 Phase 1 Abutment 4 instrumentation installation schedule 11
Table 2 Phase 2 Abutment 4 instrumentation installation schedule 12
Table 3 Field versus FEA k_o values 26
Table 4 Forward movement of wall top 28
Table 5 Property of geosynthetic from Manufacturer 30
Table 6 Data summary of geosynthetic test results 35
Table 7 Geosynthetic properties 37
Table 8 Friction angle and cohesion from triaxial tests 40
Table 9 Modulus from triaxial tests 40
Table 10 Friction angle and cohesion from direct shear tests 49
Table 11 Friction angle and cohesion of soil and geosynthetic interface from direct shear tests 51
Table 12 Parameters of the modified hyperbolic model 54
Table 13 Properties of the foundation soil 60
Table 14 Properties of the tie rod 60
Table 15 Sheet pile properties 61
Table 16 Vertical pressure 64
Table 17 Horizontal pressure 65
Table 18 Internal forces in the tie-back rod 70

1. BACKGROUND

Bridge bumps resulting from differential settlement between bridge abutment and bridge approach have caused some safety concerns, and also bridge and roadway maintenance with increased congestion. The severity of the bump problem lessened due to the increasing adoption of GRS (geosynthetically reinforced soils) backfill in providing the shallow foundation support for a bridge abutment. In this innovative approach, geosynthetic inclusions are embedded in soils to form geosynthetically-reinforcement soils (GRS, or mechanically-stabilized earth, MSE, used interchangeably), which significantly enhances the strength and stiffness of the composite over those of natural soils. In GRS, the high tensile strength geosynthetic layers are embedded in soils at a spacing of up to 12 inches to form a composite with much stronger tensile strength than that of the parent soils. The Colorado Department of Transportation was a pioneer state in the innovative utilization of GRS in supporting bridge abutment, and GRS was first used in this capacity in the Meadows and Founders Bridge (CDOT Research 2000-5-Part 1, 200-12-Part 2). The excellent performance of the Founders Meadows Bridge led to the adoption of GRS in a number of bridges in Colorado and nationwide.

CDOT and FHWA partnered to develop a comprehensive instrumentation program for abutment performance monitoring using SAA (shape accel array) for lateral and vertical displacement of sheet pile facade, Geokon 4810 for horizontal earth pressure, 4800 for vertical earth pressure, 4420 for separation measurement, 4150 for strain of anchor rod, and TenCate GeoDetect for geosynthetic strain measurement. Numerical analyses of the GRS abutment performance were performed using LS-DYNA finite element analysis software, and results were available for comparison with field measurement in April of 2014. However, field measurement data were not available until April 2015, which greatly delayed the progress of this study. Excellent agreements were achieved between the field measured performances, and the finite element analyses results. The geosynthetic tensile stresses from the finite element analyses are considered reasonable and LS-DYNA is effective as an analysis tool for GRS abutment performance calculation.

In this project, geosynthetic reinforcement installation is divided into two distinctive sections: below the bridge abutment, the geosynthetic reinforcing layers were spaced at 4 inches with alternate layer of geosynthetic of extended length, and, above the abutment base and behind the abutment, the reinforcing layers are spaced at 12 inches, as detailed in Fig. 3. The Colorado Department of Transportation used CO DOT Class 1 Backfill with minus 2-inch gravels and no

more than 10 percent fines. The low percentage of fines facilitate expedited backfill drainage to achieve greater wall stability in the event of heavy rain or snowmelt. The maximum grain size is limited to 2-inch diameter and has been a part of the CDOT Staff Bridge Abutment Worksheet, and Reinforcement Soil Abutment Specifications since 1995 (EM 074 Reinforced Soil Abutments 2012 07) and has been in use in all bridge abutments. The GRS abutment has shown to effectively reduce the overall cost of abutment construction and mitigate bridge bumps arising from the differential settlement between the abutment and the approach slab (Graeme D. Skinner, 2005). GRS is designed with a polystyrene spacer and wrapped around geosynthetics with 1 to 3-inch gap between the abutment wall and GRS backfill to avoid excessive earth pressure variation.

This CDOT Region 1 twin bridge replacement project provides an excellent opportunity for the verification of the contemporary CDOT GRS Abutment design specifications and construction practices. This twin bridge on I-70 over the Union Pacific Railroad and Smith Road incorporates innovations that implement the CDOT/FHWA mandate − EDC GRS abutment technology. Abutment #4 at the east end of the bridge is supported on GRS embankment behind a sheet-pile retaining wall. This bridge abutment seats on geosynthetic reinforced soils with run-on and approach slabs to reduce the differential settlement and bridge bumps.

A geotechnical consultant installed all the above-said field performance measurement instruments and monitored the performance of the GRS abutment along the two GRS block-faced retaining walls and provided the digital monitoring data to the TEAM. During Phase 1, the westbound traffic was rerouted, and the westbound bridge demolished. The north half of Abutment #4 was first constructed to support the new westbound bridge (E-17-AEK) along with the GRS retaining wall (E-17-DG). Once complete, Phase 2 begins and eastbound traffic was rerouted, while the construction of the remainder of Abutment #4 and the eastbound bridge (E-17-AEJ) occurred along with the GRS retaining wall (E-17-DH). The bridge was completed and opened to traffic before the Christmas holiday 2016.

While the GRS technology has progressed, there are still rooms for improvement. To realize the further advancement and improvement of the GRS technology in supporting the bridge abutment and strengthening the backfill, the Abutment #4 at the eastern end of the Region 1 Twin Bridge replacement project is comprehensively instrumented with the state-of-the-art instruments for real-time monitoring of the abutment performance. The digital performance data provided the basis for the CGES Research Team to check the effectiveness of the contemporary CDOT GRS Abutment

specifications and for checking the effectiveness of finite element analysis as a tool for abutment performance check. This study was limited to the Abutment #4 performance evaluation. The abutment performance was predicted first and then compared to the measured performances. The study of the performance of GRS block facing walls was carried out by another team of researchers. Objectives of this reported study are four-fold:

1. Validate and enhance, if appropriate, the contemporary CDOT GRS abutment and wall design specifications through both field measurements and finite element analyses,
2. Validation of finite element analysis codes, LS-DYNA, and SSI-2D using the field GRS abutment performance data.
3. Mutual validation of finite element analysis results and field performances monitoring data, and
4. Appropriateness of using finite element analysis as a means of preconstruction performance check.

Benefit of this study A geosynthetically reinforced soil is stronger and stiffer and can endure higher bearing pressure than its nature soil at a reduced settlement and deformation. This leads to the assumption of using GRS to support a bridge abutment by capitalizing on the increased strength and stiffness of GRS embankment over those of its natural soil. This study on GRS abutment aims to verify the benefit of founding a bridge abutment on a mass of GRS. When proven feasible, then the bridge abutment founded on or near the surface of a GRS mass will likely reap the benefit of cost-saving over that of deep foundations. Furthermore, the GRS abutment with the CDOT design layout will minimize the long-term bridge bumps that have annoyed traveling public for decades. So the major overall benefits of a GRS abutment are minimizing (or eliminating) the bridge bump problem and the cost-saving over that of a deep foundation-supported bridge abutment. This study is to examine if the above-stated benefit can be realized in some situations with GRS on firm subsoil or stiff rock.

Study approach and plan Laboratory tests were first performed to evaluate tensile strength of geosynthetics via wide-width strength tests, compaction tests for evaluating the maximum dry density and optimum moisture content of Colorado Class I backfill of crushed granite for QA/QC of fill compaction, sieve analysis for gradation characteristics of the backfill, and triaxial tests for

stress-stain relationship and strength parameters for evaluation the Geo-Cap model parameters for finite element analyses. Then, finite element analyses were completed for GRS abutment performance prediction in April 2014 and ready for comparison with the field performance. The CGES Team was able to perform the majority of comparisons, including vertical and horizontal earth pressures at different depths, steel sheet pile façade vertical and horizontal displacements, tie rod tensile strains, and crack meter measurements for sheet pile and bridge concrete sill corner separation. The TenCate GeoDetect optic fiber strain gauges installation was not successful then the field measurements of geosynthetic strains were not reliable for comparison. Values of geosynthetic tensile forces and strains from finite element analyses, however, were reasonable. Statistical and probabilistic studies of the spatial variation of geosynthetic strains and tensile forces were not possible due to the unsuccessful measurements from TenCate GeoDetect optic fiber measurements. In sum, all comparison efforts were successful except for the geosynthetic strain measurements. The less than successful use of optic fiber for geosynthetic strain measurement resulted in its replacement with traditional strain gauges in the Phase II study.

The use of steel tieback with steel sheet pile deadman might have contributed to the abutment stabilization after the significant forward movement of steel sheet pile façade during the 10 feet x 10 feet trench excavation for water transport pipeline along the front base of the façade around October 1, 2015. The top front of the façade was observed to move forward (away from the backfill and toward the railroad) from 0.8 to 2.0 inches in five weeks.

Construction and instrumentation Per the Attachment 3 of the RFP, the Abutment #4 construction was scheduled to start on 12/19/2013 and end on 1/10/2014. In other words, the construction was supposed to complete in a very short time, an aggressive construction schedule. However, due to the complexity of coordination efforts from various concerned parties, the construction was rescheduled for July 2014 and was not completed till March 2015. Some Phase 1 instrument monitors began to provide data in August 2014 except the optic fiber strain gage. Most of the monitors continue to provide performance readings, although most monitor data have already stabilized with periodic fluctuations and high-frequency random noises. It was followed by Phase 2 construction with a drastically reduced instrument installation program due to budgetary issues. This study only addressed the performance of Abutment #4. The Center for Geotechnical Engineering Science (CGES) Study Team, briefed as TEAM, began to visit the

construction site on monthly basis, when the Abutment #4 construction was initiated and also frequently communicated with CDOT Bridge and Construction and the engineering consultant selected to run the field performance monitoring program, to keep abreast of the progress and foster good collaboration. The instruments were approximately located in the design stage, and the selected engineering consultant made decision on final instrument installation locations. The original RFP Attachments 1 and 2 provided the type and number of instruments and their initial locations. In Phase 1 study, the field performance monitoring instruments included: horizontal and vertical pressure cells on the back of sheet piles, underneath the abutment and slabs and inside the GRS mass to monitor the change and distribution of earth pressures, Shape Accel Arrays (SAA) to monitor the deformation of the steel sheet pile façade, a pair of strain gauges for each tieback of interest for measuring tension in steel tieback and, crack meters for relative movement between the corner of concrete bridge sill and top of sheet piles. The surface displacement survey for the movement measurements of steel sheet pile façade, top of the abutment, run-on slab, and approach slab never took place. Because of the budget issue, the instrumentation program for Phase I study was drastically cut back and the optic fiber strain gage was abandoned and replaced with conventional strain gages.

The performance monitoring data of full-scale structures is very precious for it provides a validity check for finite element analysis. Thus, it is very critical to collect GRS abutment performance data. CDOT Bridge had great experience design, construction and instrumentation of GRS abutment, like the Meadows and Founders Bridge near Castle Rock, etc., and more elsewhere.

2. LITERATURE REVIEW

Geosynthetics have been applied to reinforced soil walls, slopes, and embankments for many years (Allen et al.,1992) and created new structures as Geosynthetic Reinforced Soil Walls (GRS wall) and Mechanically Stabilized Earth Walls (MSE wall). The GRS or MSE walls can support the self-weight of the backfill soil and also the roadway structures and traffic loads. The advantages of this system over the traditional concrete walls and deep foundation-supported bridge abutment are due to the cost-saving, reduction in construction time, and minimizing (or eliminating) the bridge bump problem.

Currently, the GRS or MSE walls are also used in bridge applications, which called Geosynthetic Reinforced Soil Integrated Bridge System (GRS-IBS) (Adams et al., 2011; Abu-Farsakh et al., 2017; Saghebfar et al., 2017). The GRS-IBS usually includes a GRS abutment, a GRS integrated

approach, and a reinforced soil foundation (Adams et al., 2011). Different types of facing walls can be used to support the loads, such as facing block, facing panel, and sheet pile, etc. Figure 1 shows a single-span GRS-IBS with block facing in the promotional brochure of the Center for Accelerating Innovation of the Federal Highway Administration. GRS-IBSs are designed to accelerate construction, reduce construction cost and time, and avoid the annoying bridge bumps due to the differential settlement between the abutment and approach.

Figure 1. Single-span GRS-IBS with Block Facing (Center for Innovation, FHWA)

Instrumented GRS-IBS technology has been in practice in the United States and Canada for over two decades (Adams et al., 2011). Through instrumentation, the GRS abutment settlement and lateral deformation were recorded to monitor the abutment performance under the combination of bridge dead loads and live loads. Adams et al. (2011) presents the performance of in-service GRS abutments for bridges built with GRS-IBS between 2005 and 2010. There are 5 of 30 bridges that have current monitoring data from recording settlement of both the abutment face wall and the superstructure. In those GRS-IBSs, the lateral deformation is not monitored. Fifteen-years ago, under the leadership of Dr. Trever Wang, the Colorado Department of Transportation bridge design team adopted this innovative technology in the design of construction of Meadows and Founders bridge near Castlerock, CO that carries Colorado State Highway 86 over U.S. Interstate 25 and it still stands beautifully (Abu-Hejleh et al., 2001). This is the first major bridge in the United States built on footings supported by a geosynthetic-reinforced system with Colorado Class I backfill for gravelly soils and without the use of traditional deep foundations (piles and caissons). The GRS abutment was heavily instrumented with pressure cells for measuring earth pressures

and strain gages for geosynthetic tensile for measurement. Pressure cells were also used in the Tiffin River Bridge with pressure cells behind the back wall of each abutment to measure lateral pressures between the superstructure and the GRS due to seasonal temperature-induced expansion and contraction of steel girders (Adams et al., 2011). Saghebfar et al. (2017) presented the performance of the in-service GRS-IBS abutment of Maree Michel Bridge with block facing. Instrumentations were installed in south abutment to measure the load-and environment-associated responses of the GRS-IBS abutment, including vertical and horizontal deformations near the front wall, settlements of soil foundation and GRS-IBS backfill, the stress distribution in the GRS-IBS abutments and the distribution of strains along the geosynthetic reinforcements. While most GRS-IBS façades are with block facing or concrete facing panel, other options are available, like steel sheet piles. The CDOT Region 1 Twin Bridge over the Smith Road and Union Pacific Rail Road (UPRR) on I-70 is the first project used the sheet pile as the facing wall, Figure 2.

3. GRS ABUTMENT #4 CONSTRUCTION AND INSTRUMENTATION

A comprehensive instrumentation program was implemented to monitor the performance of the Abutment #4 of the unique CDOT Region 1 Twin Bridge over the Smith Road and Union Pacific Rail Road (UPRR) on I-70 (Shannon and Wilson, Inc., 2016) to further this innovative GRS-IBS technology. This is the first time that a multi-span interstate highway was selected for a comprehensive GRS-IBS abutment performance study. Figure 3 shows the instrument layout and Tables 1 and 2 the instrument installation schedule (Shannon and Wilson, Inc., 2016). The instrumentation program includes an automatic data acquisition system (ADAS), an online integrated database management system (webIDMS), all instruments, power and communication systems, and connection of temporary and final data logger locations. Ames Construction, Inc. (Ames) was selected as the general contractor for bridge construction. The instrumentation data can access from website www.shanwil-idms.com.

This section addresses issues related to field monitoring instruments, performance, and recommendations for instrument program adjustment. The Abutment #4 project was divided into two phases: Phase I for west-bound Abutment #4 on the north side of I-70 and Phase II for eastbound Abutment #4 on the south side. In the design plan, the abutment performance was to be monitored by the following instruments: survey points on the outside face of sheet piles, top of abutment, run-on (or sleeper) slab on the surface of subgrade to monitor the surface deformations of the abutment, earth pressure cells to monitor the change and distribution of earth pressures,

Shape Accel Arrays (SAA) to monitor the deformation of GRS mass and sheet piles, crack meters (Geokon 4420) to monitor the relative settlement between the top of sheet piles and the corner of concrete bridge sill, deformation gages to monitor the settlement of the subgrade, strain gauges to measure the tensile stress of tie bar and, finally, fiber optic strain gages for geosynthetic strain measurement with the data acquisition system (multi-channel optical sensing interrogator by TenCate).

Figure 2. Facing wall of the GRS Abutment #4

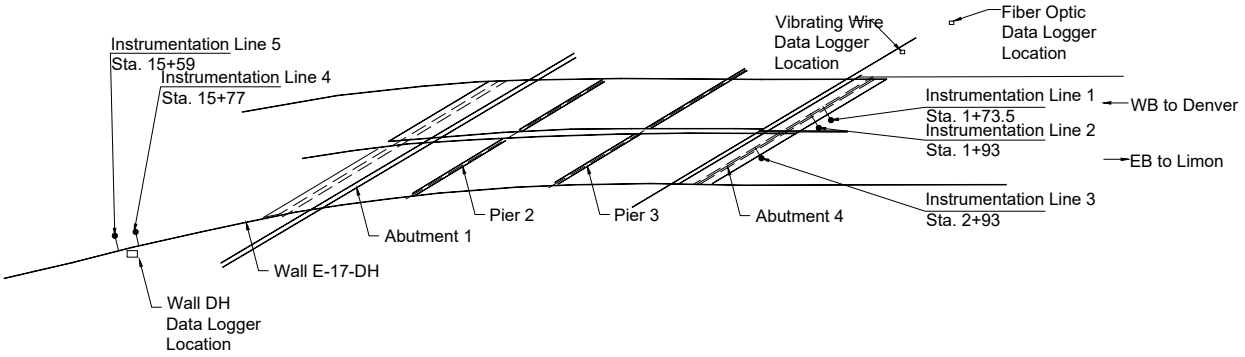

a) Plane view

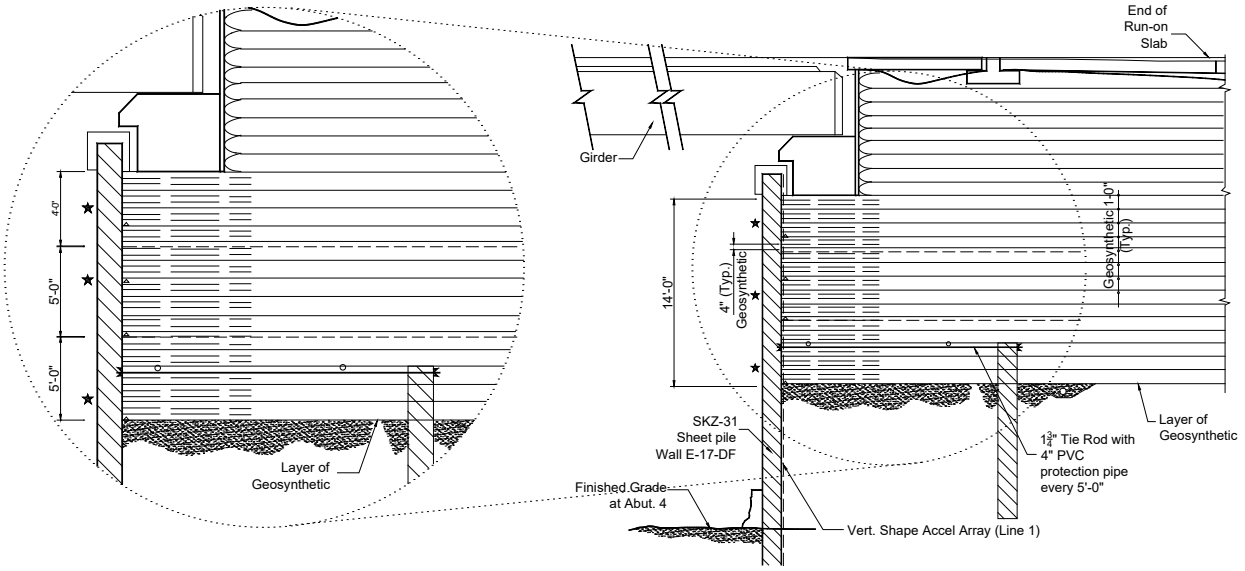

b) Cross-section

Figure 3. Plane view and cross-section of GRS Abutment #4

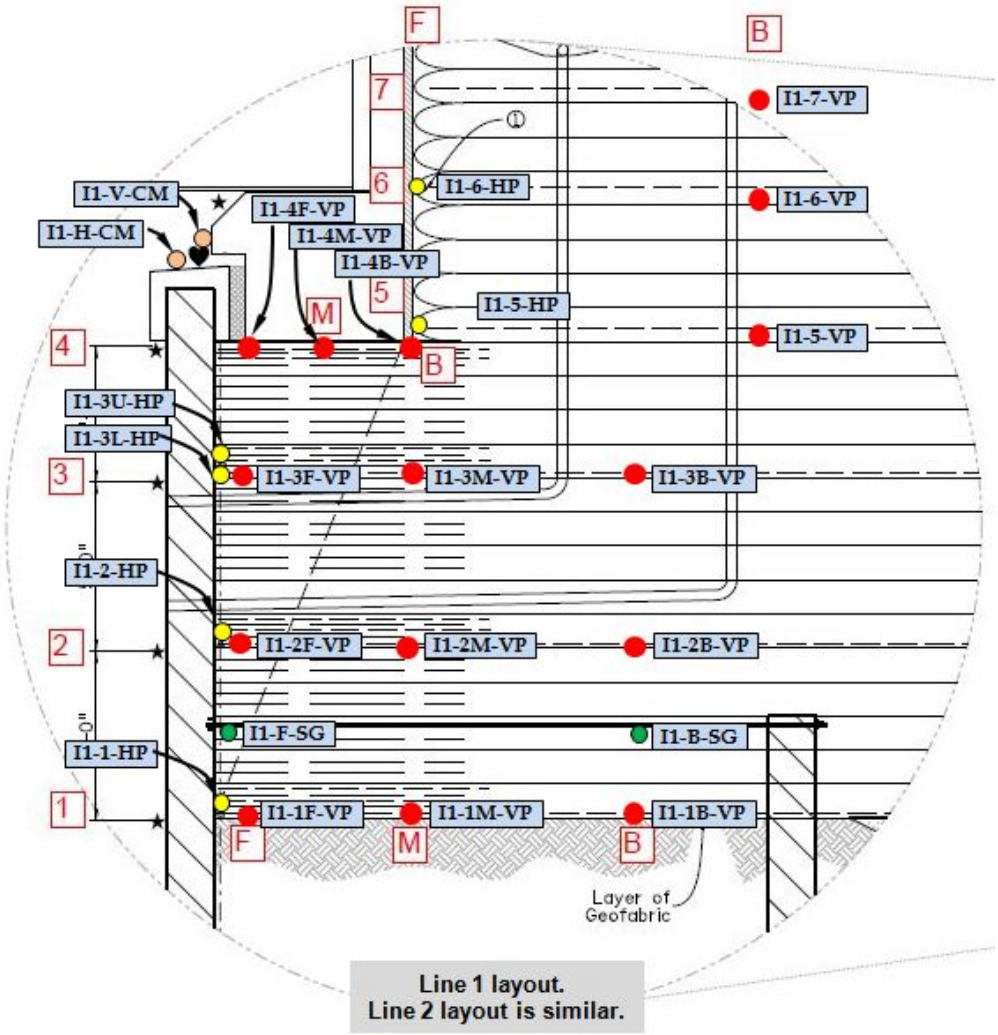

Figure 4. Instrument layout

Table 1: Phase 1 Abutment 4 instrumentation installation schedule

Date	Task	Instrumentation Line	Location
February 13, 2014	Attend GRS Coordination Meeting		
July 1, 2014	Pre-install tie-rod strain gages		
July 17, 2014	Pre-install horizontal earth pressure cells	I1 and I2	Row 1
July 21, 2014	Install vertical earth pressure cells	I1 and I2	Row 1
July 21, 2014	Install half-length GeoDetect	I1	Row 1
August 13, 2014	Pre-install horizontal earth pressure cells	I1 and I2	Row 2
August 13, 2014	Exhume fabric sample	I1 and I2	Sample 1
August 13, 2014	Install full-length GeoDetect	I1	Row 2
August 14, 2014	Install vertical earth pressure cells	I1 and I2	Row 2
August 14, 2014	Install half-length GeoDetect	I1	Row 2
August 14, 2014	Exhume fabric sample	I1 and I2	Sample 2
August 18, 2014	Pre-install horizontal earth pressure cells	I1 and I2	Row 3
August 20, 2014	Exhume fabric sample	I1 and I2	Sample 3
August 20, 2014	Install full-length GeoDetect	I1	Row 3
August 20, 2014	Install half-length GeoDetect	I1	Row 3
August 21, 2014	Exhume geosynthetic sample	I1 and I2	Sample 4
August 27, 2014	Exhume geosynthetic sample	I1 and I2	Sample 5
August 27, 2014	Install full-length GeoDetect	I1	Row 4
September 3, 2014	Install vertical earth pressure cells	I1 and I2	Row 4
September 3, 2014	Install half-length GeoDetect	I1	Row 4
September 19, 2014	Instal ShapeAccellArray	I1	
October 8, 2014	Complete temporary vibrating wire data logger setup		
October 24, 2014	Pre-install horizontal earth pressure cells	I1 and I2	Row 5 and 6
October 28, 2014	Install full-length GeoDetect	I1	Row 5
October 28, 2014	Install vertical earth pressure cells	I1 and I2	Row 5
October 30, 2014	Install crack meters	I1 and I2	
November 6, 2014	Complete temporary fiber optic data logger setup		
March 14, 2015	Install vertical earth pressure cells	I1 and I2	Row 6
March 14, 2015	Instal full length GeoDetect	I1	Row 6
March 18, 2015	Install vertical earth pressure cells	I1 and I2	Row 7
March 18, 2015	Instal full length GeoDetect	I1	Row 7

Table 2: Phase 2 Abutment 4 instrumentation installation schedule

Date	Task	Instrumentation Line	Location
July 13, 2015	Pre-install tie-rod strain gages	I3	
July 22, 2015	Pre-install horizontal earth pressure cells	I3	Row 1
August 5, 2015	Complete final vibrating wire data logger setup	I1, I2, and I3	Abutment 4 coping
August 7, 2015	Pre-install horizontal earth pressure cells	I3	Row 2 and 3
August 11, 2015	Install full-length GeoDetect	I3	Row 3
August 14, 2015	Install full-length GeoDetect	I3	Row 4

4. FIELD PERFORMANCE MEASUREMENTS OF ABUTMENT #4

Figure 2 shows the instrument layout for all pressure cells, deformation and strain gauges. The measurements are plotted in Figs. 5 to 15 from the database provided in the website database by the engineering consultant. The optic fiber strain gauge data for geosynthetic strain measurements are not included. All other measurement data are presented.

4.1 Horizontal and Vertical Earth Pressures along The Back of Sheet Pile Façade

The vertical earth pressures at the Line 1 instrument location were observed to vary with the elevation from the reference line of the subgrade-backfill interface (SBI). Along the interface, as shown in Fig. 5, the vertical earth pressures ranging from 11 psi at F to 34 psi at M are higher than those along the base of the concrete sill in Figs. 8 and 9, ranging from 11 psi at B to 22 psi at F, which also reflects the peak-to-valley variation of about 10 psi due to vertical pressure with traffic load. The vertical earth pressures along the back of sheet pile façade and sill vary from the smallest (11 psi) at the subgrade interface level 1F (Fig. 5) to the largest (33 psi) at 2F (Fig. 6) and decreases with the further elevation increase. Fig. 5 shows the smallest value at 1F that needs additional attention and discussion.

Horizontal earth pressures Figs. 12 to 15 show that they are slightly negative at - 0.2 psi at SBI, and increase to 4.0 psi at the next level up and decrease as the elevation further increases until it reaches a value of around zero near the sill base. The horizontal earth pressure variation is believed to be due to the Soil-Structure interaction effect between the GRS and steel sheet pile façade. This reduction of the horizontal earth pressure from those calculated from the classical earth pressure theories is definitely resulted from the increasing stiffness of GRS from its parent soils and the increasing flexibility of the steel sheet piles over that of the traditional rigid concrete walls. The cap beam may cause a pressure applying on GRS Wall of about 4 psi as shown in Figs. 8 and 9.

Pressure from girders and bridge structure is about 10 to 12 psi as shown in Figs. 8 and 9. The traffic load caused another pressure increase of 0.5 psi.

The horizontal and vertical pressures also vary with seasonal temperature variations, as shown in Figs. 6 to 15. During fall and winter, the pressures decreased, and during spring and summer, the pressures increased. Pressure differences between the fall and winter and the spring and summer are about 3 psi to 9 psi for the vertical pressures and 0.5 psi to 2.3 psi for the horizontal pressures. As shown in Fig. 5, the vertical pressures located at the sill base level are not affected much by the temperature variations. Currently, there is no study or analysis performed for GRS-IBS wall taking into account the thermal effects.

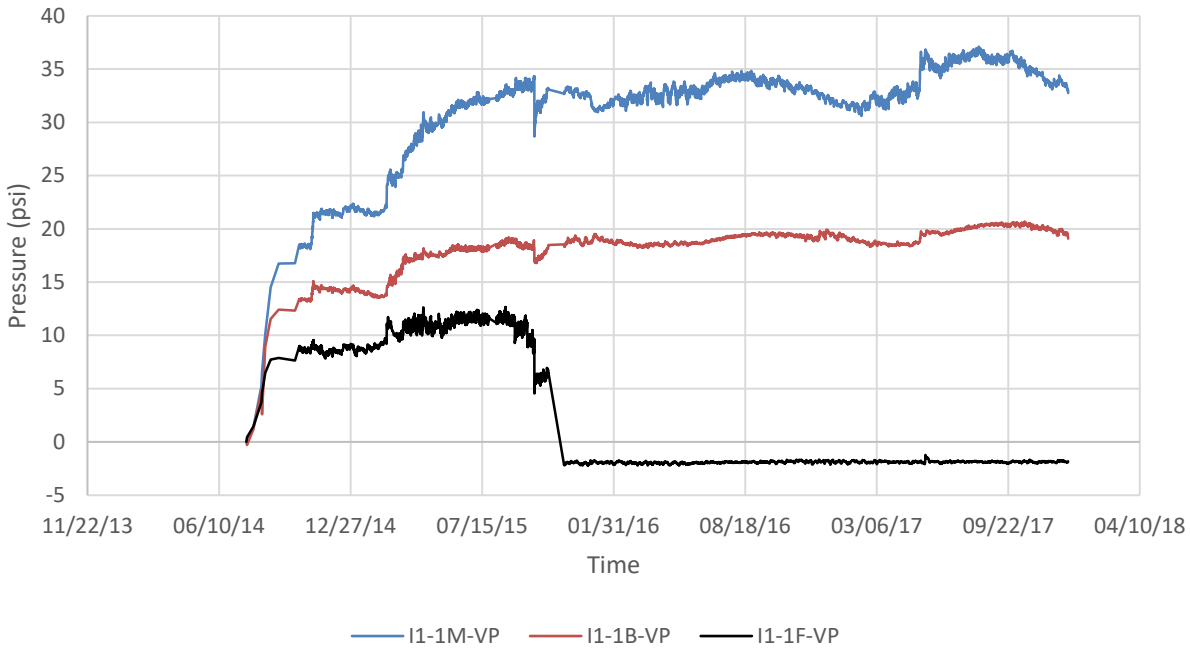

Figure 5. Data from vertical pressure cells I1-1-VP

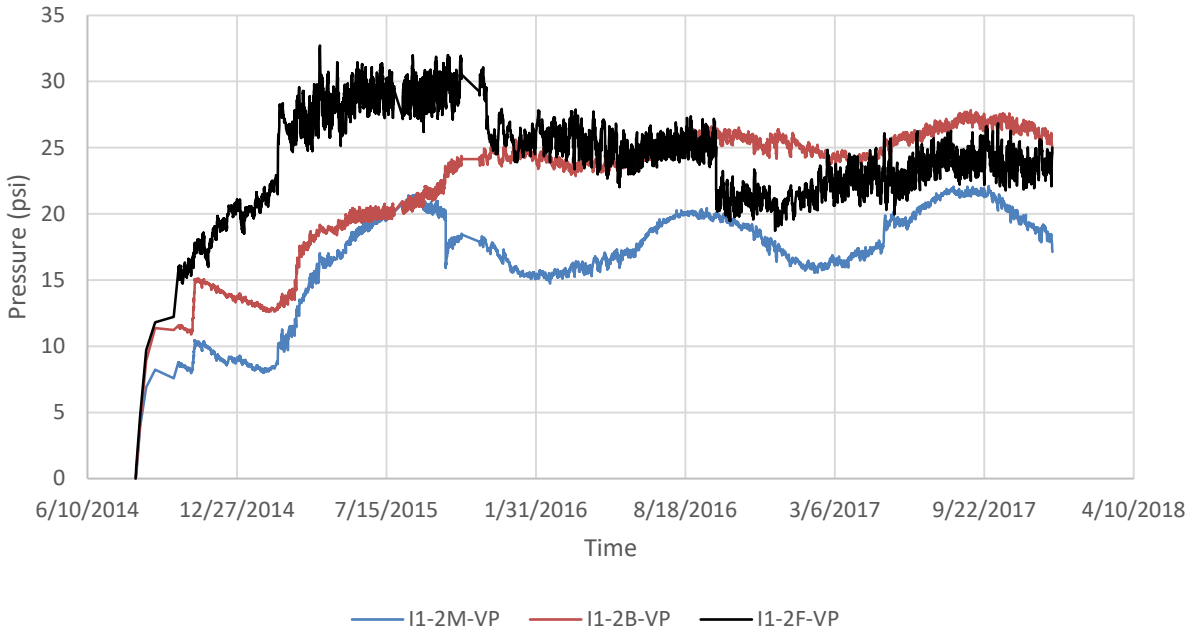

Figure 6. Data from vertical pressure cells I1-2-VP

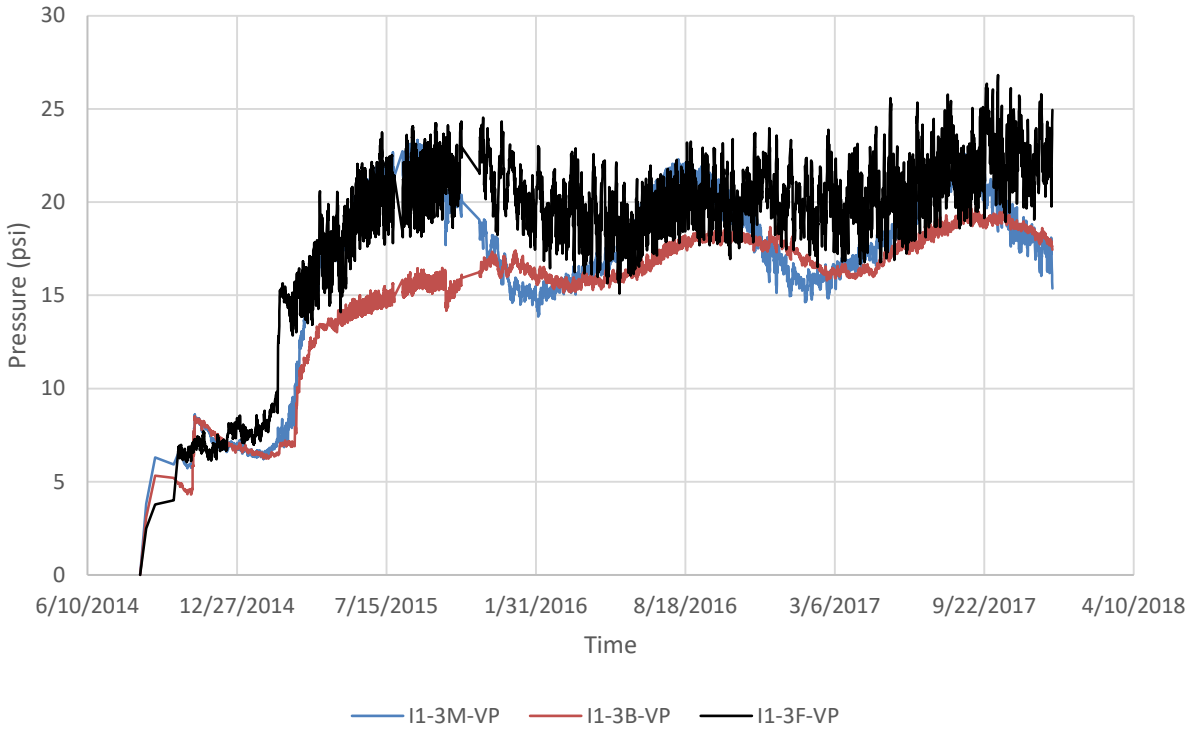

Figure 7. Data from vertical pressure cells I1-3-VP

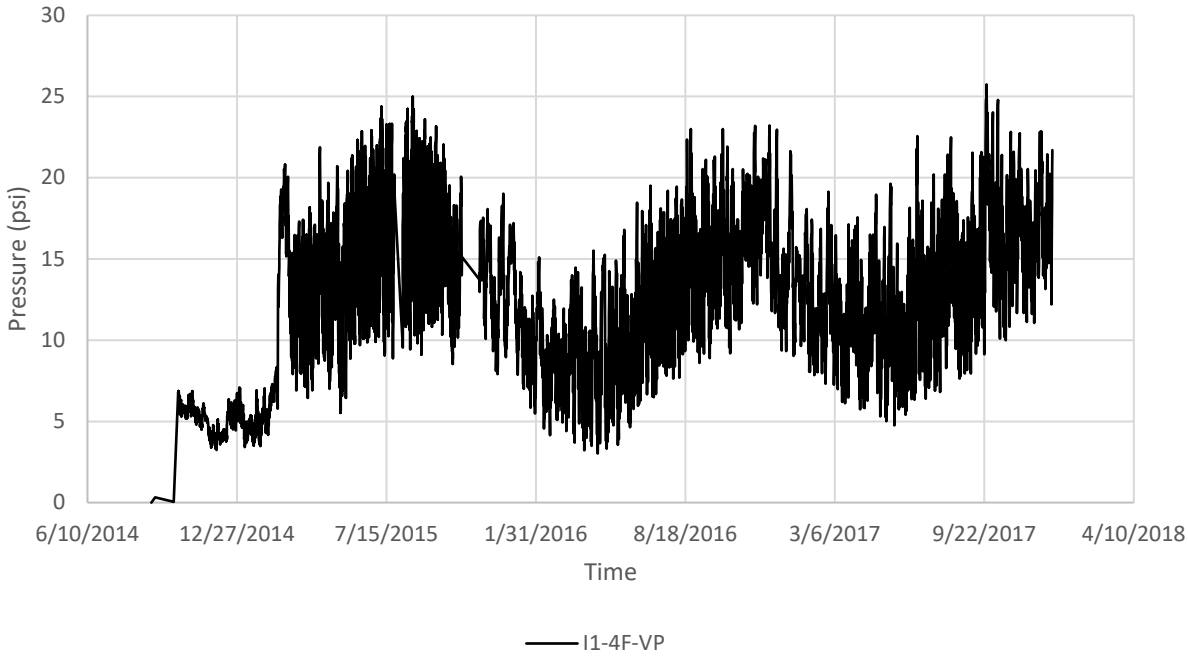

Figure 8. Data from vertical pressure cell I1-4F-VP

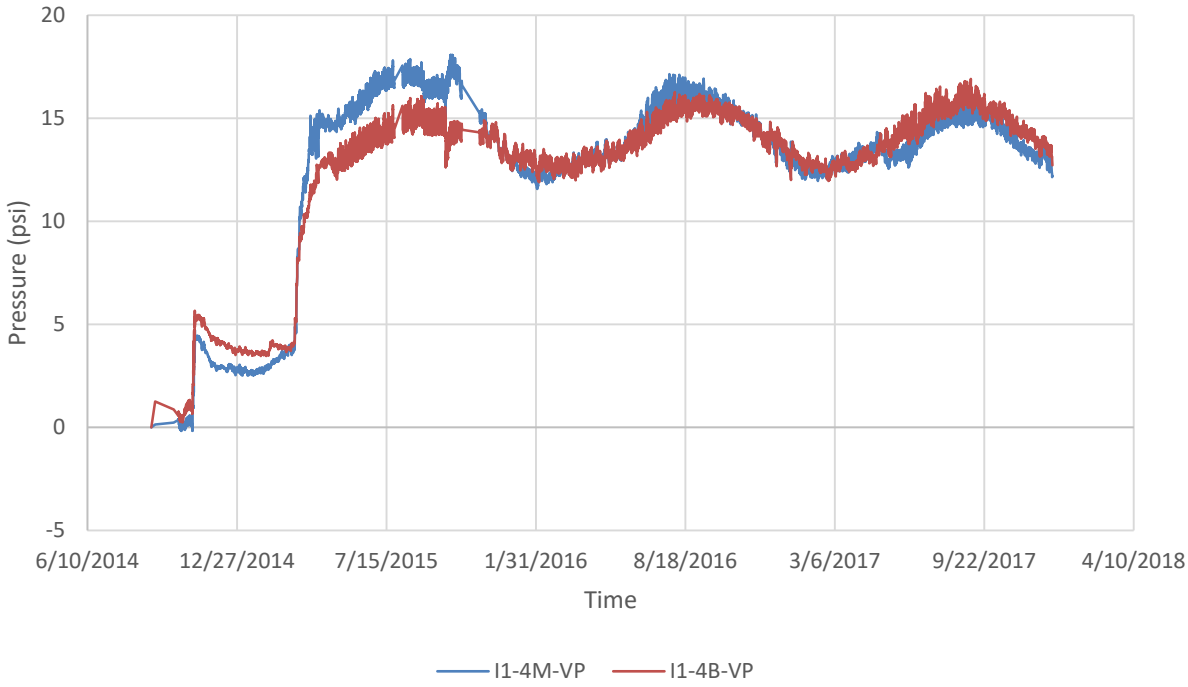

Figure 9. Data from vertical pressure cells I1-4M-VP and I1-4B-VP

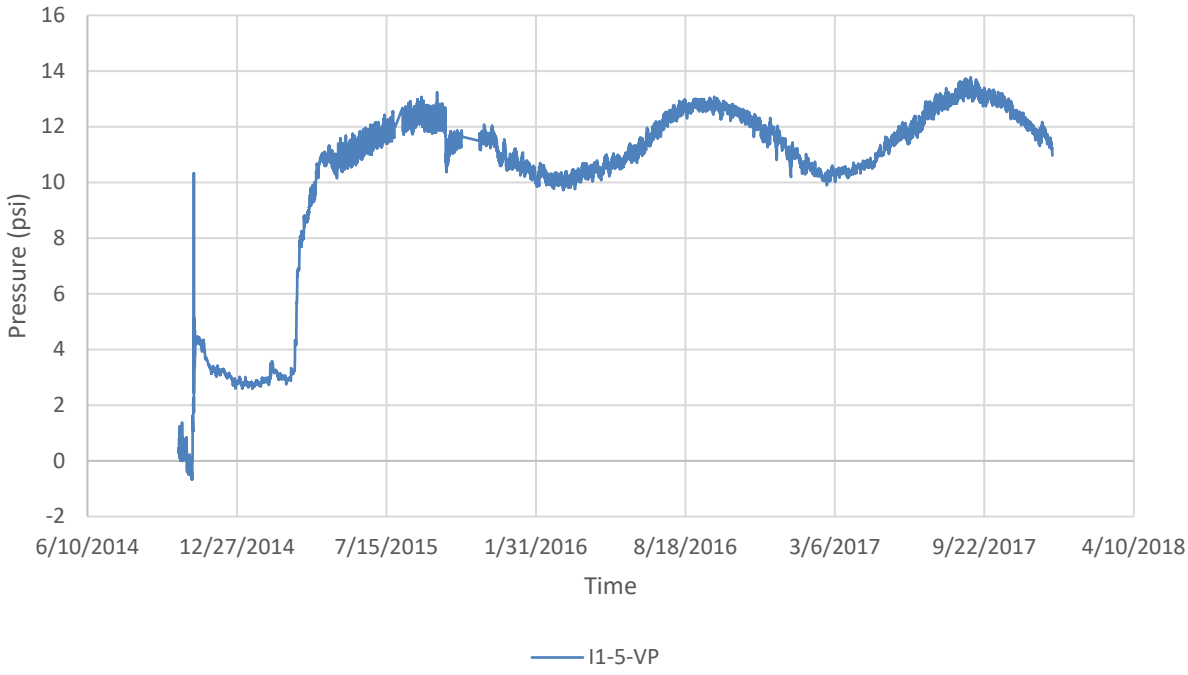

Figure 10. Data from vertical pressure cell I1-5-VP

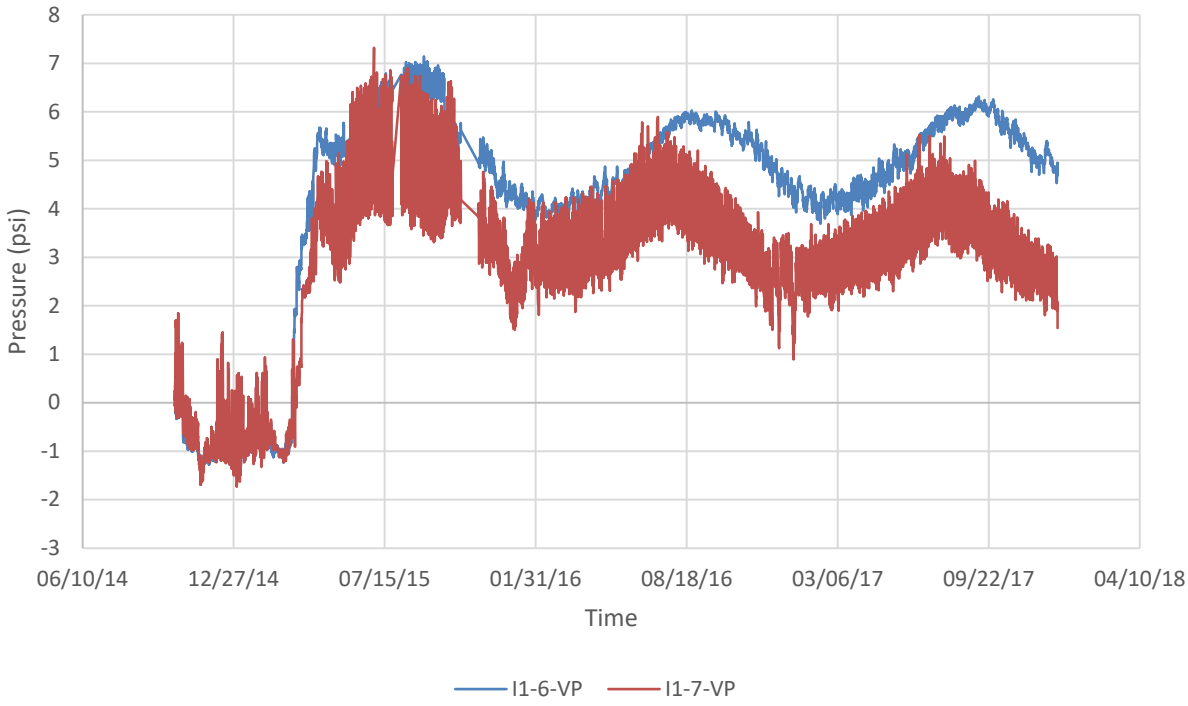

Figure 11. Data from vertical pressure cells I1-6-VP and I1-7-VP

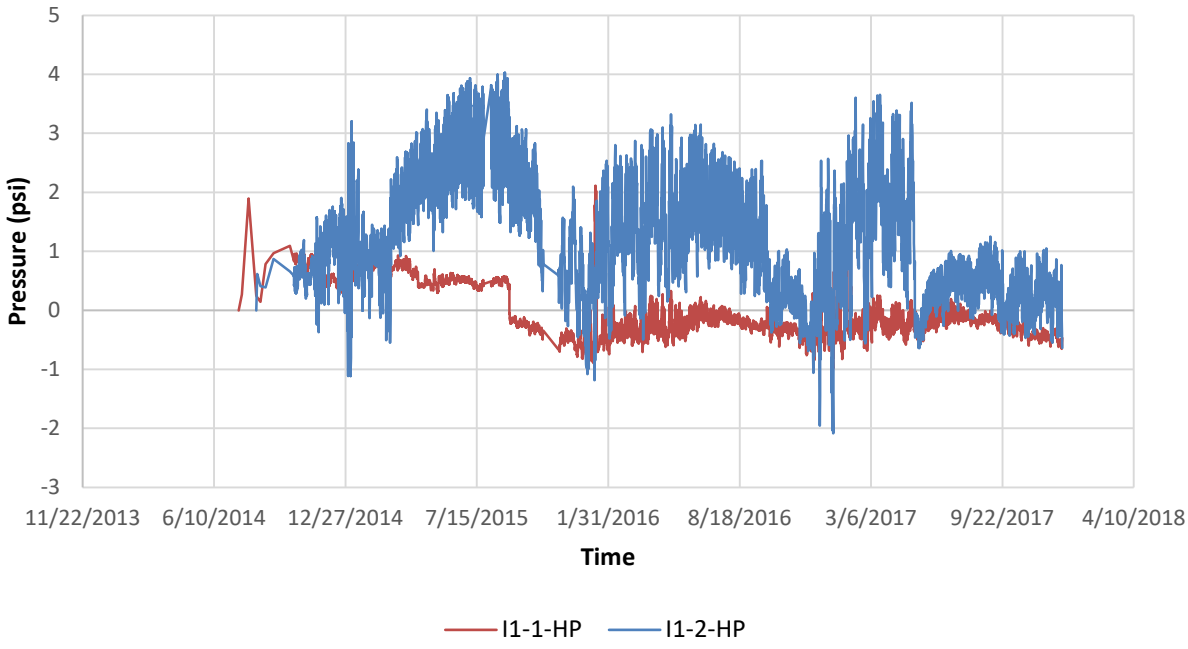

Figure 12. Data from horizontal pressure cells I1-1-HP and I1-2-HP

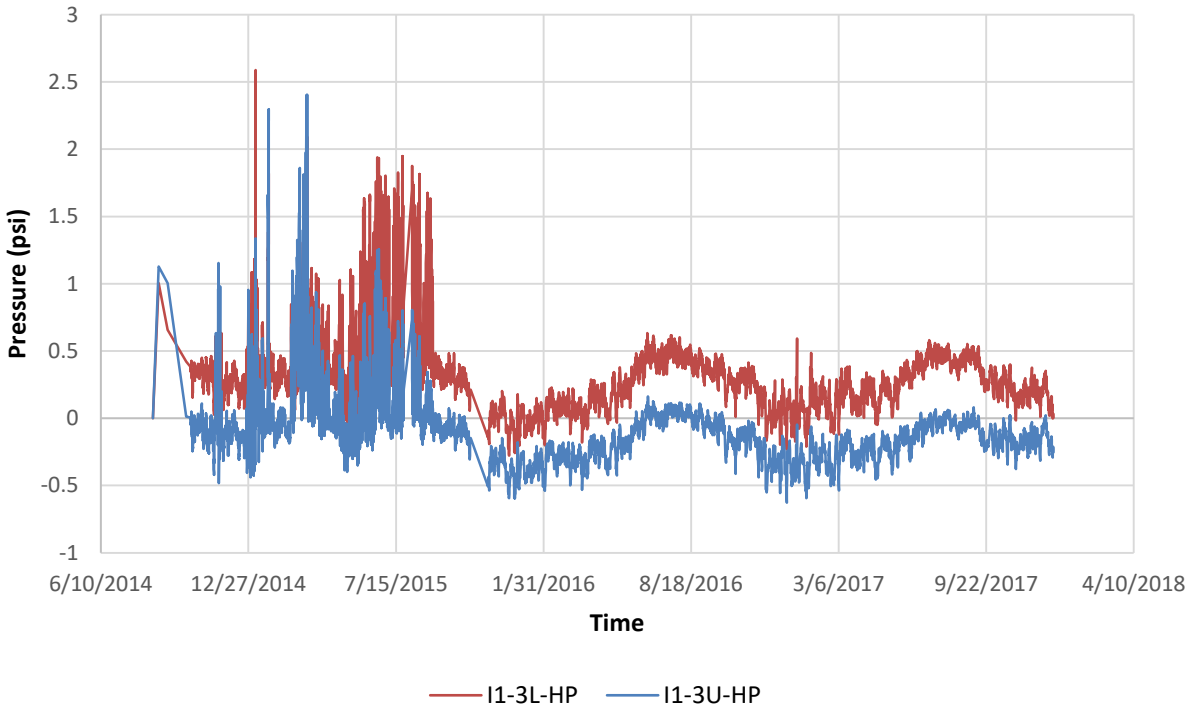

Figure 13. Data from horizontal pressure cells I1-3L-HP and I1-3U-HP

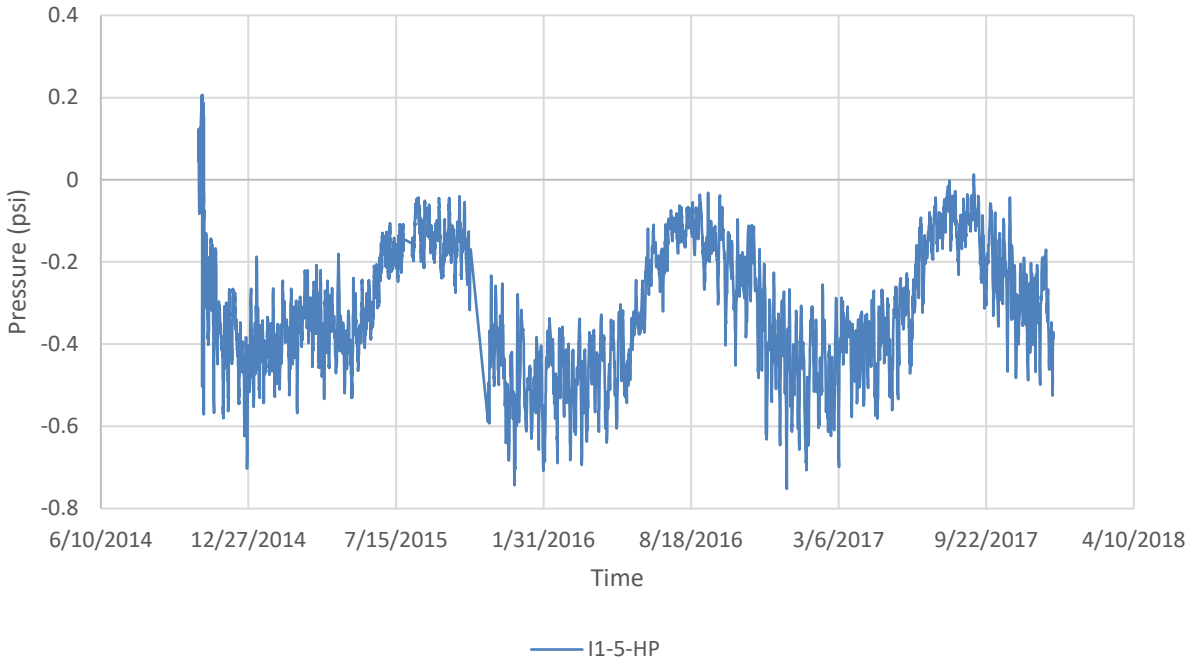

Figure 14. Data from horizontal pressure cell I1-5-HP

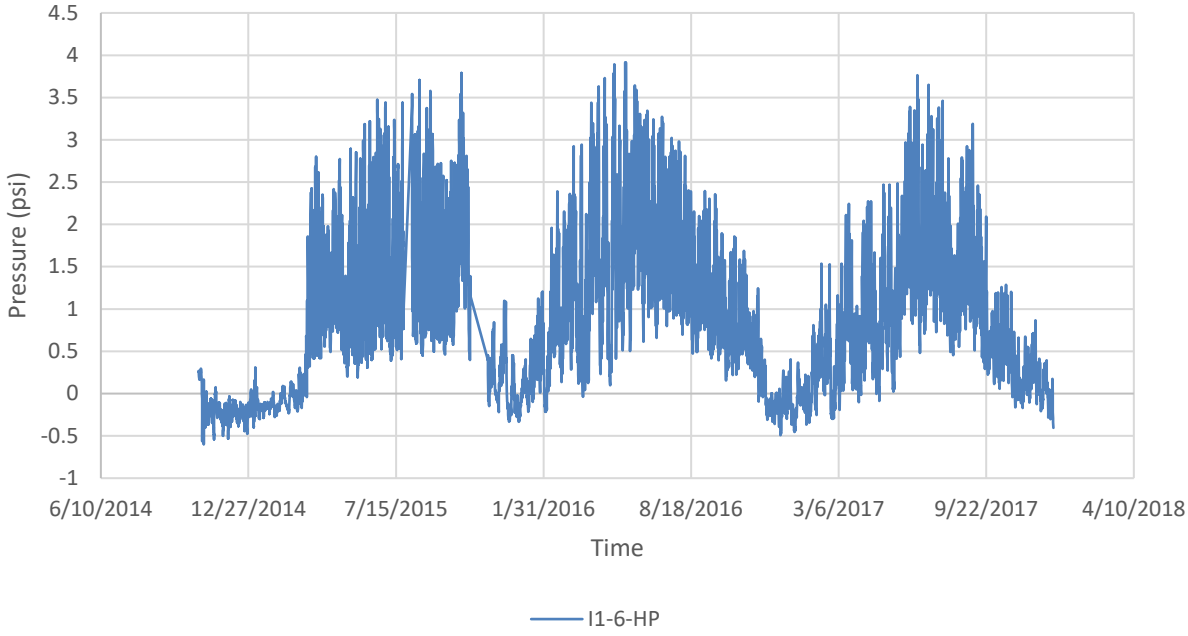

Figure 15. Data from horizontal pressure cell I1-6-HP

4.2 Sheet Pile Façade Movement

Sheet pile façade southward deformation, away from the backfill and toward the railroad track, as shown in Figs. 16 and 17, the Shape Accel Array (SAA) shows that the top of the sheet pile façade

displaced southward (or toward the Smith Road or Union Pacific Railroad) by about 0.65 inches and westward by about 0.75 inches before October 1st, 2015 or before the initiation of water transport pipeline excavation directly adjacent and in front of the base of the steel sheet pile façade. As indicated in Fig. 17, after the initiation of the excavation, the wall top displacement reached a maximum value of about 2 inches.

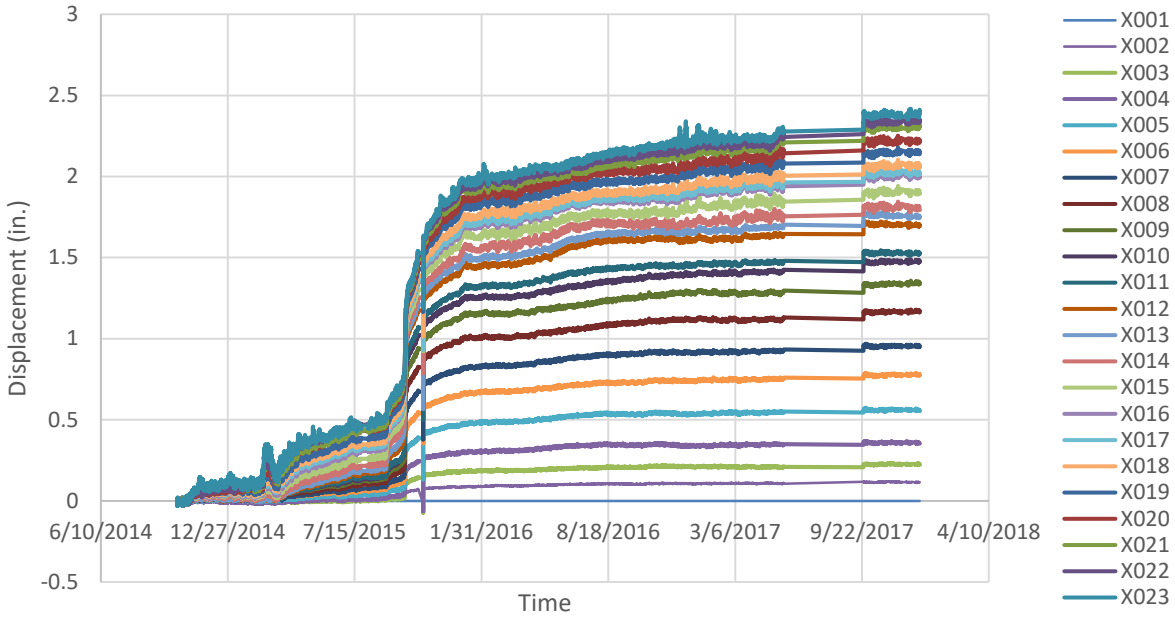

Figure 16. Data from Sensors

Fig. 17 shows the last data recorded on December 22nd, 2017, and the wall top moved another 0.5 inches since then. The wall top is still moving 22 months after SAA was installed because of creep. The Creep rate is about 0.0006 in./day.

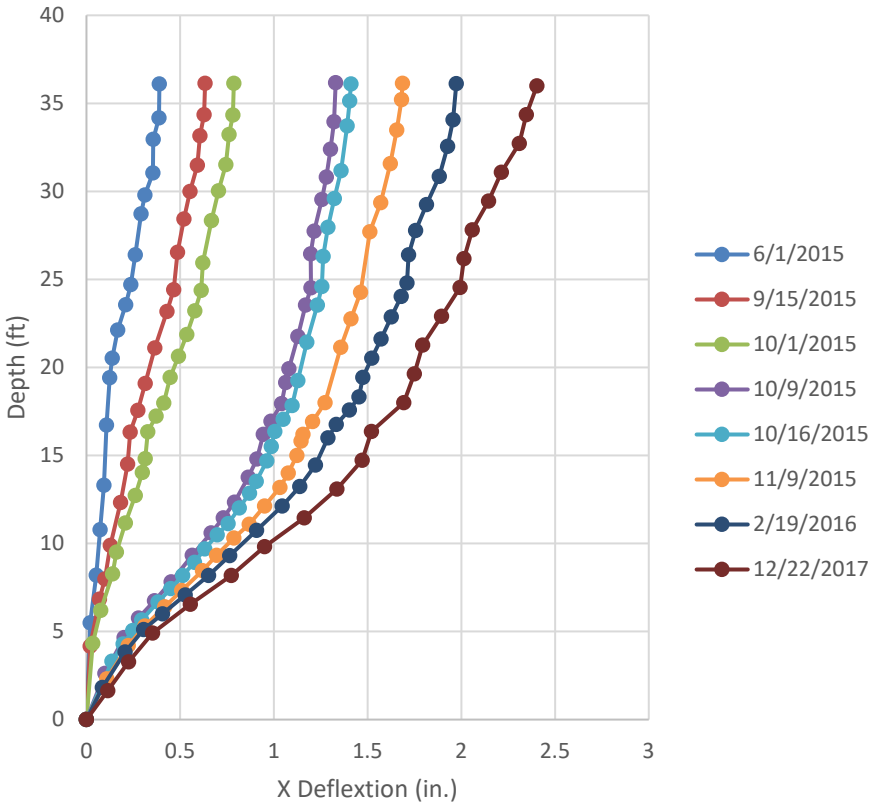

Figure 17. Wall deflection

4.3 Wall Top and Sill Corner Separation from Crack Meter

The crack meter readings are shown in Fig. 18 indicated that the relative displacement between the top of sheet pile façade and sill corner is about 1.2 inches, which might be acceptable per CDOT bridge design specifications.

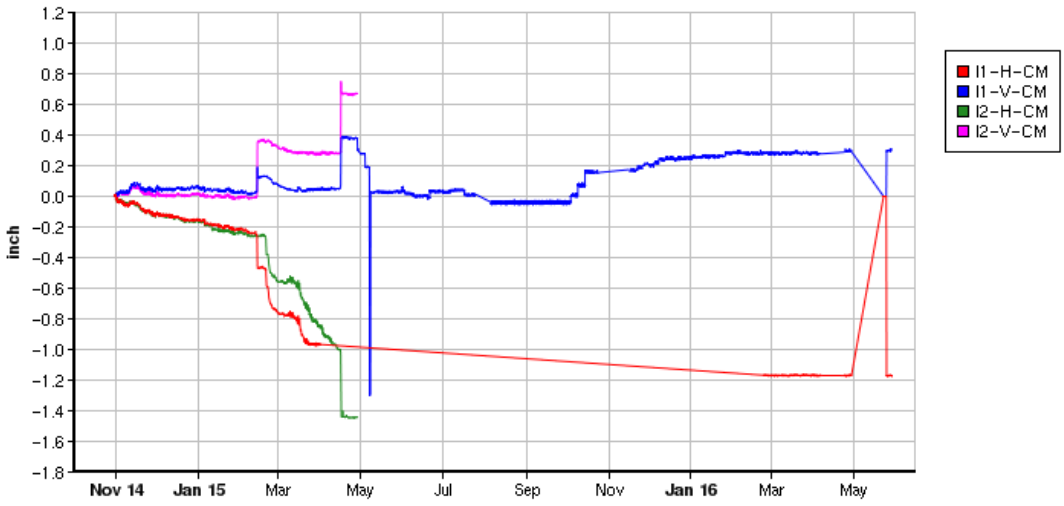

Figure 18. Gap history of sill front corner vs. top of sheet pile façade (inches)

4.4 Tie Rod Strain

Tie rod strains in Fig. 19 show that the tie rod tension is larger near the sheet pile façade and the tie rod strain is higher in Line 2 instrumentation (I2-F-SG) and reached a maximum value of 500 micro strains (equivalent of 15,000 psi tensile stress) near façade, which is much smaller than the yield strength of steel. Beyond the peak value, strain in the tie rod reduced to values between 0 and 100 micro strains. This variation in tensile stresses need further check with finite element analysis results for its validity. The strain gauges in the Line 1 tie rod did not function properly: first, the micro strain levels are much smaller and the removal of the berm in early September 2015 did not lead to any micro strain changes (Fig. 20). The construction of deadman and tie rod are shown in Figs. 21a and b.

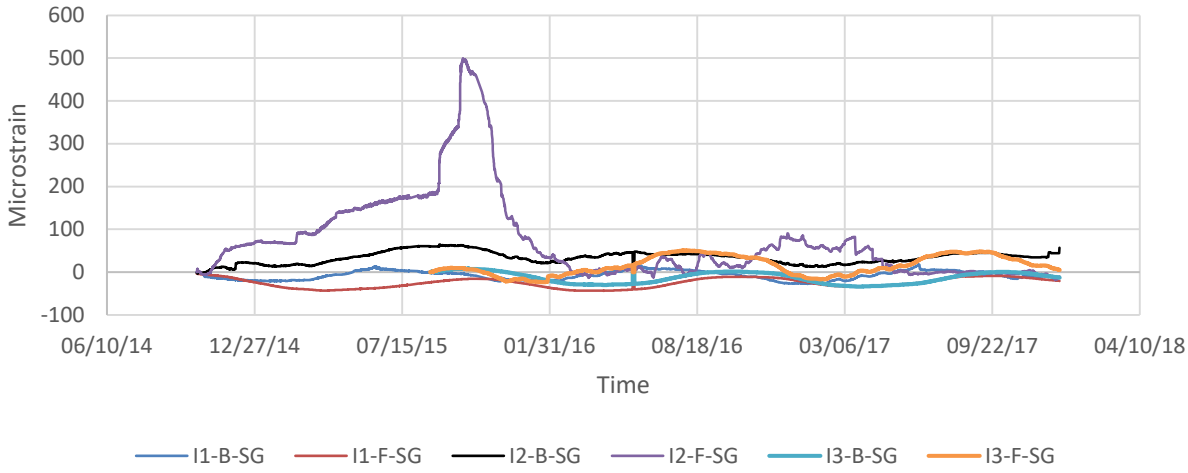

Figure 19. Tieback strain in micro strain

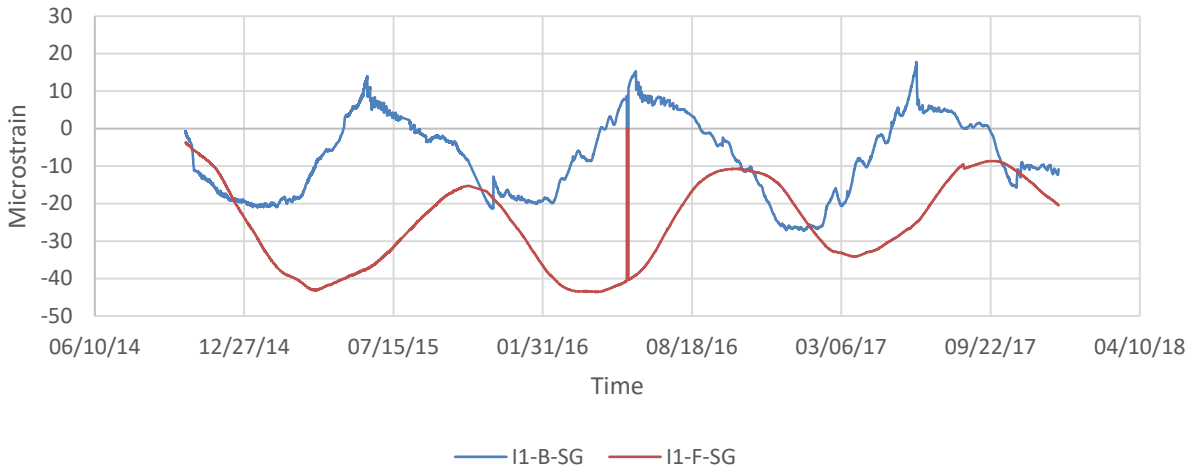

Figure 20. Tieback strain in micro strain I1-B-SG and I1-F-SG

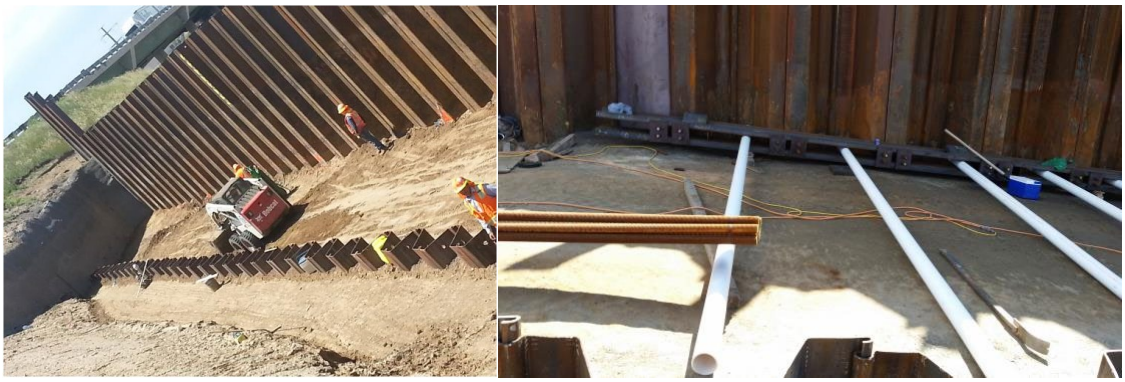

a) b)

Figure 21. Deadman and tie rod installation

4.5 Geosynthetic

The attempt for geosynthetic strain measurement using fiber optic strain gauges were not successful and needed a further study for any further implementation. Fig. 22 demonstrates the installation of the optic fiber strain gages. The optic fiber strain gage readings were delayed and, when it became available at a late date, the results were not reasonable. This means the unsuccessful attempt to measure strains along geosynthetics in the GRS mass. This could be resulted from the gauge damage during the compaction of the Colorado Class I backfill of crushed granite, which has the knife-edge like sharp grains.

Figure 22. Fiber optic strain gauge field installation

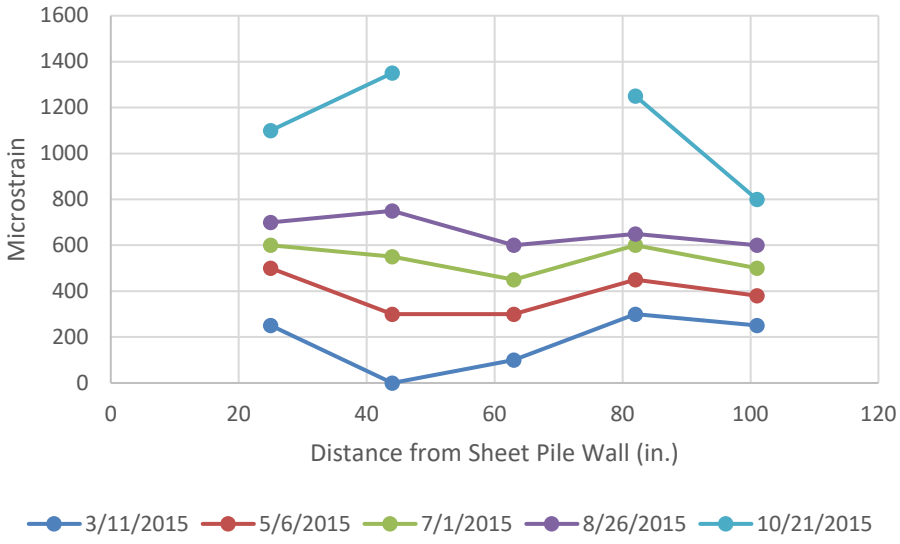

a) Level 1 (4” from the base of excavation)

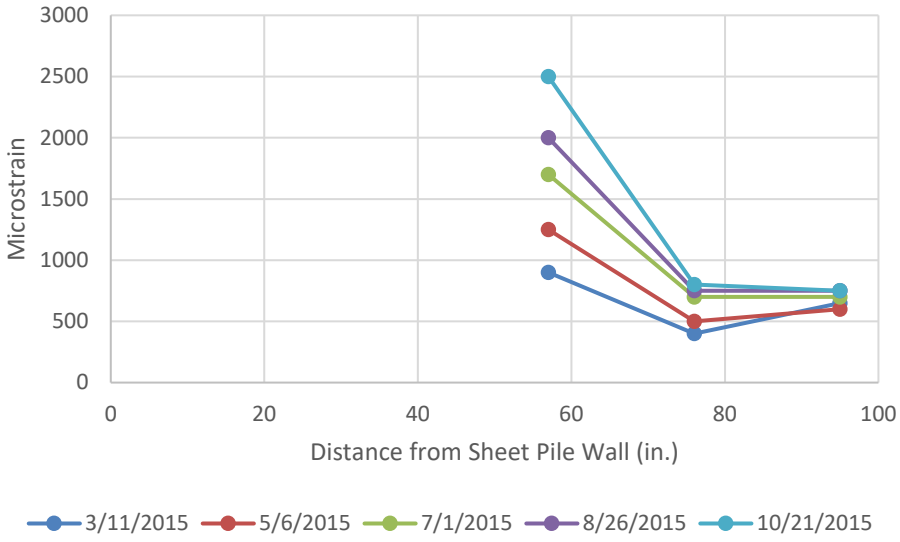

b) Level 3 (10’4” from the base of excavation)

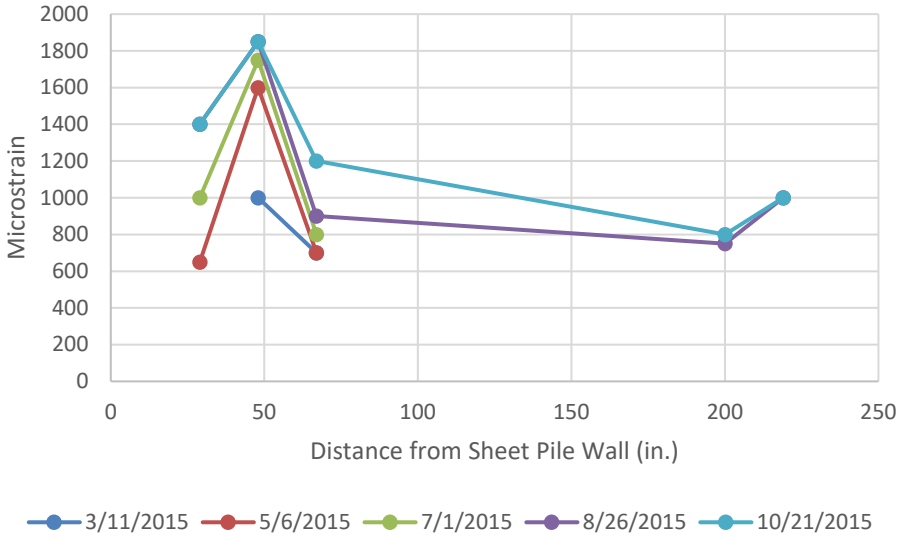

c) Level 4 (12’8” from the base of excavation)

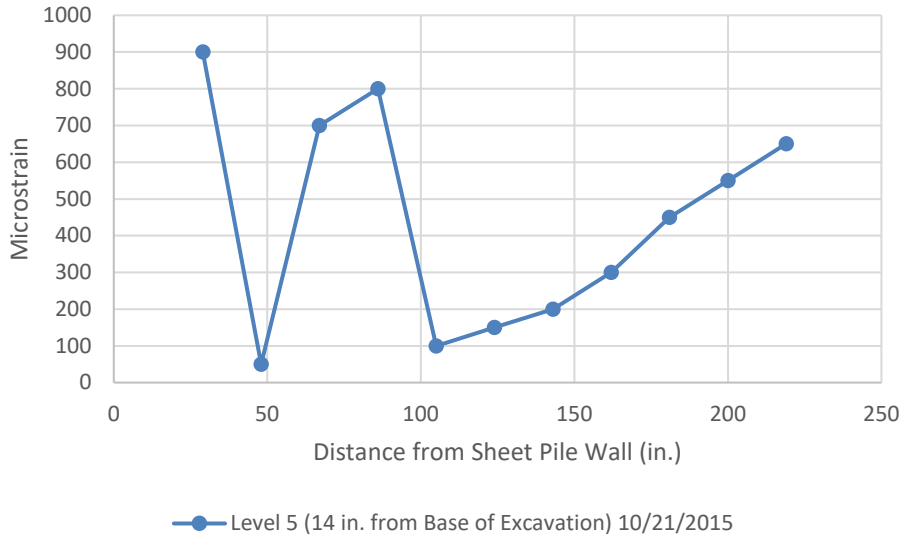

d) Level 5 (14' from the base of excavation)

Figure 23. Measurement of fiber optic strains

4.6 Adjust the Instrumentation Program

This study is a collaborative research effort. The CGES TEAM collaborated with CDOT study panelists, bridge and geotechnical engineers, geotechnical engineering consultants involved in abutment performance monitoring and construction contractor to assure the success of this study through meetings and personal contact. The abutment wall height reached about 21.5 feet at completion. This complex collaboration structure has the potential for significant project delay and subsequent change of order and exhaustion of budget. The performance monitor aspect of this project is the victim of problems experienced in this complex project and overspending, as expected. To enforce the original budget limit led to unfortunate drastic reduction in the planned instrumentation effort in Phase II construction as shown in the revised Phase II instrumentation plan.

5. COEFFICIENT OF EARTH PRESSURE AT REST

Earth pressure cells measured both horizontal and vertical earth pressures. Figures 5 to 11 showed the Earth pressures were monitored throughout the construction. As shown in these figures, 15 vertical and 5 horizontal earth pressure cells were installed in Phase I of the study on Abutment #4. Through the continuous monitoring of earth pressures during construction, time-dependent k_o can be recorded. But the values of k_o on July 1, 2015, based on the measured values of vertical and horizontal earth pressures, are as follows:

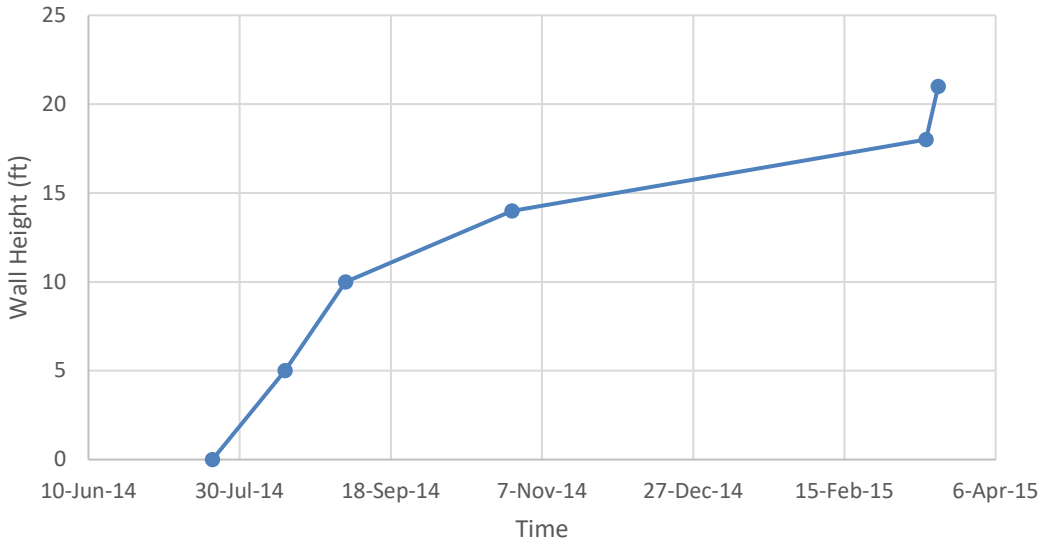

Figure 24. Wall height and construction time

Table 3: Field versus FEA k_o values

Transducers	Depths (in.)	Measured Pressure (psi)	K measured lateral earth pressure coeff..	k_0 (FEA)
1F-VP	168	12	0.042	0.12
1-HP	162	0.5		
2F-VP	108	30	0.093	0.11
2-HP	102	2.8		
3F-VP	48	22	0.055	0.11
3-HP	42	1.2		

The above table shows that the k_o values from the measured earth pressures immediately adjacent to the back of steel sheet pile façade are much smaller than those from the finite element analysis. This shows that the measured horizontal earth pressures are approaching active earth pressures and much smaller than earth pressures at rest. This is believed to be caused by the forward deformation of the steel sheet pile façade and the measured horizontal earth pressures were no longer the at-rest earth pressures but approached the active earth pressures due to the façade forward movement with a maximum displacement of 2 inches at the wall top. This is further evidenced by the

following k_o values from different sources:

$$k_0 = 1 - \sin\varphi = 1 - 0.682 = 0.318$$

where φ is equal to 43^0, and is the angle of internal friction of Colorado Class I backfill of crushed granite of minus ½ inch grain size.

$$k_0 = \frac{\nu}{1-\nu} = \frac{0.25}{1-0.25} = 0.333$$

where ν is Poisson's ratio of the Colorado Class I backfill, the selected value of 0.25. $k_0 = 0.17$ measured from the Colorado Class I backfill specimen compaction in the 12-inch direct shear machine under Oedometer condition.

The above discussion on k_o is summarized as follows:

1) The horizontal earth pressures measured along the back of façade are much smaller than the at-rest earth pressure. These earth pressures decreased from the at-rest values to the values of active earth pressures due to the forward movement of the façade.
2) While the maximum movement at the wall top is limited to 2 inches, it was sufficient to arrive at the active state and active earth pressures, as evidenced in the earth pressure tests carried in the Tiger Cage. This shows that the active earth pressures are extremely sensitive to the lateral wall movement.
3) The classical at-rest earth pressure coefficient theories need to be re-examined for their reliability.

The topic of the at-rest earth pressures will be further discussed in the research report on "GRS wall earth pressures" for the CDOT/FHWA sponsored report. The Rankine active earth pressure coefficient is equal to $k_a = (1-\sin\varphi) / (1+ \sin\varphi) = 0.189$. Table 3 gives the average measured horizontal earth pressure of 0.063, which is smaller than the active earth pressure coefficient of 0.189. This indicated some soil-wall separation.

6. ABUTMENT PERFORMANCE DURING PIPELINE TRENCH EXCAVATION

Around October 1, 2015, a 10' x 10' trench excavation was initiated to prepare for the installation of a large-diameter water transport pipeline. During the excavation, the steel sheet pile façade experienced immediate forward movement from 0.8 inches on Oct. 1 before excavation to 1.3 inches on Oct 9, 1.4 inches on October 16, 1.7 inches on Nov. 9 and 2.0 inches on Feb. 19, 2016, as shown in Table 4 and Figure 17.

Table 4: Forward movement of wall top

Date	Movement in inches
10/1/2015	0.8
10/9/2015	1.3
10/16/2015	1.4
11/9/2015	1.7
2/19/2016	2.0
2/22/2018	2.4

This showed the following important observations for reference in similar construction projects in the future:

1) A large trench excavation like this can lead to an undesirable immediate forward movement of the steel sheet pile façade,
2) Immediate remedial measures are required to arrest the situation, as evidenced by the quick request for the action of backfilling the trench by the personnel from the CDOT Bridge Branch and Construction Branch,
3) After backfilling, the façade still experienced further lateral displacement, and this movement is caused by the time-dependent soil-structure interaction, which shows the nature of creep at a reducing creep rate. This indicates that the wall movement is stabilized and further drastic movement is not expected without additional drastic action,
4) Fig. 19 showed that the Tieback I2-F-SG experienced a drastic increase in tension, peaked out on October 1, 2015. The installation of the tiebacks in this project saved the façade from even more drastic forward movement and might have even saved it from imminent failure. This tieback-deadman system should be made an integral part of the steel sheet pile wall system, when the wall toe might suffer gross outward movement, such as that caused by the excavation along the wall toe.
5) At the level of subgrade, the measured earth pressures are much smaller than calculated values as shown in Table 3. Fig. 5 shows that the vertical earth pressure measured at Pressure Cell I1-1F-VP and Fig. 12 for horizontal Pressure Cells I1-1-HP and I1-2-HP suffered significant drops. The vertical Pressure Cell I1-1F-VP might have been torn for it no longer function after October 1, 2015.

7. LABORATORY TESTING OF BACKFILL AND GEOSYNTHETIC

7.1 General

The study TEAM carried out a laboratory test program that covers the following tests to provide all necessary soil parameters for use in finite element analysis:

1) Wide-Width Tension Tests of UD4800 geosynthetics,
2) Triaxial compression tests on Colorado Class I backfill of crushed granite,
3) Oedometer and direct shear tests
4) Index property tests and density-moisture relationship

7.2 Wide-Width (WW) Tension Tests of US4800 Geosynthetic

WW tensile tests, ASTM D-4595, were performed on three intact and twelve exhumed samples (six from I1 and I2 each) of Amoco woven geosynthetic US4800 used in the construction using 220-kip MTS Hydroelectric Servo Control universal testing machine. The engineer from the Shannon and Wilson, Inc. provided all geosynthetic samples for testing. The tests provided geosynthetic design parameters for the numerical analysis of GRS abutment performance. Since ASTM requires the use of "Mean Average Roll Value (MARV)" in design, sufficient statistical sample size of a test type is needed, where MARV is defined as sample mean minuses two times the standard deviation (MARV = statistical sample mean – two times the standard deviation). In the WW tensile tests, geosynthetic samples are typically 8" x 8" and the clamps are 8" in length x 2" in width x 0.25" in thickness. After a test, the tensile force is divided by the width of 8 inches and then multiplied by 12 inches to obtain the geosynthetic strength in lbs/ft. The Wide-Width tensile test provides a more reliable assessment of geosynthetic strength and, for critical applications, it is the method engineers use to determine the required tensile strength. It is typically performed only on woven (reinforcement) geosynthetics. ASTM D-4595 requires the entire width of the sample to be clamped with the clamps of 8" x 2". The geosynthetic sample is 8" wide x 8" long (minimum length exposed to tension during the test not including the 2" clamped length at each end with the minimum total length of 12 inches. Since the entire width of the sample is held by the clamps, the test is considered to provide a true tensile strength. US4800 shows its peak strength at around 20% strain. The tensile force versus elongation curves for the WW tensile tests of Amoco US4800 Geosynthetic are summarized in Figs. 25 to 29. Table 6 shows a summary of the test results. The average tensile strength of the new geosynthetic samples is 495 lbs/inch (or 5940 lbs/ft). The tensile strength is direction-dependent and is smallest at 30^0 angle to the main

direction of geosynthetics. Refer to the manufacturer's websites for more information on typical properties of Woven Geosynthetics tested by following ASTM Test Methods for Geosynthetics.

Table 5: Property of geosynthetic from Manufacturer

Property	Test Method	Manufacturer	Tests at UCD
Tensile Strength	ASTM D-4632	550 x 550 lbs	
Elongation @ Break	ASTM D-4632	20 x 20 %	22.6 %
Wide Width Tensile	ASTM D-4595	5,070 x 5,070 lbs/foot	5,847 lbs/foot
Wide Width Tensile @ 2% Strain	ASTM D-4595	960 x 1,096 lbs/ft	-
Wide Width Tensile @ 5% Strain	ASTM D-4595	2,740 x 2,740 lbs/ft	1,948 lbs/ft
Wide Width Tensile @ 10% Strain	ASTM D-4595	4,800 x 4,800 lbs/ft	3,060 lbs/ft
CBR Puncture	ASTM D-6241	1,700 lbs	-
Trapezoidal Tear	ASTM D-4533	180 x 180 lbs	-
Apparent Opening Size	ASTM D-4751	40 US Sieve	-
Permittivity	ASTM D-4491	0.15 Sec-1	-
Water Flow Rate	ASTM D-4491	11.5 g/min/sf	-
UV Resistance @ 500 Hours	ASTM D-4355	80%	-

Three new samples with force in the main geosynthetic direction and other three new samples with the test force in 15º, 30º and 45º direction, respectively, to the main geosynthetic direction, six exhumed samples from each site were tested and the results summarized in Table 6.

Figure 25. Wide width tension test sample preparation parts and layout

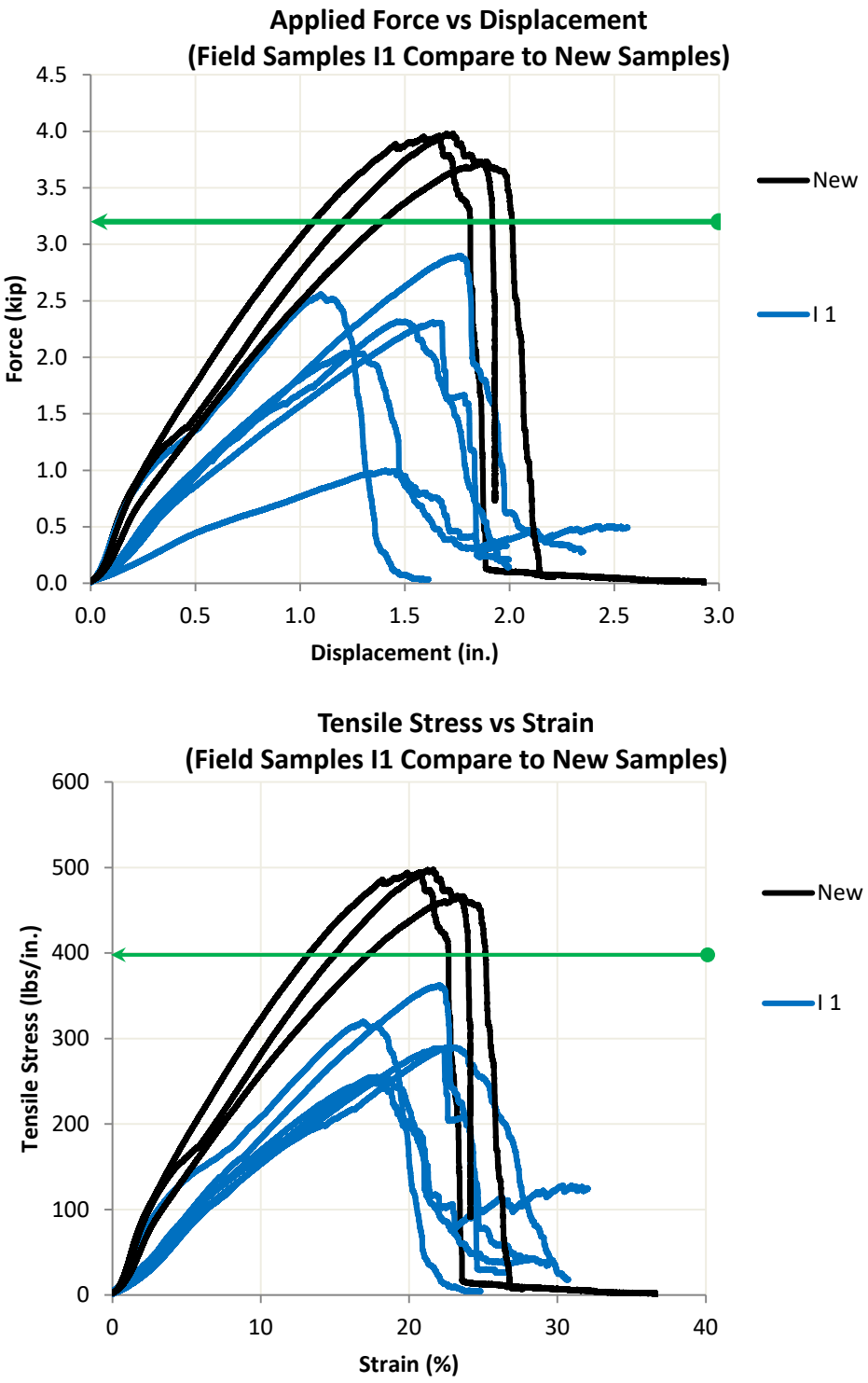

Figure 26. Tests of I1 new and field geosynthetic samples

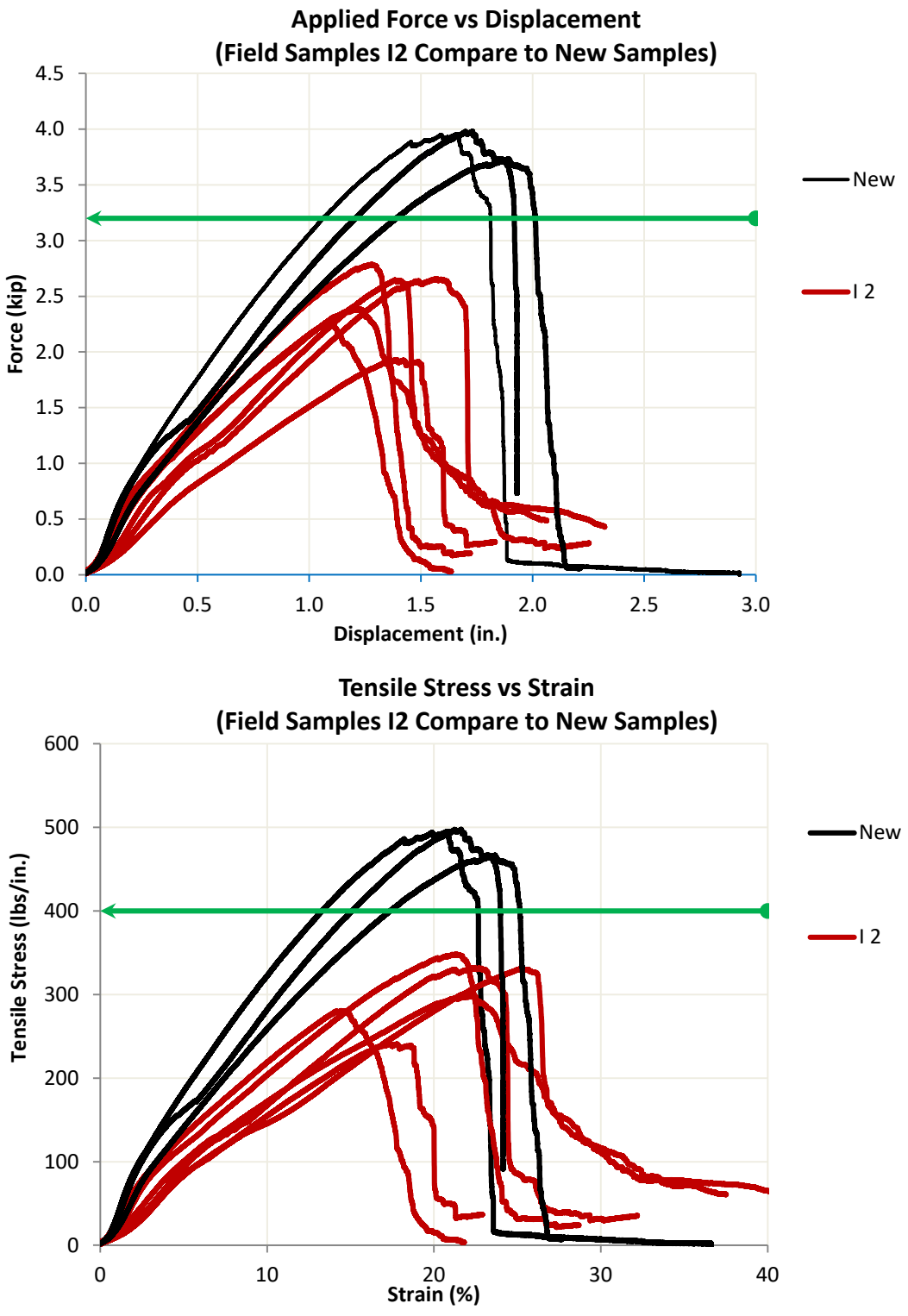

Figure 27. Tests of I2 new and field geosynthetic samples

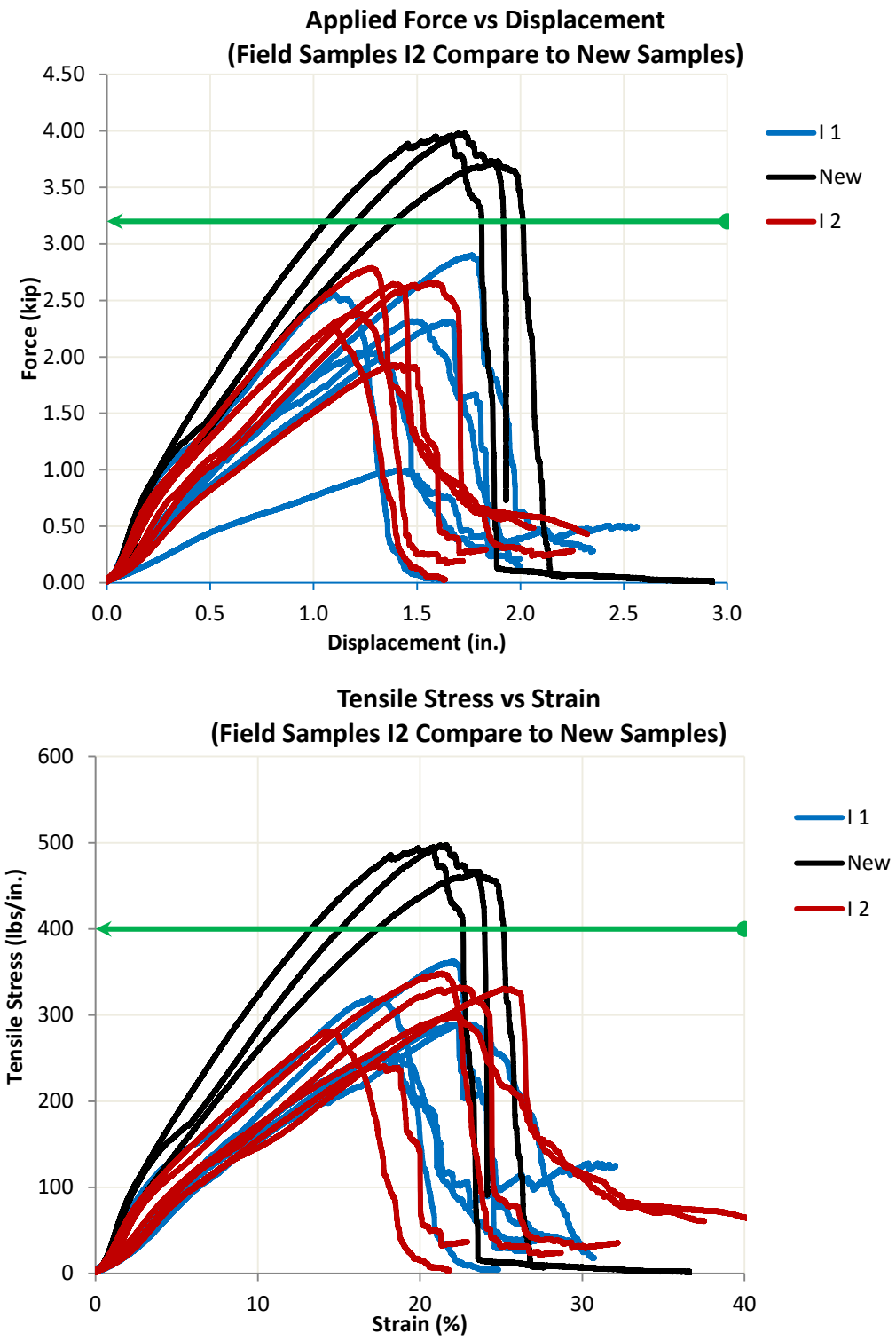

Figure 28. Tests of all new and field geosynthetic samples

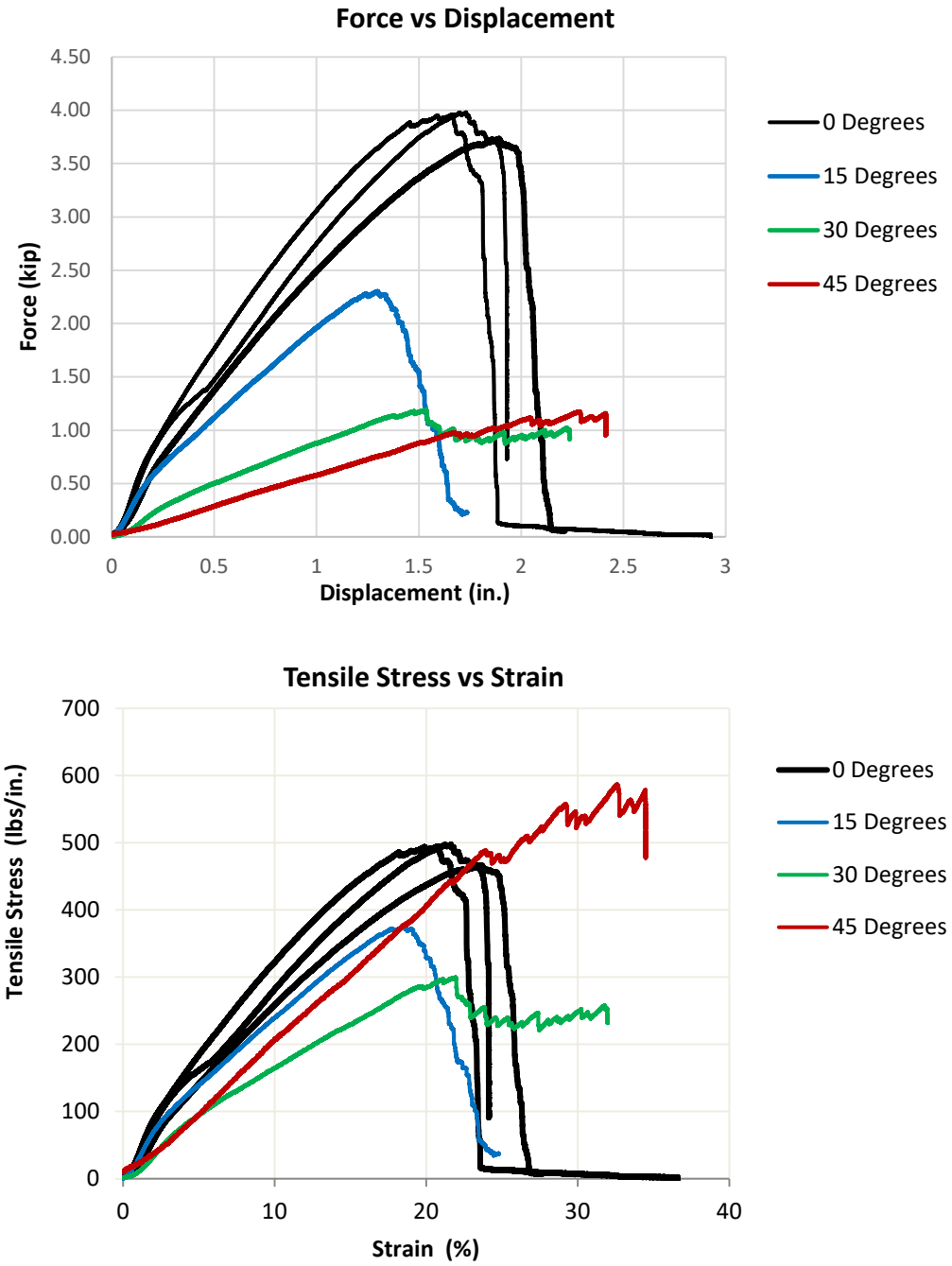

Figure 29. Tests of geosynthetic samples in different directions

Table 6: Data summary of geosynthetic test results

Test Results												Note
Sample	Location	Symbol	Sample Dimension W × L (in)	Maximum Applied Force (lbf)	Tensile Strength (lbf/in)			Strain at Maximum Tensile Strength (%)	Tensile Modulus (lbf/in)			
					Maximum Tensile Strength	Tensile Strength at 5%	Tensile Strength at 10%		Peak Tensile Modulus (K_P)	Tensile Modulus at 5% ($K_{5\%}$)	Tensile Modulus at 10% ($K_{10\%}$)	
New with Main Direction		No.2	8 × 8	3960	495	184	225	22	2574	3635	3225	Angle direction is zero
		No.3	8 × 8	3981	498	161	282	22	2300	3220	2818	
		No.4	8 × 8	3754	467	142	258	24	1975	2814	2591	
New with Angle Direction		15 deg.	8 × 7	2302	376	140	239	19	2028	2794	2394	Angle direction is the angle between tensile direction and main direction
		30 deg.	8 × 7	1188	300	95	264	22	1567	1825	1643	
		45 deg.	8 × 7	1174	485	95	207	24	1995	1905	2068	
Exhumed Field Sample I1	STATION 1 + 73.5	I1 - 51	8 × 8	2901	365	95	285	22	1645	1861	1850	
		I1 - 52	8 × 6.5	2318	290	76	153	23	1273	1517	1533	
		I1 - 53	8 × 8	998	252	89	161	28	1431	1783	1606	Not along principle direction
		I1 - 54	8 × 7.5	2510	289	85	155	22	1520	1657	1551	
		I1 - 55	8 × 7	2042	266	91	169	28	1431	1824	1688	Heavily soiled
		I1 - 56	8 × 6.5	2559	320	136	208	27	1891	2725	2079	Heavily soiled
Exhumed Field Sample I2	STATION 1 + 93	I2 - 51	8 × 5.5	2647	331	84	246	25	1514	1685	1459	
		I2 - 52	8 × 7	2659	332	95	288	22	1450	1809	1677	
		I2 - 53	8 × 5.5	2385	298	100	172	22	1334	2007	1720	
		I2 - 54	8 × 8	2789	349	118	200	22	1655	2568	2055	
		I2 - 55	8 × 8	1929	241	83	255	17	1385	1667	1550	Heavily soiled
		I2 - 56	8 × 7.5	2246	281	151	228	24	1946	2624	2185	Heavily soiled

Statistics										
Sample	Location	Value	Maximum Applied Force (lbf)	Tensile Strength (lbf/in)			Strain at Maximum Tensile Strength (%)	Tensile Modulus (lbf/in)		
				Maximum Tensile Strength	Tensile Strength at 5%	Tensile Strength at 10%		Peak Tensile Modulus (K_P)	Tensile Modulus at 5% ($K_{5\%}$)	Tensile Modulus at 10% ($K_{10\%}$)
New with Main Direction		Minimum	3734	467	141	259	21	1973	2814	2591
		Maximum	3981	493	184	323	24	2374	2085	3225
		Average	3892	486	162	238	22	2216	3240	2878
New with Angle Direction		Minimum	1174	300	96	164	19	1367	1893	1643
		Maximum	2302	485	140	239	24	2028	2794	2394
		Average	1555	387	110	204	22	1797	2197	2035
Field Sample I1	STATION 1 + 73.5	Minimum	993	252	76	153	17	1273	1517	1531
		Maximum	2901	363	136	208	23	1891	2725	2079
		Average	2183	296	96	171	20	1499	1896	1711
Field Sample I2	STATION 1 + 93	Minimum	1929	241	83	146	14	1314	1667	1459
		Maximum	2789	349	131	219	25	1946	2624	2185
		Average	2443	305	102	177	21	1515	3037	1771

Additional tension tests of three geosynthetic samples with unloading-reloading are shown in Fig. 30. The sample dimensions are 8 in. in width and 12 in. in length. The properties of the geosynthetic used in analyses are shown in Table 7.

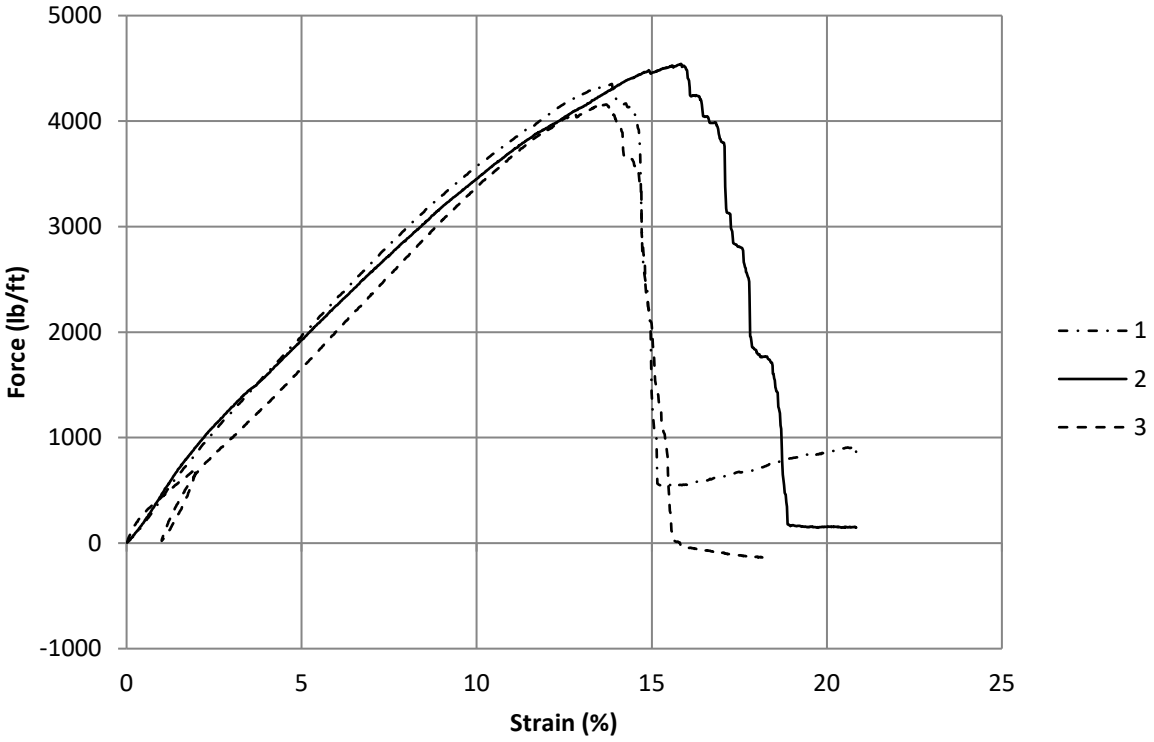

Figure 30. Load-Displacement curves of geosynthetic from tension tests

Table 7: Geosynthetic properties

Properties	Unit	Value
EA_i	lb/ft [kN/m]	44250 [659]
EA_{ur}	lb/ft [kN/m]	69000 [1028]
Fmax	lb/ft [kN/m]	4353 [65]

7.3 Triaxial Compression Tests on Colorado Class I Backfill of Crushed Granite

Both conventional compression and hydrostatic compression triaxial tests were performed and results presented in Figs. 31 to 34 and summarized in Tables 8 and 9.

7.3.1 Hydrostatic Compression Tests

Hydrostatic compression (or isotropic compression) tests are performed and shown in Fig. 8.

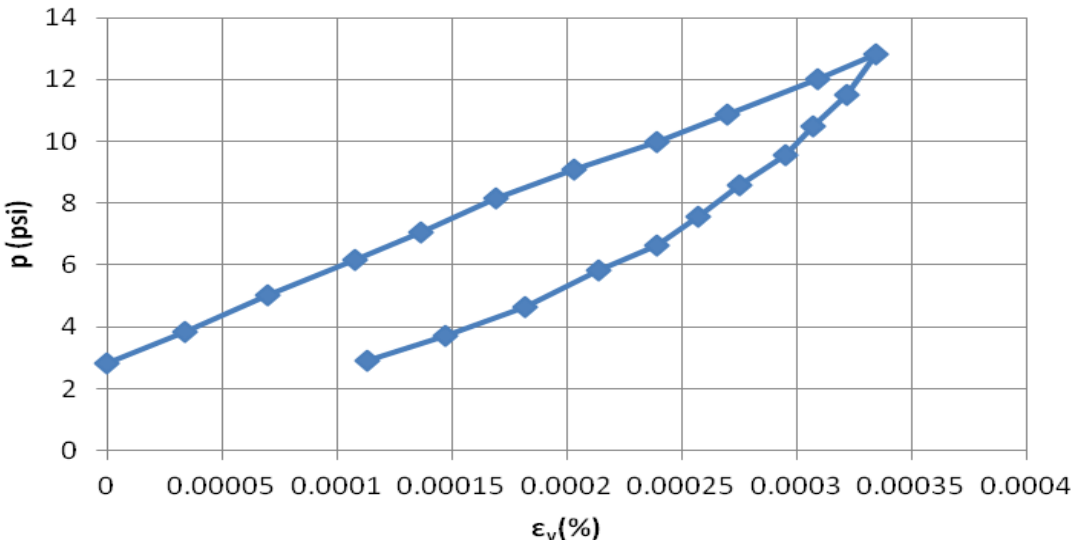

Figure 31. Hydrostatic test

7.3.2 Conventional Triaxial Compression Tests

Several conventional triaxial compression tests were conducted in the UCD laboratory. Samples were 6 inches in diameter, 12 inches in length. Dry soil was mixed with water to attain its optimum moisture content and compacted in a mold using the modified Proctor compaction. Three confining pressures were selected as 10 psi, 20 psi and 30 psi which represent corresponding common heights of GRS walls. Test results of three samples are shown in Fig. 32 without volume change measurement. From these tests, the soil strength parameters are determined and shown in Table 8. The method to determine the friction angle and cohesion is presented in Figs. 33 and 34. Two isotropic compression tests, one on dry soil and other on moisture soil, were performed to assess the effect of moisture on volume change (Fig. 35). Both tests yielded similar results. This test is also used to determine the dilatancy angle, as shown in Figs. 36 and 37 and Table 8.

The Young's moduli can be determined from triaxial tests as follows:

$$E_i = K_L P_a \left(\frac{\sigma_3}{P_a} \right)^{n_L} \quad (1)$$

$$E_{ur} = K_{ur} P_a \left(\frac{\sigma_3}{P_a} \right)^{n_{ur}} \quad (2)$$

where E_i and E_{ur} are initial tangent modulus and unloading-reloading modulus, respectively, as functions of confining stress, σ_3; K_L and K_{ur} are loading and unloading-reloading moduli,

respectively; p_a is atmospheric pressure (used as a normalizing parameter); σ_3 is confining stress; and n_L and n_{ur} are exponents for defining the influence of the confining pressure on the moduli. The Poisson's ratio is back-calculated from the coefficient of the lateral earth pressure at rest $k_0 = 0.17$ as $\nu = k_0/(1+k_0) = 0.17/1.17 = 0.145$. The elastic parameters are presented in Table 9.

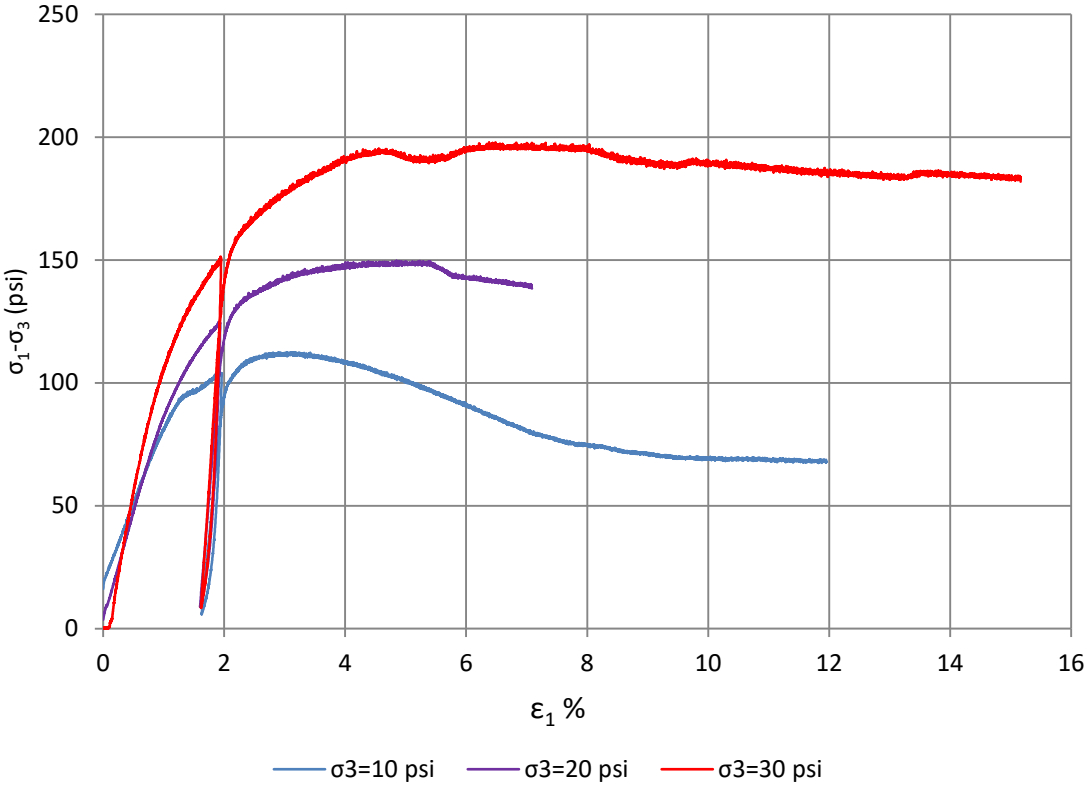

Figure 32. Triaxial test results

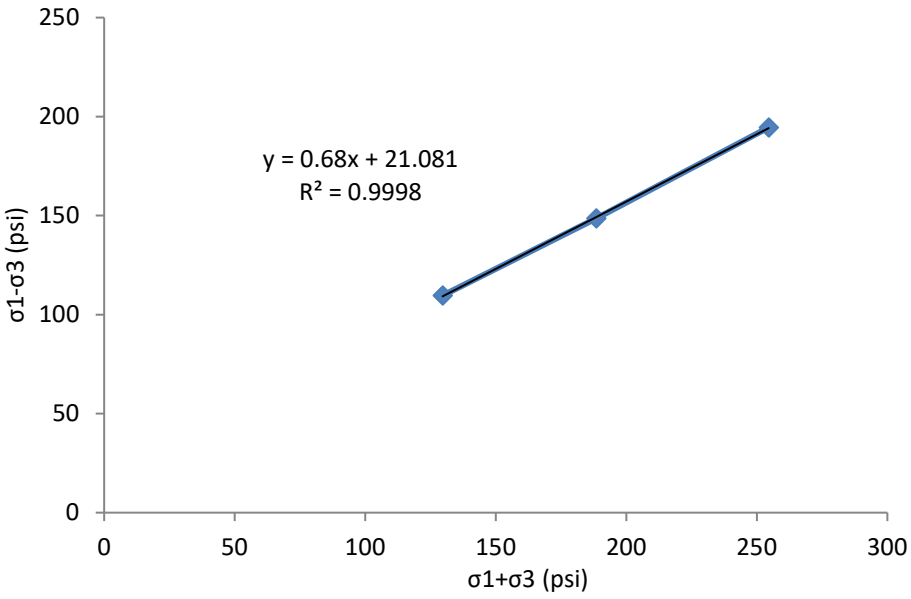

Figure 33. Determination of friction angle and cohesion

Table 8: Friction angle and cohesion from triaxial tests

Properties	Units	Value
Friction angle, φ	(^{0})	42.8
Cohesion, c	(psi)	14.4
Dilatancy angle, ψ	(^{0})	8.7

Table 9: Modulus from triaxial tests

Parameter	Value
K_L	532.4
n_L	0.477
K_{ur}	1975.6
n_{ur}	0.344
ν	0.145

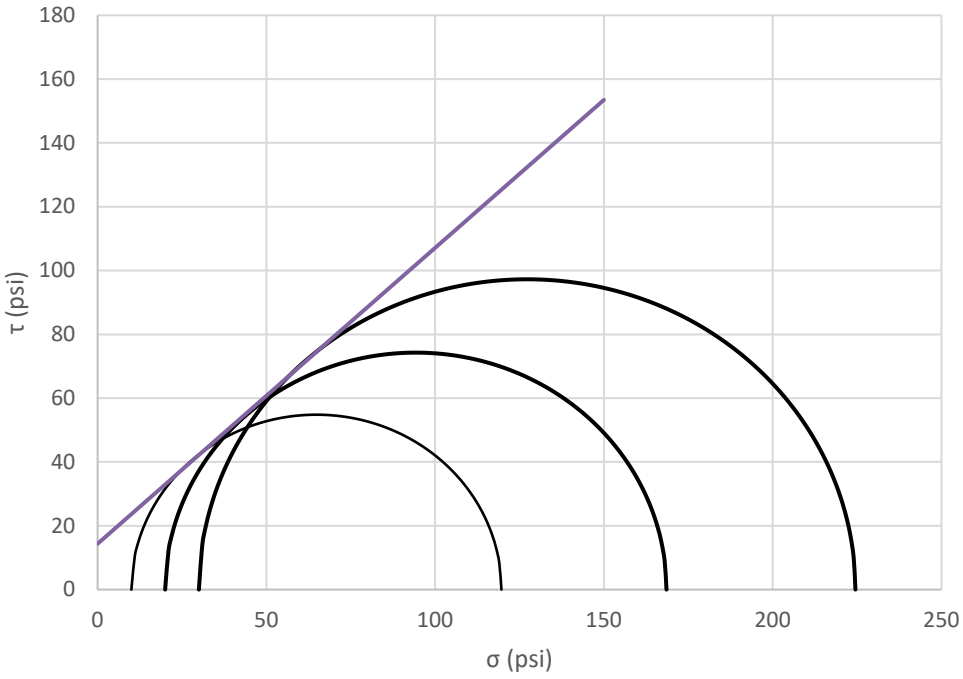

Figure 34. Mohr circle and failure line

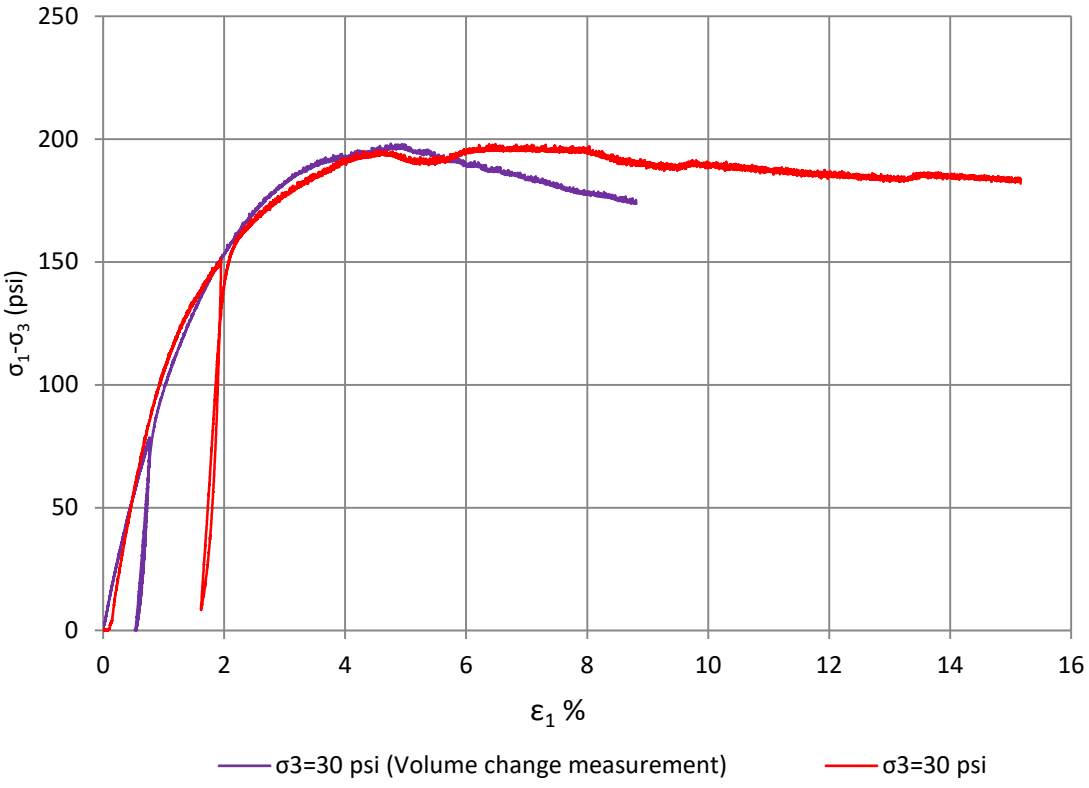

Figure 35. Comparison of triaxial compression tests (σ_3=30 psi)

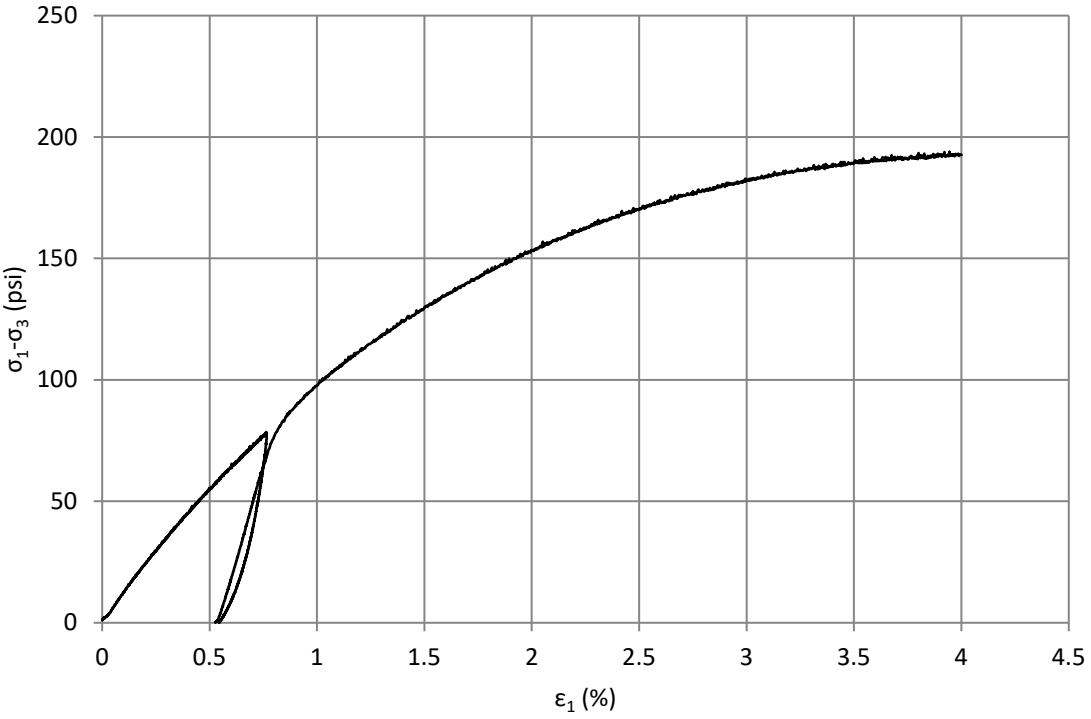

Figure 36. Triaxial test (σ_3=30 psi) with volume change measurement

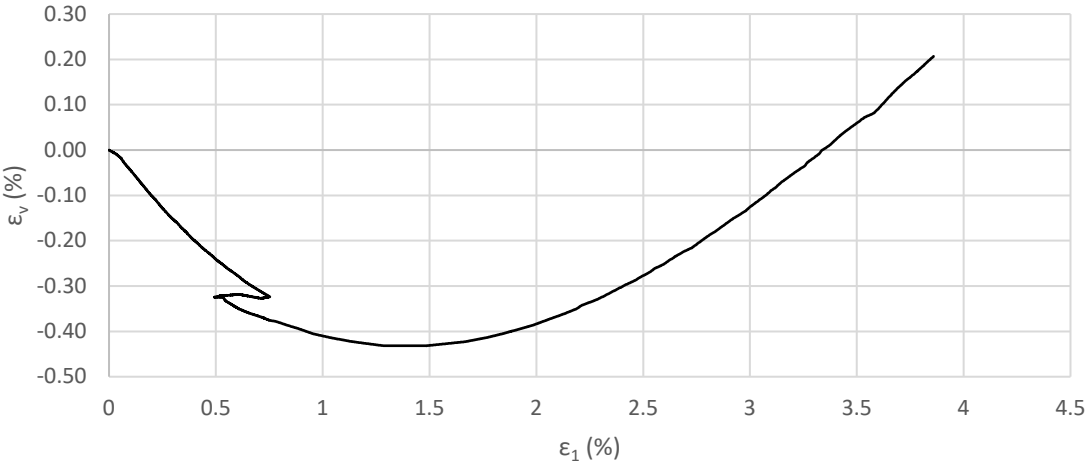

Figure 37. Volume change measurement

7.4 Oedometer and Direct Shear Tests

7.4.1 Device Description

The 305MM with 12" x 12” square direct shear box was specifically designed for testing large soil sample sizes with soil and geosynthetics for evaluating the interface coefficient of friction. It could

also be used in testing: soil to soil, soil to geosynthetic, geosynthetic to geosynthetic, and GCL to GCL (geosynthetic clay liner).

The device utilizes the Karol Warner “CONBEL” concept for the consolidation loading of the sample. One of two pneumatic pistons provides a vertical load on the sample, and this concept increases the accuracy and sensitivity of light load settings. A small diameter rolling diaphragm piston is capable of applying light loads to 454 kg (1,000 lbs) and larger piston applies loads up to 45 kN (10,000 lbs).

The machine and compaction table is easy to move in the lab. The machine and the compaction table are designed with the same height to give the operator a convenient level for setting up, operating the machine, transferring the sample from the compaction table, and making the sample easy to prepare in the shear rings. Installing and removing the rings from the water chamber and the compaction table are easy to handle.

Applying the vertical load is accomplished by setting the precision regulator to the required pressure per the pressure to load the calibration chart. A pressure readout that reads to two decimal places and is accurate to 0.25% to verify load settings. The digital thumb wheels on the control panel are used to set a constant rate of displacement for the horizontal shear rate. Limit switches control the home position and limit the travel to 102 mm (4.0"). The limit switches are located on the control cabinet.

Linear displacement transducers measure and the digital readout displays the consolidation and shear displacements along with shear load from the load cell attached to the water chamber. Data is via an RS232 Serial Port in ASCII format output to the computer and can be exported to spreadsheet programs like “Excel”. Viewing of displays is not dependent on a computer hookup and readout is capable of showing a peak shear load.

The direct shear is designed for harsh lab environments with all steel parts are powder coated and aluminum parts are hard coat anodized for corrosion resistance. Several parts of the device are made from stainless steel.

Figure 38. Direct shear test device

SPECIFICATIONS

Machine Dimensions: 58.4 cm x 109 cm x 102 cm high (23" x 43" x 40" high)

Compaction Table Dimensions: 356 mm x 508 mm x 551 mm high (14” x 20” x 21.69” high)

Power: 110 Volts 60 Hz - 220-240 Volts 50 Hz

Net Weight: 381 kg (840 lbs)

Shipping Weight: 465 kg (1,025 lbs)

Shear Box

- Top 100 mm deep x 305 mm sq (3.97" x 12" sq), area = 929 cm (144” sq)

- Bottom 305 mm x 406 mm x 100 mm deep

(12" x 16" x 3.97” deep)

Easy-access water chamber Aluminum with hard coat anodize finish with water control valves

Horizontal and Vertical Load 45 kN (10,000 lbs)

Consolidation Loading Pistons (2) 4 kN & 45 kN (809 lb & 10,000 lb) capacity

Four-Channel Readout With RS232 output

Displays - Pressure for setting consolidation load

- Horizontal Load

- Horizontal Displacement

- Vertical Displacement

RS 232 Serial Output - ASCI Format Cable included

Get Data Software Export of data into “Excel” in computer

Horizontal Load Cell 45 kN (10,000 lbs)

Vertical Displacement Transducer: 50 mm (2.0")

Horizontal Displacement Transducer: 100 mm (4")

Geosynthetic Platform: 303 mm x 405 mm x 100 mm H (11.94" x 15.94" x 3.94")

100 mm (4.0") sq Filler Block 100 mm sq x 304 mm long (4.0" sq x 11.95")

Air Pressure Required 827 kPa (120 psi) for max sample load of 45 kN (10,000 lbs)

Horizontal Strain Rate: 0.0508 mm to 5.08 mm/min (0.002" to 0.20”/min).

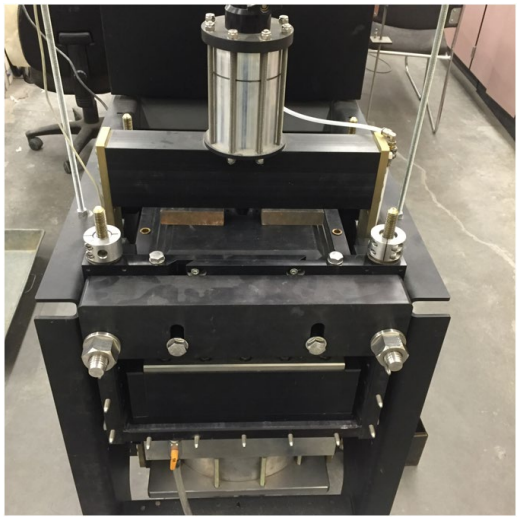

Figure 39. Loading system of direct shear box

7.4.2 Oedometer Tests

Direct shear device is used for one-dimensional compression test. Three samples of 12"x12"x7.94” was compressed under vertical load. The relationship between vertical pressure and vertical strain are shown in Fig. 40. From the curves, constraint moduli are computed and shown in Fig. 41.

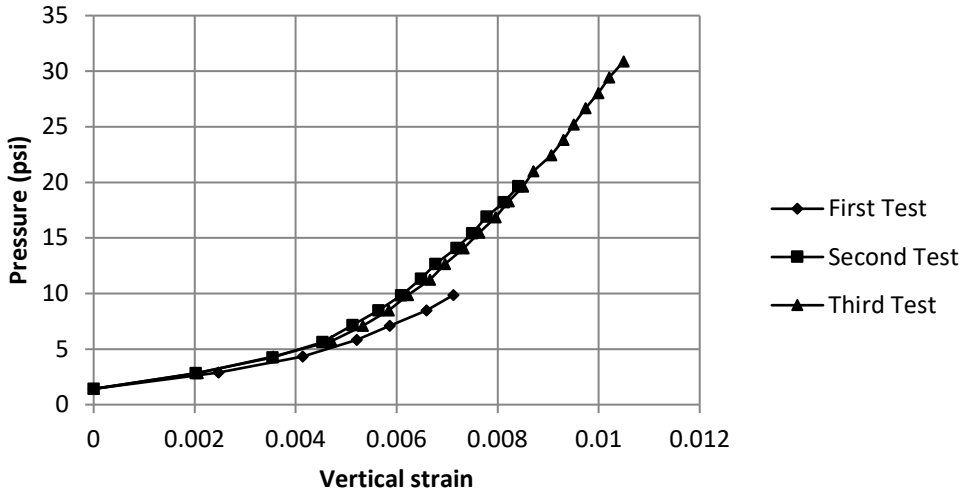

Figure 40. Oedometer tests

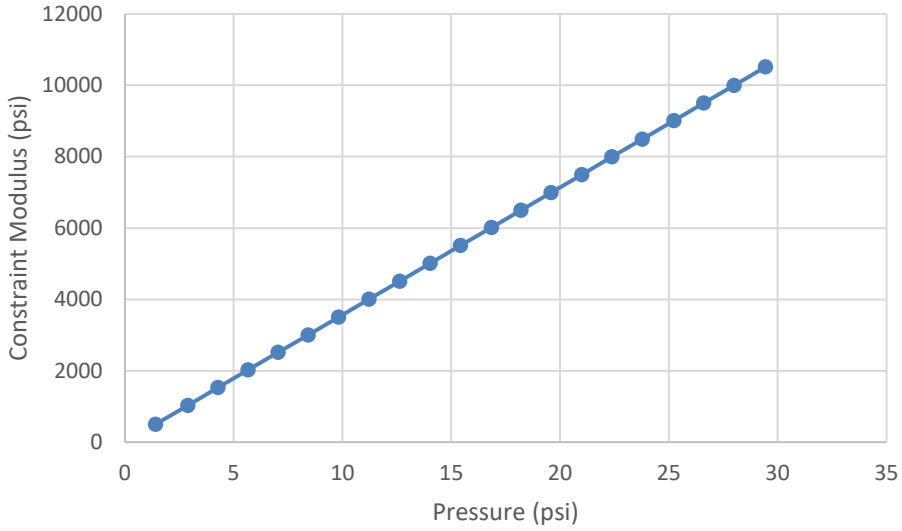

Figure 41. Constraint moduli

7.4.3 Direct Shear Tests

Three direct shear tests at different normal stresses were conducted to determine the shear strength of the soil. Soil sample after shearing is shown in Fig. 42. Shear stress-displacement curves are shown in Fig. 43 and vertical displacements and horizontal displacements curves are shown in Fig. 44.

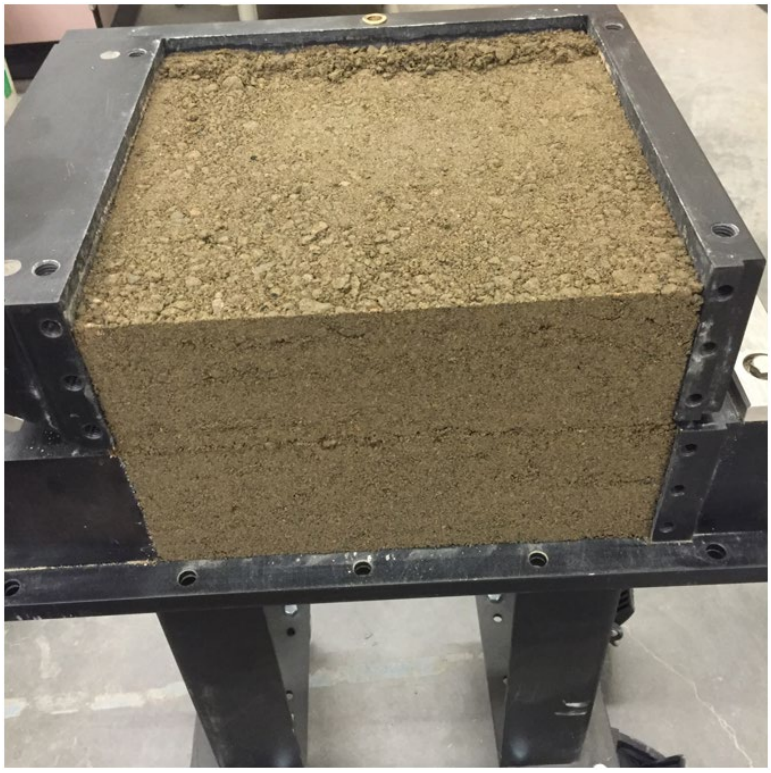

Figure 42. Soil sample after shearing

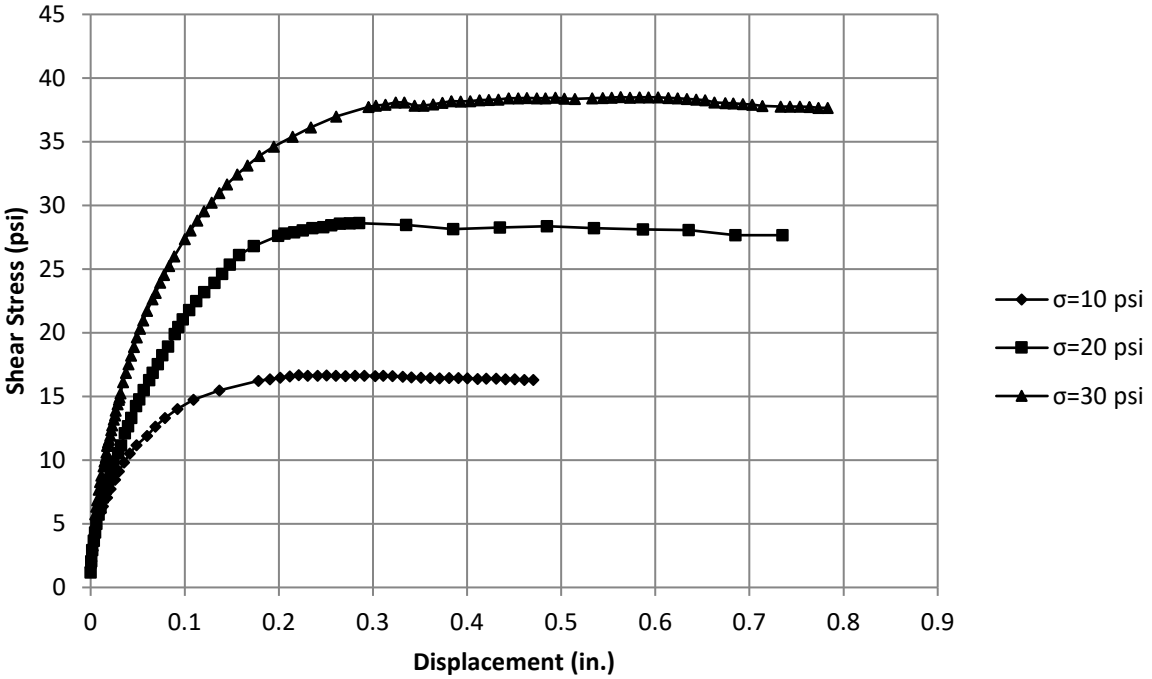

Figure 43. Shear stress and displacement curves

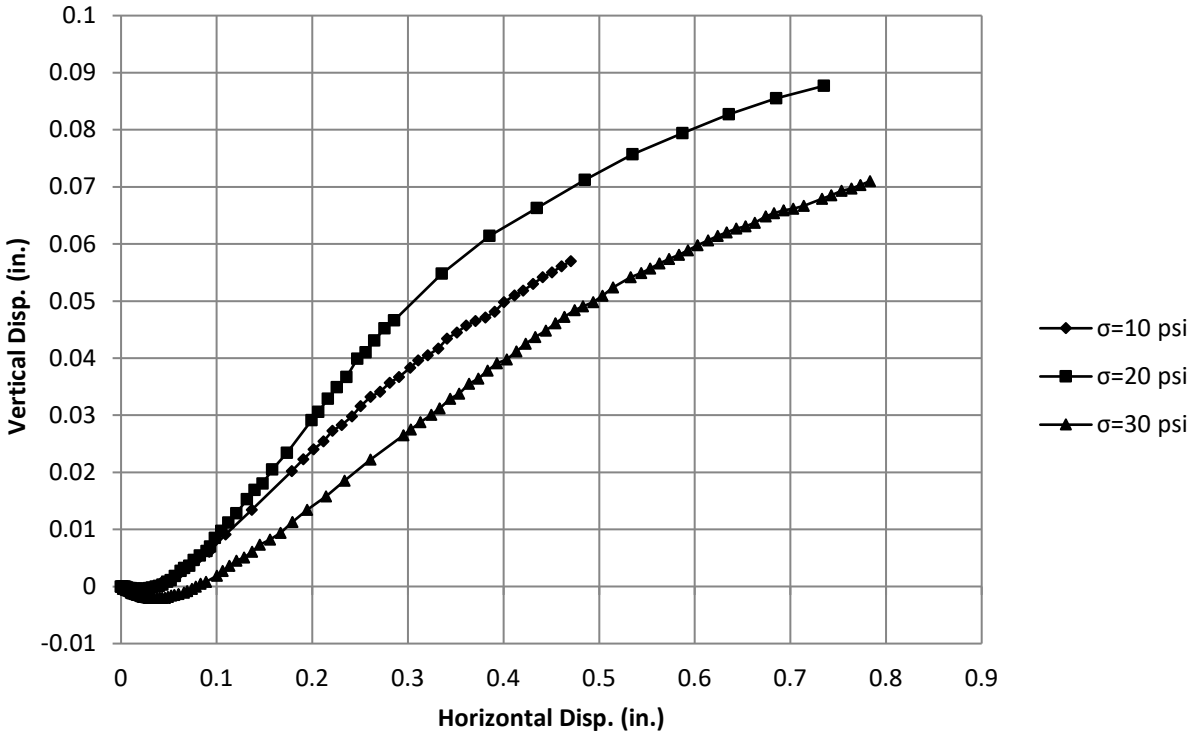

Figure 44. Vertical displacement and horizontal displacement curves

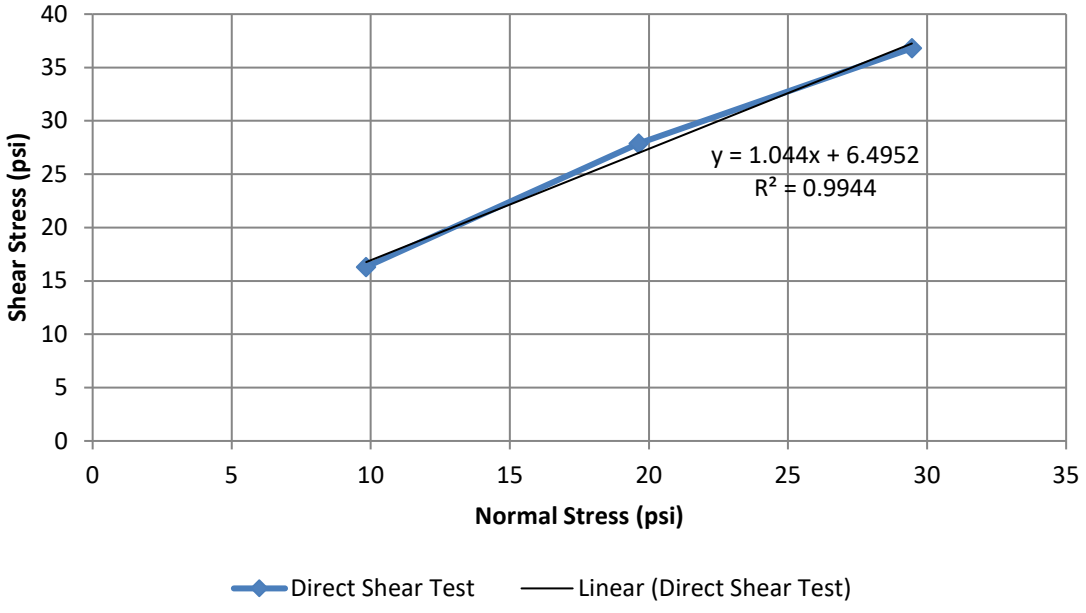

Figure 45. Determination of shear strengths

Using the Mohr-Coulomb criterion, $\tau = \sigma \tan \varphi + c$, friction angle and cohesion from these tests are calculated as shown in Fig. 45.

Soil strength properties are shown in Table 10 as below:

Table 10: Friction angle and cohesion from direct shear tests

Properties	Units	Value
Friction angle, ϕ	(^{0})	45
Cohesion, c	(psi)	6.49

7.4.4 Interface between Soil and Geosynthetic

The direct shear device was also used to determine friction angle and cohesion of the interface between soil and geosynthetic. Figure 46 shows the failure line between soil and geosynthetic after a test. Test results are shown in Fig. 47 to Fig. 48.

Figure 46. Backfill with geosynthetic inclusion after shearing

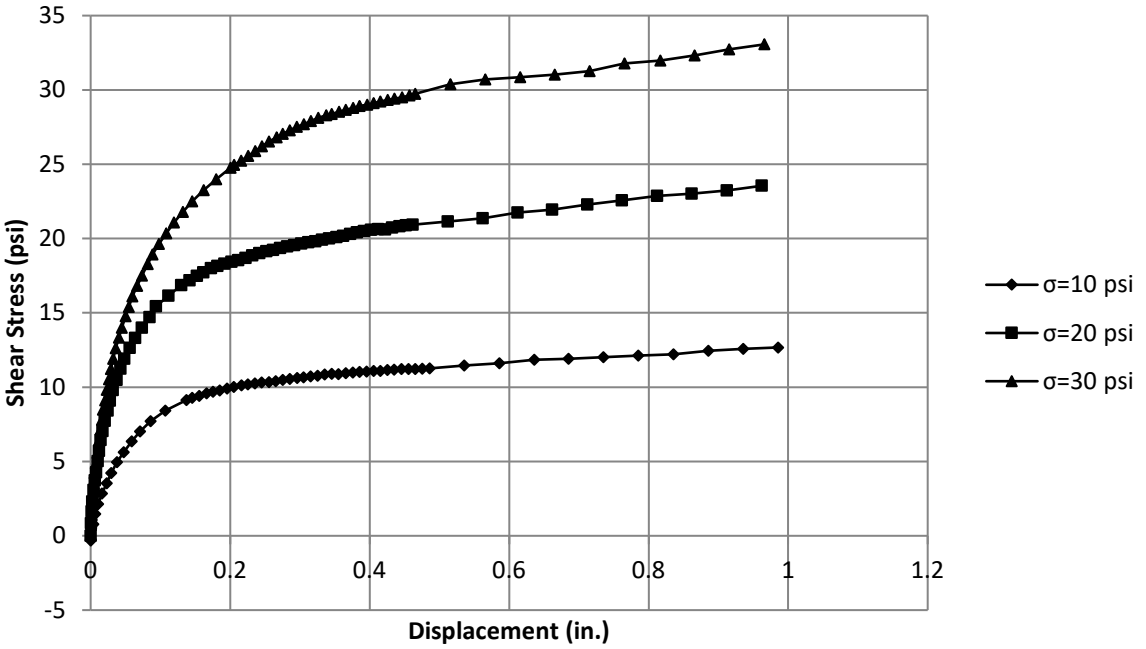

Figure 47. Shear stress and displacement curves for the backfill

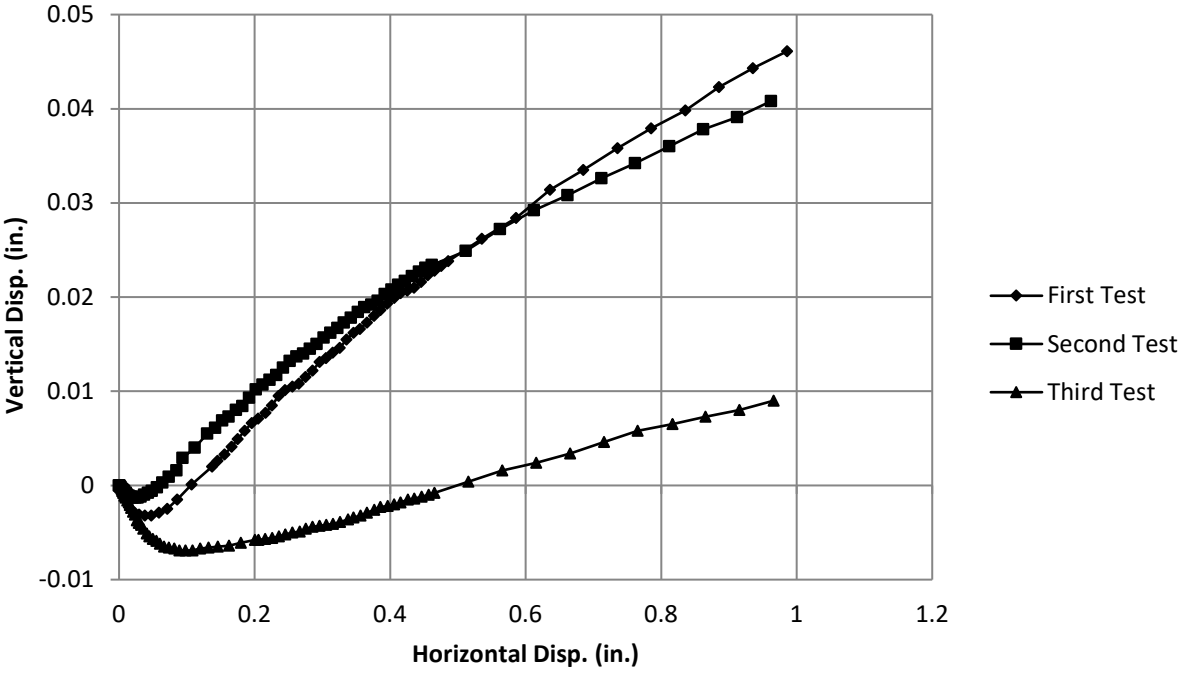

Figure 48. Vertical displacement and horizontal displacement curves

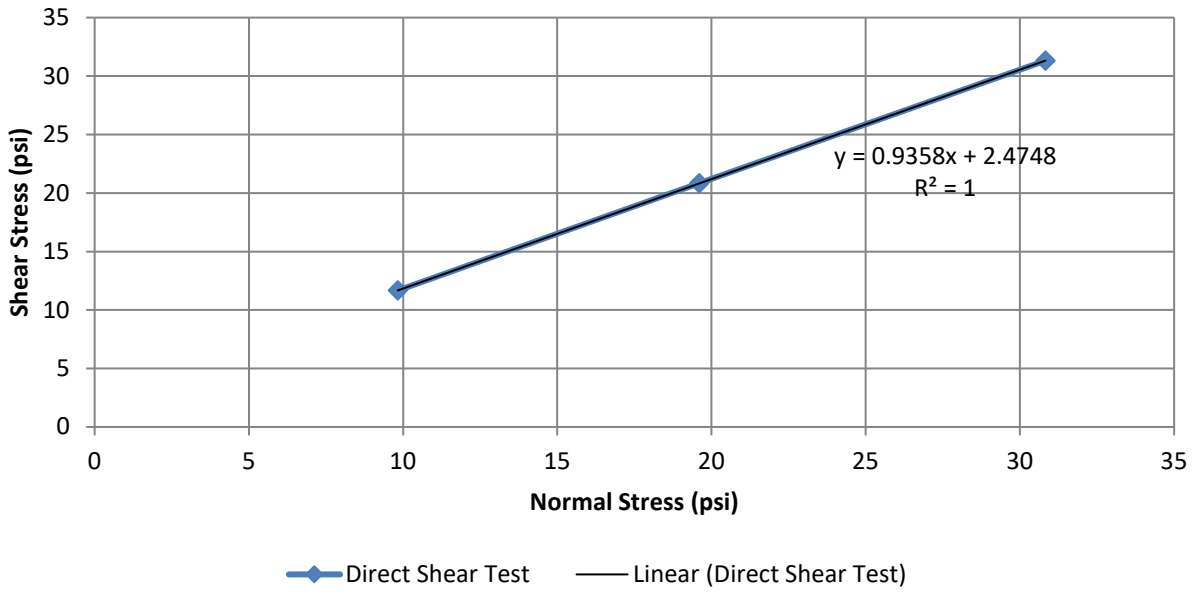

Figure 49. Interface shear strengths

The friction angle, cohesion, and dilatancy angle are computed from these tests for the interface by using the same method for the backfill soil, as shown in Fig. 49 and also shown in Table 11 as below:

Table 11: Friction angle and cohesion of soil and geosynthetic interface from direct shear tests

Properties	Units	Value
Friction angle, ϕ	(^{0})	43
Cohesion, c	(psi)	2.47

As can be seen, the frictional angle and cohesion of soil and soil-geosynthetic differ insignificantly.

7.4.5 Index Property Tests and Density-Moisture Relationship

Index properties and density-moisture relation of the backfill were also evaluated via corresponding tests, and their results are:

1) **S**pecific gravity test gave the specific gravity value of 2.80,
2) Gradation analysis gave the following results: D_{60} = 3.64 mm, D_{30} = 1.05mm, D_{10} = 0.16 mm, Cu = 22.75 and Cc = 1.86.
3) Both Standard Proctor Compaction and Modified Proctor Compaction tests were performed and their results are:

a. Standard Proctor Compaction Test: maximum dry density, γ_{dmax} = 131.5 pcf and Optimum moisture content, ω_{opt} = 10%
b. Modified Proctor Compaction Test: maximum dry density, γ_{dmax} = 142 pcf and optimum moisture content, ω_{opt} = 6.5%

Details of the above tests are given in Appendix A.

8. FINITE ELEMENT ANALYSIS OF GRS ABUTMENT #4

8.1 CDOT Finite Element Analysis Requirements for #4 Abutment

The CDOT Bridge Branch specifically requested the implementation of the following requirements in the finite element modeling:

1. The modeling and dimension shall include sheet pile and of the tip of sheet pile (bottom of the FEM boundary),
2. Deadman tied back sheet pile shall also be modeled with tied rod,
3. The dimension directly below the centerline of sleeper slab shall be representative,
4. Instead of one step or several cut steps, a neat 2(H) to 1(V) cut slope shall be extended to the right side boundary,
5. Reinforcing zone shall extend to the right-most boundary,
6. 3-inch polystyrene behind the abutment back wall shall be included in the modeling as an alternate detail,
7. Boring logs shall be included and simplified under the GRS backfill zone.

8.2 Finite Element Analysis Program Development

8.2.1 Introduction

To investigate the GRS Abutment Performance requires a comprehensive numerical analysis program to simulate and cross-check the measured field abutment performance to assure the accurate computation results and field measurements. A general-purpose computer software, SSI2D, was selected to serve the purpose. Dr. Hien Nghiem at the CGES, when working toward his doctoral degree at the University of Colorado Denver developed SSI2D. The program was further enhanced after joining the Hanoi Architectural University and tested in the recent analyses of the performance of truncated base MSE walls with the final report to be submitted to CDOT shortly. This program will be further tested for their effectiveness in finite element analyses of GRS/MSE walls and abutments. The calibration of SSI2D showed it to be an effective numerical

modeling computer code for this study.

8.2.2 Soil Model

Triaxial and direct shear test results show that this soil is highly dilative and the geologic cap model may not be the most suitable soil model for simulating its dilation behavior and the modified hyperbolic model is adopted, instead. The Duncan and Chang model (Duncan and Chang, 1970) represented the nonlinear stress-strain curve as a hyperbola in the shear stress, $\sigma_1 - \sigma_3$, versus axial strain space as shown in Fig. 50. The hyperbolic relationship between stress and strain can be written as the following equation:

$$\left(\sigma_1 - \sigma_3\right) = \frac{\varepsilon_1}{a + b\varepsilon_1} \tag{1}$$

where a and b are related to the initial tangent modulus and asymptotic deviator stress:

$$E_i = \frac{1}{a};\ \left(\sigma_1 - \sigma_3\right)_{ult} = \frac{1}{b} \tag{2}$$

where E_i is initial tangent modulus as a function of confining stress, σ_3.

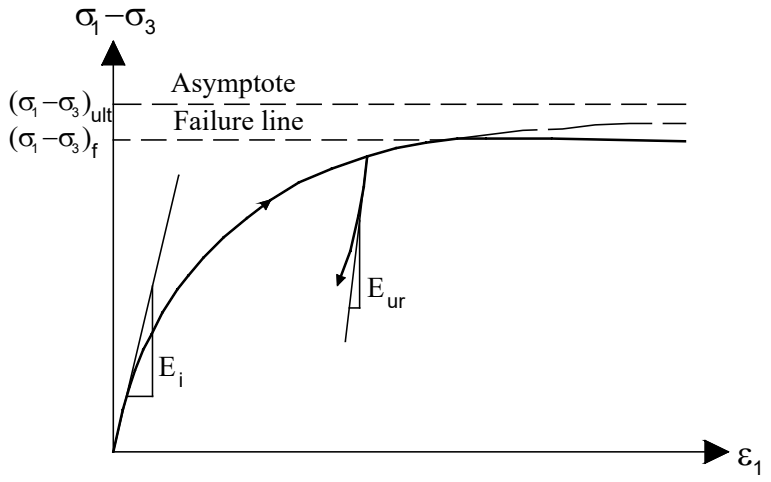

Figure 50. Nonlinear stress-strain behavior

The ultimate shear stress, $\left(\sigma_1 - \sigma_3\right)_{ult}$ related to shear stress at the failure of the Mohr-Coulomb criterion by model parameter, R_f. The following equation determines the value of failure ratio R_f for each of the tests:

$$R_f = \frac{\left(\sigma_1 - \sigma_3\right)_f}{\left(\sigma_1 - \sigma_3\right)_{ult}} \tag{3}$$

where $(\sigma_1 - \sigma_3)_f$ is deviator stress at failure determined from the stress-strain plots of the tests. Typical values of R_f range from 0.5 to 0.9 for most soil (Duncan et al., 1980). The modified hyperbolic model adopted the Mohr-Coulomb failure surface. The failure occurs when the state of shear stress, τ, and the normal stress, σ, on any surface in the material, satisfy the equation below:

$$|\tau| + \sigma \tan\varphi - c = 0 \tag{4}$$

where φ and c denote the friction angle and cohesion of soils.

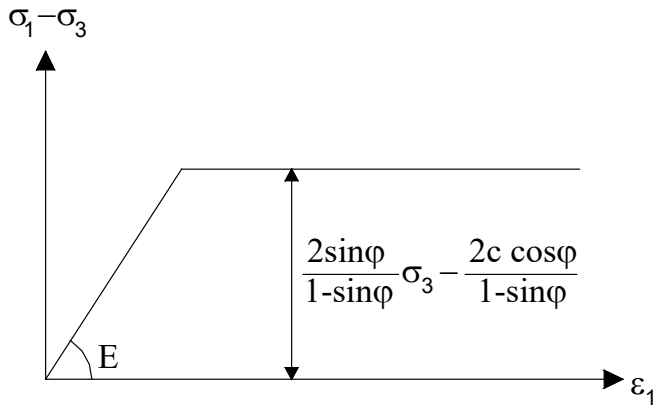

Figure 51. Mohr-Coulomb failure criteria

The Mohr-Coulomb criterion as shown in Fig. 51 can be written in terms of principle stresses as follow:

$$-\frac{1}{2}(\sigma_1 - \sigma_3) = -\frac{1}{2}(\sigma_1 + \sigma_3)\sin\varphi + c\cos\varphi \tag{5}$$

The full Mohr-Coulomb yield criterion takes the form of a hexagonal cone in principal stress space as shown in Fig 52. Main stress can be related to invariant stresses as:

$$(\sigma_1 - \sigma_3) = \frac{2}{\sqrt{3}}\sqrt{J_2}\left(\sin\left(\theta - \frac{2\pi}{3}\right) - \sin\left(\theta + \frac{2\pi}{3}\right)\right) = -2\sqrt{J_2}\cos\theta \tag{6}$$

$$(\sigma_1 + \sigma_3) = \frac{2}{\sqrt{3}}\sqrt{J_2}\left(\sin\left(\theta - \frac{2\pi}{3}\right) + \sin\left(\theta + \frac{2\pi}{3}\right)\right) + \frac{I_1}{3} = -\frac{2}{\sqrt{3}}\sqrt{J_2}\sin\theta + \frac{2I_1}{3} \tag{7}$$

Substitute Eqs. (6) and (7) to Eq. (5), and failure criterion can be written in invariant shown as following (Smith and Griffiths, 1997):

$$f_1 = \frac{I_1}{3}\sin\varphi - \sqrt{\frac{J_2}{3}}\sin\theta\sin\varphi + \sqrt{J_2}\cos\theta - c\cos\varphi \tag{8}$$

where θ is the Lode angle.

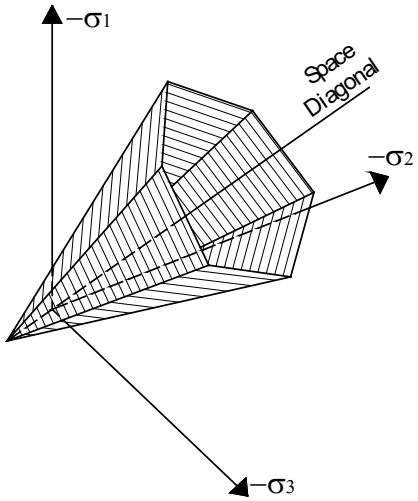

Figure 52. Mohr-Coulomb failure criteria in principal stress space

In this plastic behavior of soil, unassociated flow rule is followed and the potential function has the same form as the associated yield function and is defined for the Mohr-Coulomb model by replacing friction angle φ by dilation angle ψ in the yield function. The potential function is given by:

$$g_1 = \frac{I_1}{3}\sin\psi - \sqrt{\frac{J_2}{3}}\sin\theta\sin\psi + \sqrt{J_2}\cos\theta - c\cos\psi \qquad (9)$$

The dilatancy angle, ψ, is requires to model positive plastic volumetric strain increments as actually observed for dense soils. Soil starts to dilate when the stress state reaches the Mohr-Coulomb failure surface.

In reality, soil can sustain none or small tensile stress. This behavior can be specified as a tension cut-off. The functions of tension cut-off (which is related to maximum principal stress) are:

$$f_2 = \sigma_3 - T \qquad (10)$$

where T is maximum tensile stress. For these three yield functions, an associated flow rule is adopted.

Yield and cap surfaces for modified hyperbolic model are shown in Fig. 53 and Fig. 54. Parameters for this model are shown in Table 12.

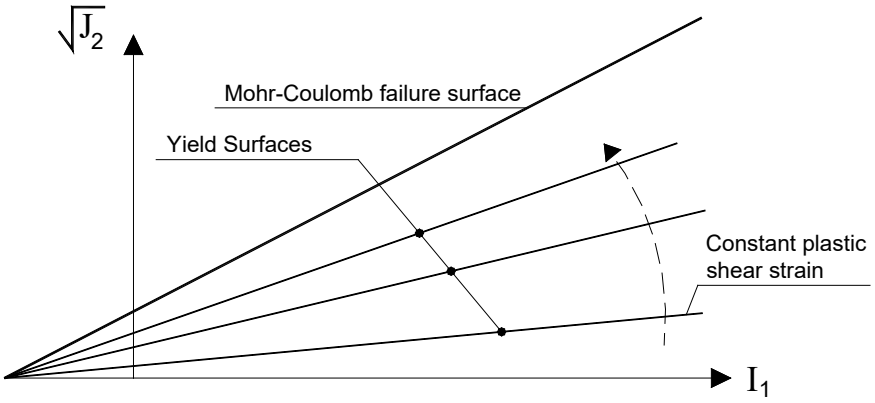

Figure 53. Yield surface of modified hyperbolic model

The plastic volume strain measured in the hydrostatic compression test is not explained in shear hardening yield surfaces as in Fig. 53. It requires a second yield surface, cap yield surface, to explain the contractive soil behavior. This cap yield surface is defined as:

$$f_c = 4J_2\left(\cos\theta - \sqrt{\frac{1}{3}}\sin\theta\sin\varphi\right)^2 + \left(2\frac{I_1}{3} - c\cot\varphi - \frac{I_{1c}}{3}\right)^2 - \left(c\cos\varphi - \frac{I_{1c}}{3}\sin\varphi\right)^2 \qquad (11)$$

The hardening law relating I_{1c} to plastic volumetric strain is:

$$d\varepsilon_v^p = -\kappa\frac{dI_{1c}}{I_{1c}} \text{ or } \varepsilon_v^p = -\kappa\ln\left(\left|\frac{I_{1c}}{3}\right|\right) \qquad (12)$$

Table 12: Parameters of the modified hyperbolic model

Parameter	Description
K_L	Loading modulus number
K_{ur}	Unloading-reloading modulus number
n_L	Exponent for defining the influence of the confining pressure
n_{ur}	Exponent for defining the influence of the confining pressure
R_f	Ratio between the asymptote to the hyperbolic curve and the maximum shear strength
c	Cohesion
φ	Friction angle
ψ	Dilatancy angle
OCR	Over-consolidation ratio
κ	Cap surface parameter

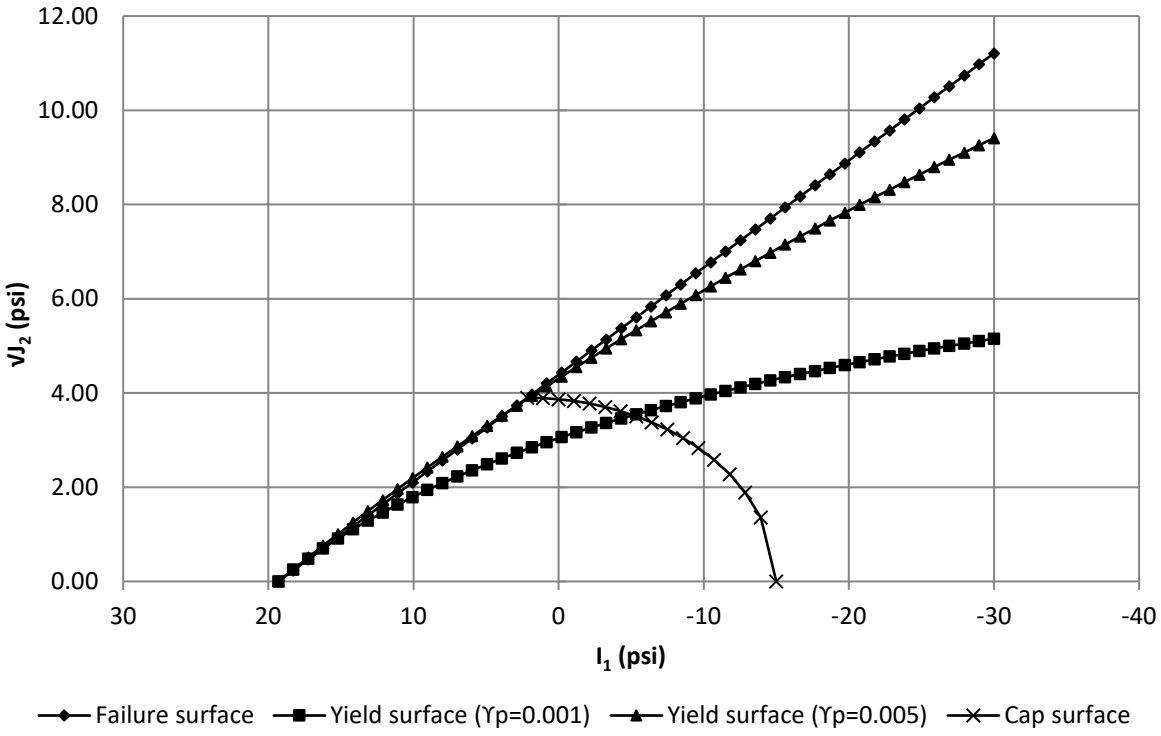

Figure 54. Yield, cap and failure surfaces

8.3 Model Geometry and Boundary Conditions

The GRS bridge abutment was modeled in plane strain condition with a thickness of one meter. In the FE model, soil areas were discretized by 6-node plane-strain elements to describe the stress-strain behavior. The default 6-node plane element uses three integration points.

The interface specified in this study was modeled by 4-node interface elements. Interfaces, the same as those observed in the physical structure, were specified between two distinct materials in the FE model. Since geosynthetic reinforcements were simulated by bar elements, interface elements are connected on the top and the bottom of bar elements.

In the GRS bridge abutment, steel sheet piles are utilized as the facing element and the anchored deadman. In 2-D analysis, the sheet pile and deadman are modeled by two-node beam elements. In the FE mesh, beam elements connect two nodes on a side of an interface or plane elements.

In the tie rod, when only axial forces prevail, then, a bar element is used to simulate its behavior. It is also assumed that no contact exists between the tie rod and the surrounding soil. It is also assumed that the boundary deformation is negligible. Figure 56 shows the FE mesh for the GRS-IBS Abutment #4 of the unique CDOT Region 1 Twin Bridge over the Smith Road and Union Pacific Rail Road (UPRR) on I-70. A fine mesh is used for the area below the abutment because of concentrated pressures.

The boundary conditions specified in the FE model are shown in Fig. 56. The FE model was fixed at the base both in the horizontal and vertical directions (i.e., X- and Y-directions). The front and back ends of the model were constrained in the horizontal direction (X-direction) but were free to move in the vertical direction (Y-direction).

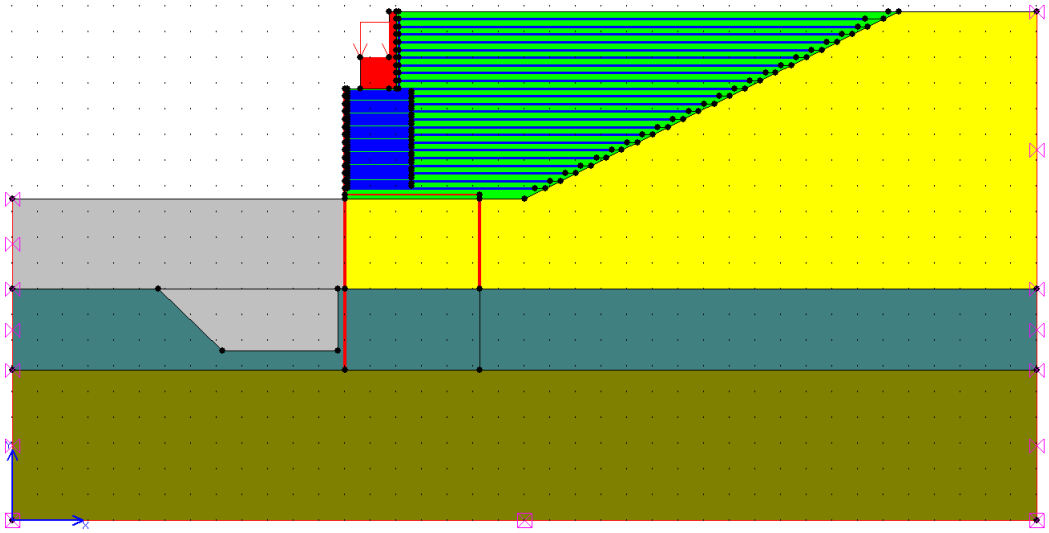

Figure 55. Model geometry

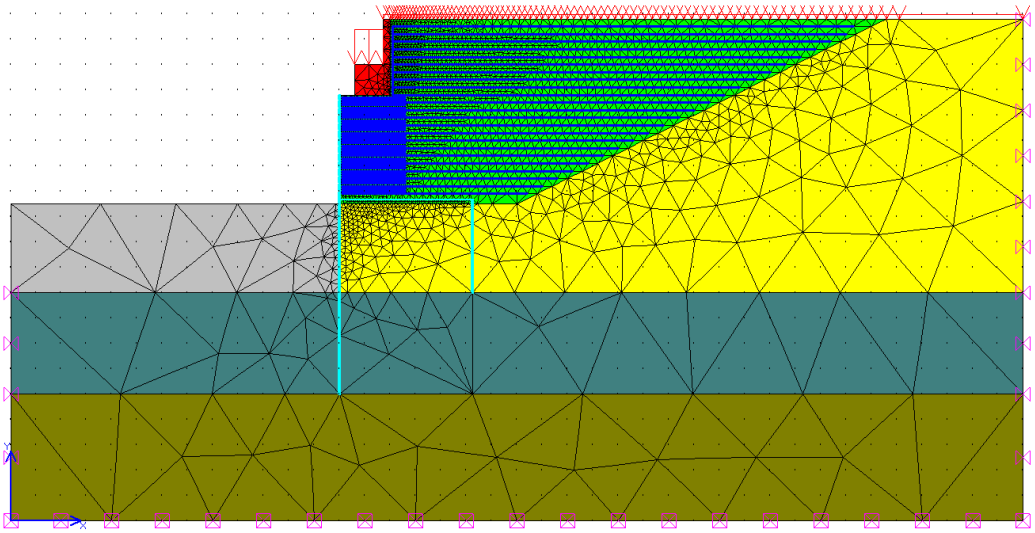

Figure 56. Element mesh

8.4 Model Materials and Properties

Constitutive model parameters are required for the following materials: (1) concrete for the bridge sill structure and slabs, (2) steel for the sheet pile facing, tie rod, and deadman, (3) geosynthetic reinforcement, (4) backfill, and (5) foundation and backfill clay soil. Concrete and steel were modeled as linear elastic materials.

Soil

Properties of backfill were selected from Oedometer tests, triaxial tests and direct shear tests, as presented in Table 8 and 9. A standard penetration test (SPT) was conducted to evaluate the foundation soil properties. The properties of the foundation and backfill clay soil are given in Table 13.

Table 13: Properties of the foundation soil

Soil	Properties	Units	Value
Foundation	Young's Modulus	psi	22000
	Undrained shear strength	psi	22
	Poisson's Ratio (Assumed value)	-	0.4
Backfill Clay	Young's Modulus	psi	5010
	Undrained shear strength	psi	11
	Poisson's Ratio (Assumed value)	-	0.4

Tie rod

The stiffness of the tie rod computed for 5-ft spacing is adjusted for one-meter spacing. This configuration allows the tie rod to be included at the mid-thickness. The circular tie rod of 1.75-inch diameter was modeled as a linear elastic material with the material parameters shown in Table 14.

Table 14: Properties of the tie rod

Diameter (in.)	Young's Modulus (psi)
1.75	29000000

Sheet pile wall

The sheet pile section SKZ-31 was specified in the construction drawing, and the dimensions of the SKZ-31 section are shown in Fig. 57. To simplify the FE model, Z section sheet pile was converted to an equivalent rectangular section. The conversion was achieved by requiring the same section modulus as the Z section. Determination of the equivalent rectangular section is shown in Table 15.

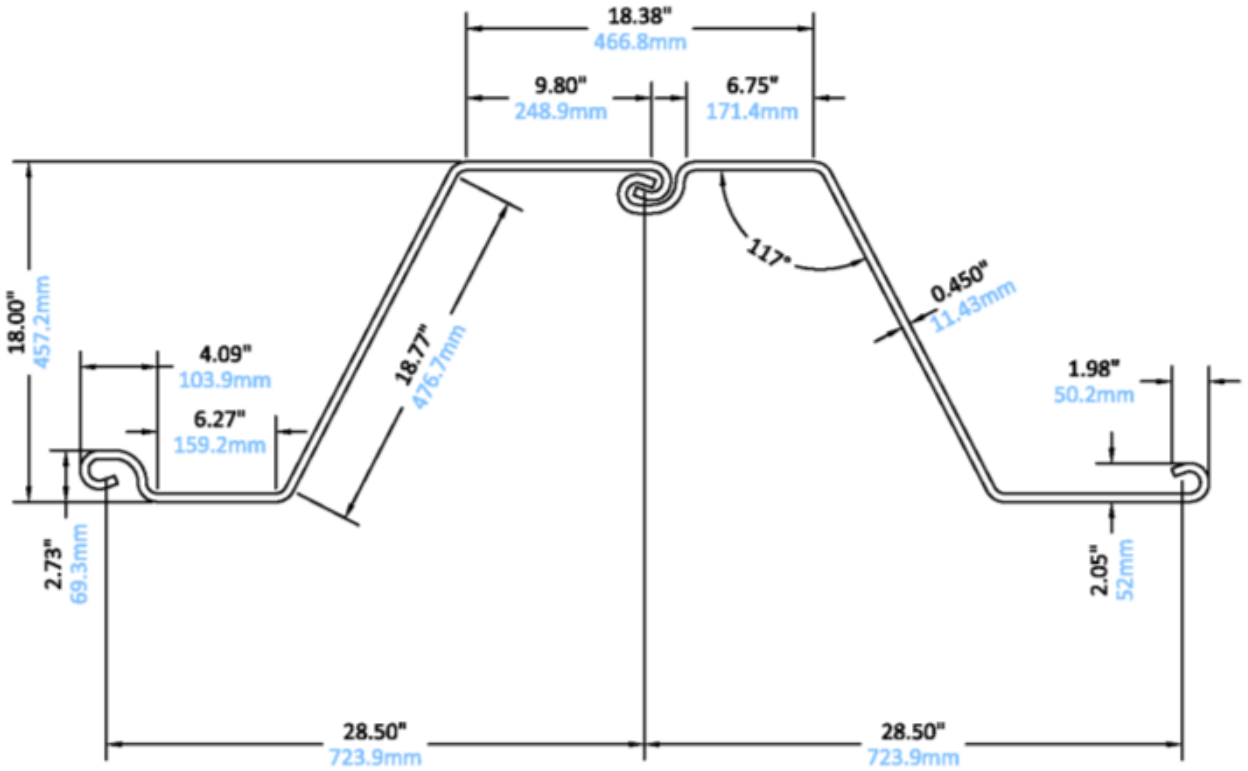

Figure 57. Sheet pile dimensions

Table 15: Sheet pile properties

Width (in)	Height (in)	Thickness (in)	Cross-sectional area (in^2/ft)	Weight		Section modulus		Moment of inertia (in^4/ft)
				Pile (lb/ft)	Wall (lb/ft^2)	Elastic (in^3/ft)	Plastic (in^3/ft)	
28.5	18	0.45	9.07	78.32	31.08	51.56	60.51	464.05

The equivalent thickness and width of the wall is 24.8 in. and 0.37 in., respectively.

Geosynthetic

The geosynthetic reinforcement was modeled as a linear elastic perfectly-plastic material, in which four parameters are required. The linear elastic perfectly-plastic model possesses a bilinear stress-strain curve. Note that the slope of the tensile load-strain curve is the product of modulus (e.g., Young's modulus E or tangent modulus E_t) and thickness of the geosynthetic. The tensile load is typically expressed in units of force per unit width of the reinforcement. Inversely, the modulus

was calculated by dividing the slope of the tensile load-strain curve by the geosynthetic thickness. Similarly, the yield stress f_y for the bilinear model was found by dividing the yield tensile load by the thickness of the geosynthetic.

The model parameters assumed for the geosynthetic reinforcement are presented in Table 7. A geosynthetic reinforcement manufactured by Tensar Corporation (i.e., US 4800) will be used in the GRS bridge abutment construction, which has a wide width tensile strength of 4353 lb/ft (or 65 kN/m). According to the assumed load-strain curve, the tensile strength of 4353 lb/ft would occur at a strain of 14%. The geosynthetic reinforcement mesh modeled with two-node tension bar elements. The thickness of geosynthetics was assumed as 0.06 in. or 1.5 mm.

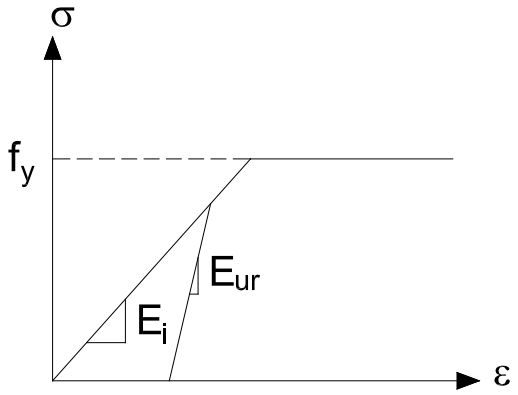

Figure 58. Stress-strain curve for geosynthetic

Interface

The interface is characterized by friction angle φ, cohesion, c, and dilatancy angle ψ. In the FE model, the parameters for all interfaces between soil and geosynthetic are given in Table 11.

8.5 Loadings

In FE model, gravity was simulated as a body load and was applied as self-weight load at every stage of construction. A uniform pressure was applied on the top surface of the sill, Fig. 59, to simulate dead loads applied to the bridge abutment. The uniform pressure is estimated at q = 14 psi, measured pressure from pressure cells, I1-4M-VP and I1-4B-VP. The nonlinear analysis is performed by increasing the pressure step by step from zero to its maximum pressure.

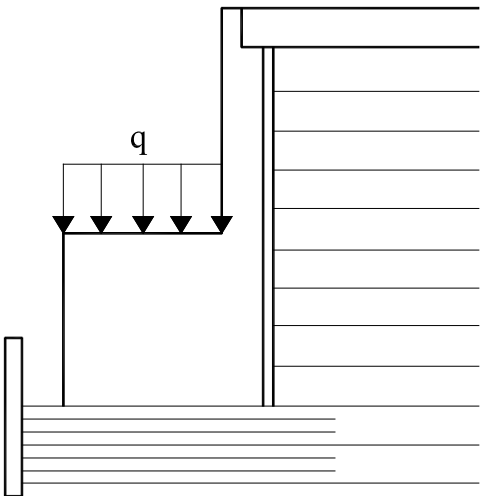

Figure 59. Applied load on abutment

8.6 Field versus FEA Performance Comparison

The GRS-IBS is an innovative technology increasingly adopted in modern-day bridge design in transportation infrastructure construction. It not only is cost and time effective but it also virtually eliminates the bridge bump problems because of its founding on GRS mass and adoption of approach (or sleeper) slap. This is the first GRS-IBS demonstration project with comprehensive instrumentation for the abutment performance monitoring. The Shannon and Wilson, Inc. provided all service on instrumentation program design and implementation with the performance database available 24/7 on the website for access by all interested researchers and practitioners. The FHWA/CDOT funded project serves as an invaluable case study for the GRS-IBS technological development. The CGES at the University of Colorado Denver is honored for the opportunity to participate in this developmental mission. Besides the field monitoring, finite element analyses were also performed as a means of mutual calibration for the validity of the instrumentation program and the finite element analysis software through the comparison of numerical and field measurement results. The major components of the abutment performance monitoring are compared in the following sections.

Earth pressures

Vertical stresses in GRS are measured with earth pressure cells. The results are compared with the finite analysis results in Table 16. As observed, the comparison was very favorable with good agreement. Horizontal earth pressures, Table 17 and Fig. 60, along the back of the sheet pile façade were also measured using earth pressure cells. While the cell number is limited, they do provide precious horizontal earth pressure data during and after construction. Because of the lateral movement of the sheet pile façade, the horizontal earth pressure comparison was not as ideal as shown in Table 16 for vertical earth pressure comparison, Figs. 60 and 61.

Table 16: Vertical pressure

Location	Depth (in)	Measured pressure (psi)			Computed pressure (psi)
		Max.	Min.	Ave.	
I1-1F-VP	168	12	0	6	16
I1-1M-VP	168	35	31	33	20
I1-1B-VP	168	20	18	19	22
I1-2F-VP	108	30	20	25	27
I1-2M-VP	108	22	15	18.5	18
I1-2B-VP	108	28	23	25.5	21
I1-3F-VP	48	22	18	20	29
I1-3M-VP	48	22	15	18.5	16
I1-3B-VP	48	19	15	17	14
I1-4F-VP	0	18	8	13	16
I1-4M-VP	0	17	12	14.5	15
I1-4B-VP	0	15	13	14	16
I1-5-VP	120	13	10	11.5	11
I1-6-VP	72	7	4	5.5	6
I1-7-VP	36	5	3	4	3

Table 17: Horizontal pressure

Location	Depth (in)	Measured pressure (psi)	Computed pressure (psi)
I1-1-HP	162	0-1	2.6
I1-2-HP	102	1.6-4	2.3
I1-3L-HP	42	0-2	1.6
I1-3U-HP	42	0-2.4	1.6
I1-5-HP	114	0	1.6
I1-6-HP	66	0.5-3.5	1.6

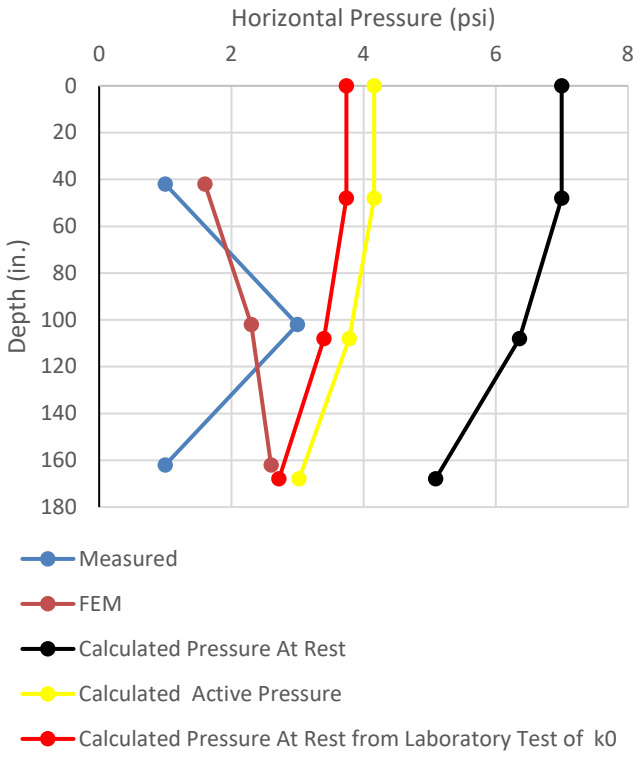

Figure 60 Comparison of final lateral pressure façade at final stage

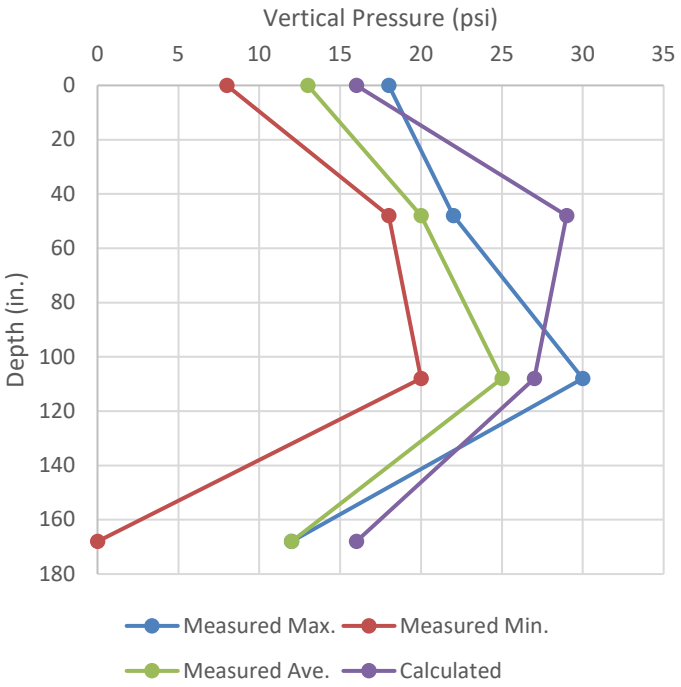

a) Front vertical pressures

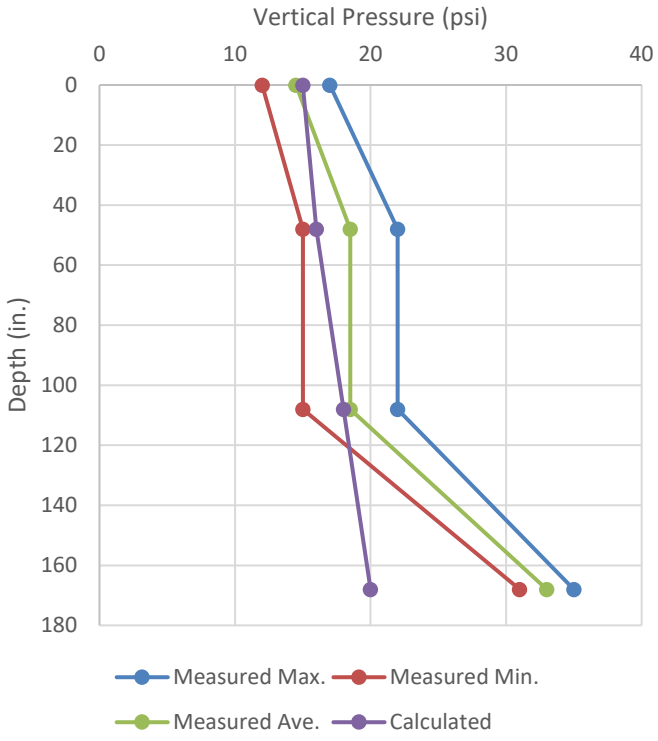

b) Middle vertical pressures

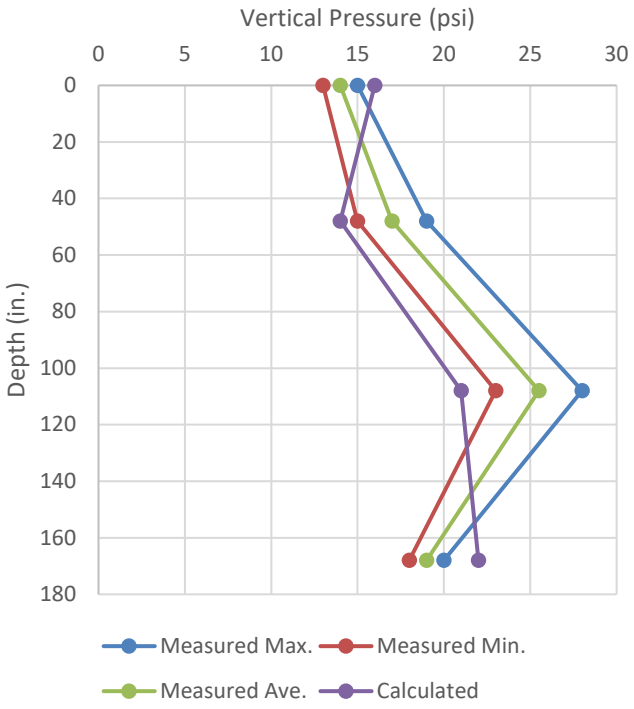

c) Back vertical pressure

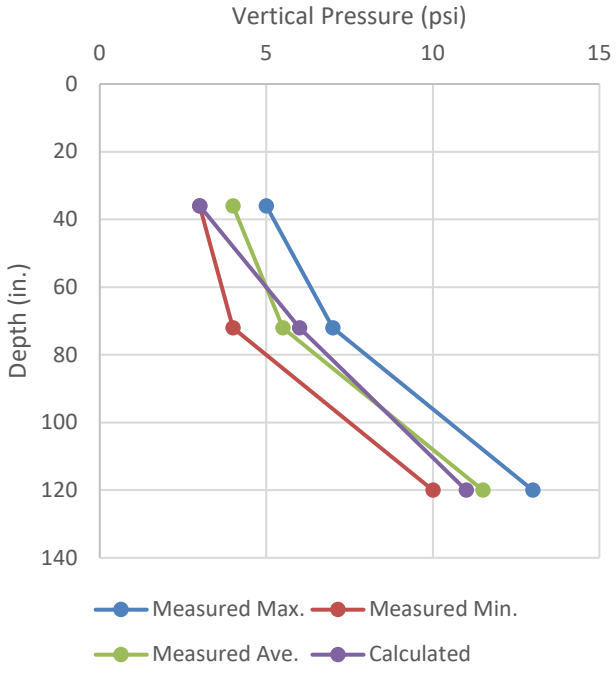

d) Vertical pressures at I1-5-VP, I1-6-VP, and I1-7-VP

Figure 61. Comparison of final vertical earth along the back of pressures along the back of façade

Tensile force in geosynthetics

Optic fiber strain gauges were installed, but the measurement results were not as good as anticipated. The tensile force in the geosynthetics ranges from very small tension to mostly compression, while the finite element analysis results as shown in Fig. 62 are compressive and much more reasonable and acceptable. It is, therefore, recommended to perform a large in-house model test to check proper installation and compaction damage protection before the next full-scale installation.

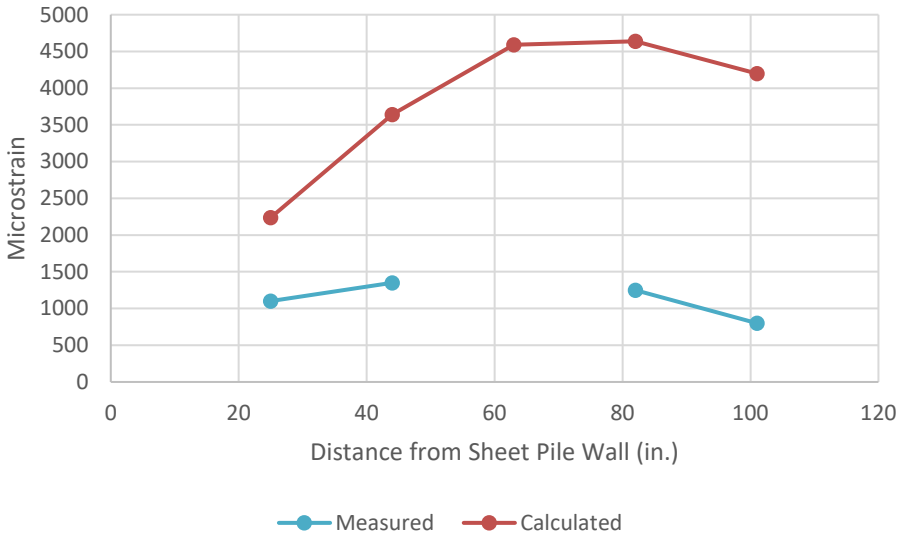

a) Level 1 (4” from the base of excavation)

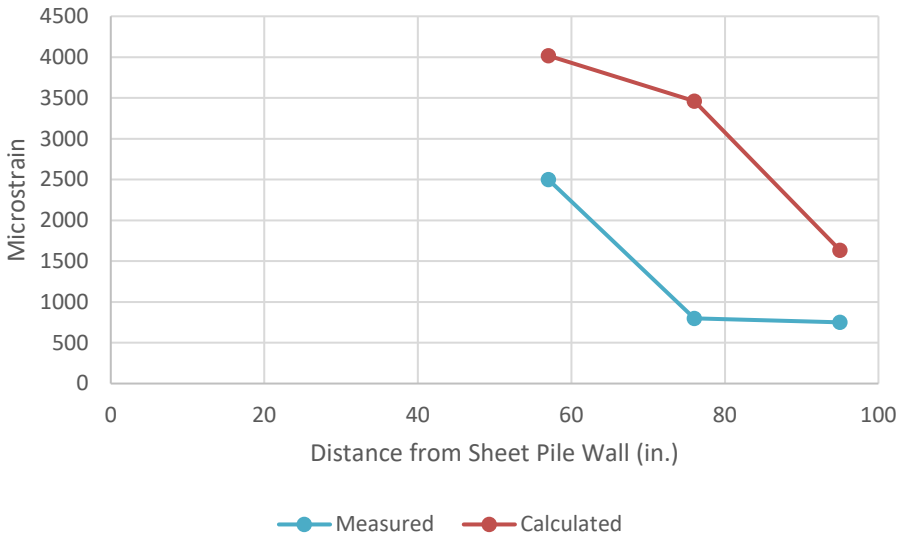

b) Level 3 (10’4” from the base of excavation)

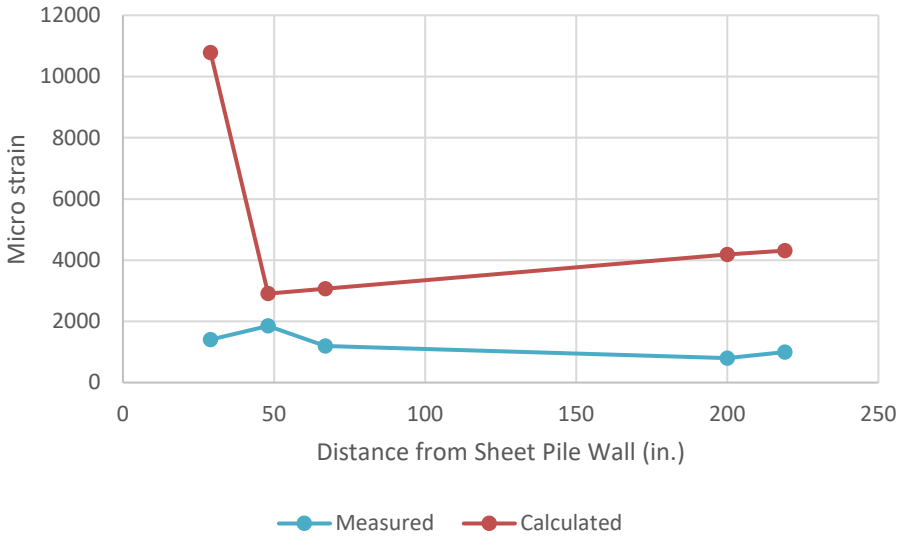

c) Level 4 (12'8" from the base of excavation)

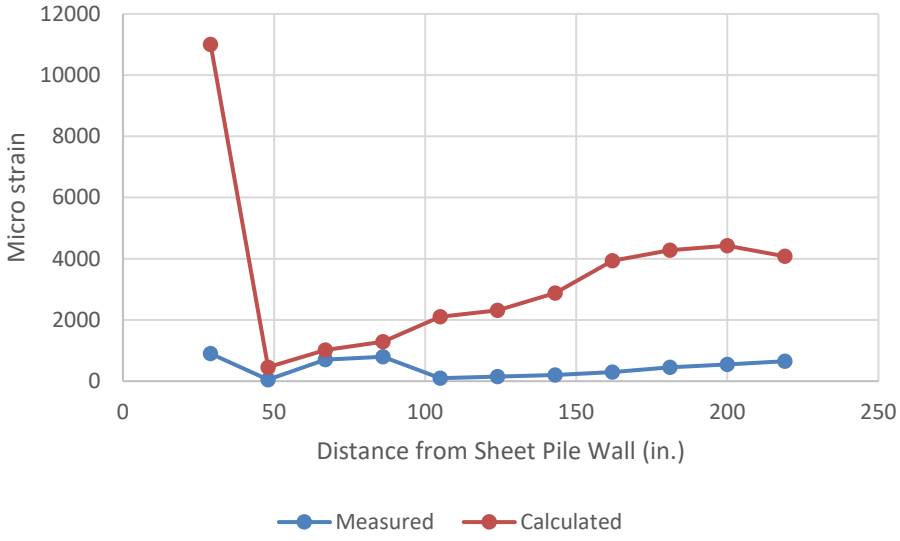

d) Level 5 (14' from the base of excavation)

Figure 62. Comparison of measurement and calculated fiber optic strains

Tieback tension

Steel Sheet pile deadman with 1.75-inch diameter steel tieback at a spacing of 5 feet was installed along the sheet pile façade. Four tiebacks were installed with strain gages to measure tieback tension. All tiebacks were also cased with PVC tubes for corrosion protection. The spacing between the steel tie backs and PVC tubes were cement grouted. This grout hinders the development of tieback tension and further led to the failure of three out of four tiebacks to provide

tensile force data. The tension force in the tieback I2-F-SG, only functional one, is given in Table 18 and the maximum measured tension is 0.0005.

Table 18: Internal forces in the tie-back rod

Stage	Force (lb)	Computed strain	Measured strain
Applying vertical load	31713	0.000455	0.000337
After Excavation	35539	0.000509	0.000500

Displacement of retaining wall

The steel sheet pile wall top displacement was measured at 0.8 inches on October 1, 2015. Upon the 10' x 10' excavation at the base and along the longitudinal direction of the façade, the wall top moved drastically forward toward the rail track south of the façade. Fortunately, upon the emergency call for the backfill of the trench, the wall movement gradually slowed down and crept to 2.0 inches. Figure 65 shows the results of finite element analysis are in close agreement with the field monitored wall movement.

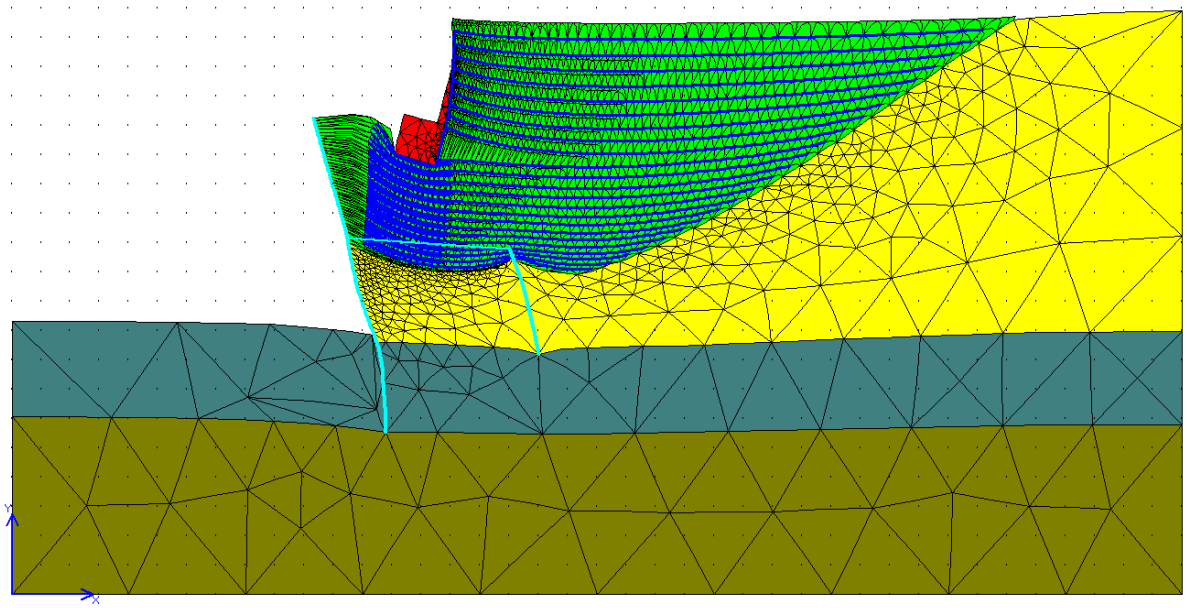

Figure 63. Abutment displacement before excavation

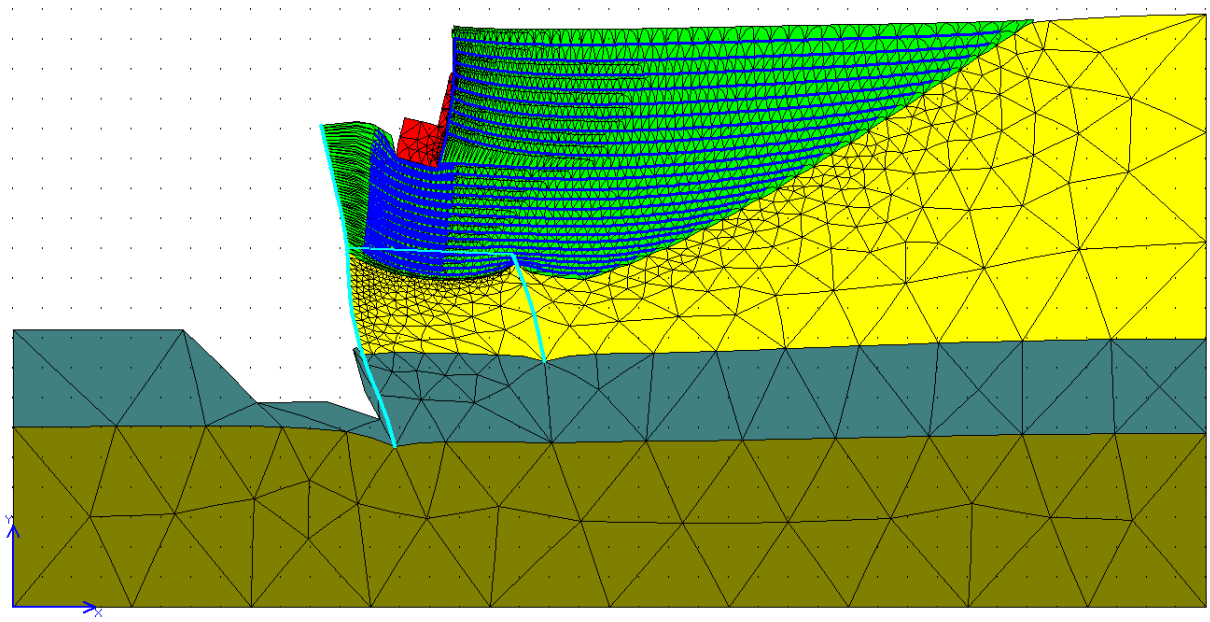

Figure 64. Abutment displacement after excavating

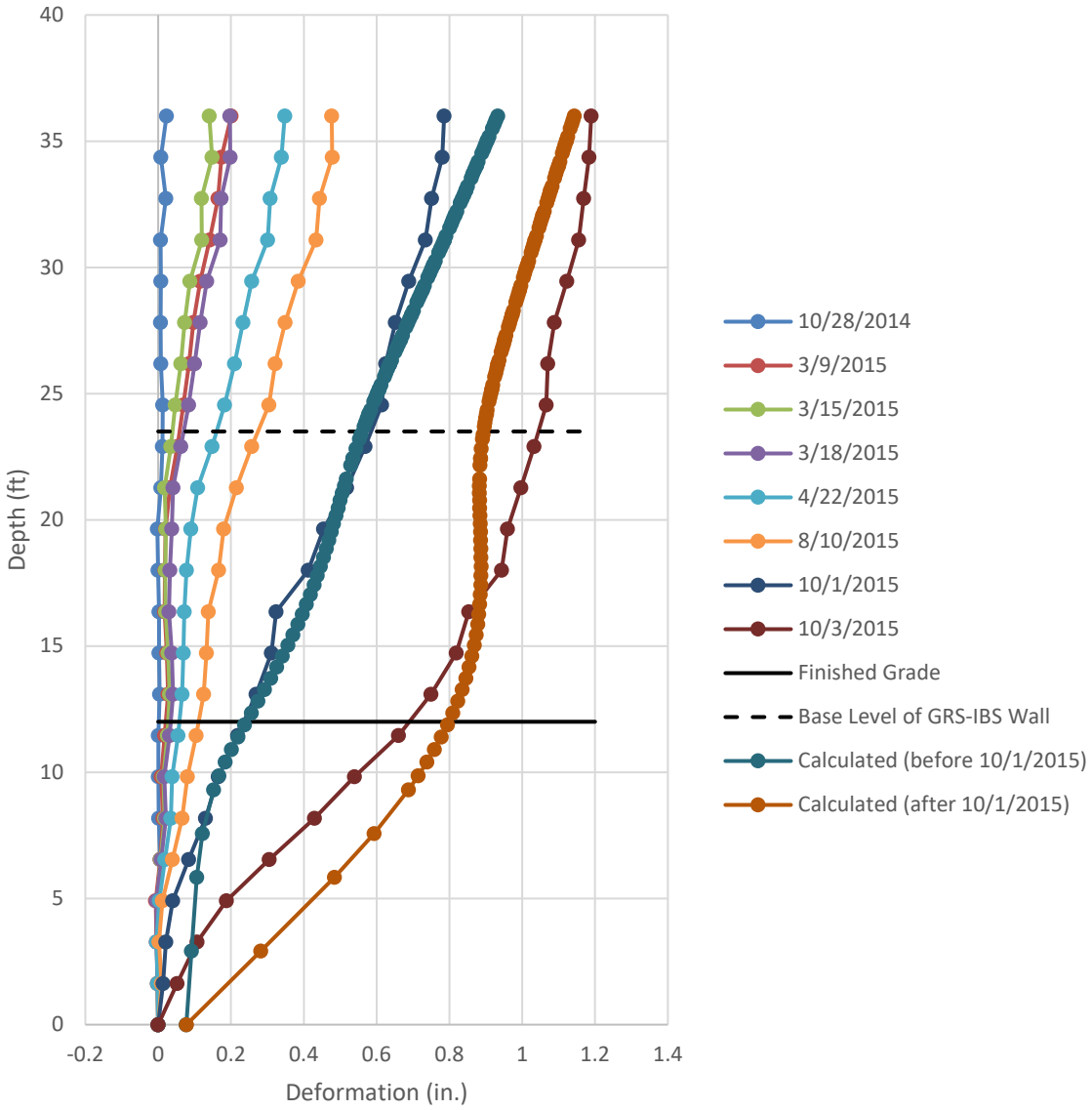

Figure 65 Comparison of wall displacements

9. SUMMARY, CONCLUSIONS, AND RECOMMENDATIONS

9.1 Summary and Conclusions

The CDOT Twin Bridge replacement project over Smith Road and Union Pacific Rail Road (UPRR) on I-70 was selected as the first multi-span GRS-IBS bridge with steel sheet pile façade for comprehensive instrumentation for abutment performance measurements. The field measurements include vertical earth pressure measurement in GRS and horizontal earth pressure measurement on the back of steel sheet pile façade using earth pressure cells, the lateral movement of the façade using SAA (shape acceleration array), tensile force in steel tie rod with strain gages, differential movement between the wall top and sill corner using crack meters, and geosynthetic strain using optic fiber strain gages. The field measurement provides an excellent opportunity for construction safety control, the abutment system performance measurements and the mutual validity check for the instrumentation and numerical analysis software.

The conclusions of this study are summarized as follows:

1) All instruments performed well as expected except the optic fiber strain gages. The heavy machinery compaction might have altered the strain gages during construction and rendered it ineffective. The optic fiber strain gauges are not recommended for future full-scale installation until proven effective,

2) Vertical and horizontal earth pressure measurements provided valuable data for the study of construction-induced earth pressures and coefficient of earth pressures. The lateral deformations of the façade led to small measured lateral earth pressures. In fact, the lateral earth pressure coefficient was much smaller than its at-rest value and was close to or smaller than the coefficient of active earth pressure for GRS walls,

3) SAA is very effective in the lateral deformation measurement of steel sheet pile façade and is highly recommended for future projects,

4) The tieback-deadman system is highly effective for the stability assurance of steel sheet pile façades, as evidenced during the trench excavation of a large water transport pipeline installation along the front of the façade. The instrumented tiebacks should not be cement grouted until instrumentation objective is achieved,

5) Numerical analysis is effective in assessing GRS-IBS performance before and during construction and is recommended as a preconstruction design tool for complex design configurations such as this project,

6) Measured earth pressures are higher in summer and fall and lower in winter and spring due to seasonal temperature effects,

7) Optic fiber strain gauges are not recommended for field installation, until proven effective in field or large-scale model tests and strain gages are recommended, instead,

9.2 Recommendations

Following recommendations are made for the future study and design:

1) In future projects, SAA for deformation measurements of steel sheet pile facade, tieback-deadman system for stability enhancement of wall system and abutment, more horizontal earth pressure cells, crack meters are recommended,

2) Do not grout tie rod before its tension force measurement is complete,

3) Numerical analysis is recommended for the preconstruction assessment of abutment performance for complex structures,

4) Conduct a study to prove the effectiveness of optic fiber strain gages for geosynthetic strain measurements before further full-scale installation,

5) Good planning and coordination are needed for effective and timely construction and instrumentation operations.

REFERENCES

ASTM D-4595. Standard Test Method for Tensile Properties of Geotextiles by the Wide-Width Strip Method.

AASHTO, LRFD Bridge Design Specifications, 2014, seventh ed. American Association of State Highway and Transportation Officials, Washington, D.C.

Abu-Hejleh, N., Wang, T., Zornberg, J.G., McMullen, M., Outcalt W., 2001. Performance of geosynthetic reinforced walls supporting the Founders/Meadows bridge and approaching roadway structures. Report No. CDOT-DTD-R-2001-12.

Adams, M., Nicks, J., Stabile, T., Wu, J., Schlatter, W., Hartmann, J., 2011a. Geosynthetic Reinforced Soil Integrated Bridge System. Synthesis Report (No. FHWA-HRT-11-027).

Adams, M., Nicks, J., Stabile, T., Wu, J., Schlatter, W., Hartmann, J., 2011b. Geosynthetic Reinforced Soil Integrated Bridge System. Interim Implementation Guide (No. FHWA-HRT-11-026).

Allen, T.M., Christopher, B.R., Holtz, R.D., 1992. Performance of a 41 Foot High Geotextile Wall. Final Report, Experimental Feature WA87-03. Washington State Department of Transportation, Planning, Research and Public Transportation Division.

Ardah, A., Abu-Farsakh, M., Voyiadjis, G., 2017. Numerical evaluation of the performance of a Geosynthetic Reinforced Soil-Integrated Bridge System (GRS-IBS) under different loading conditions. Geotextiles and Geomembranes, 1-12.

Duncan, J.M., Chang, C.Y., 1970. Nonlinear analysis of stress and strain in soils. J. Soil Mech. Found. Div. 96 (5), 1629e1653.

Graeme D. Skinner, R.K.R. (2005). "Design and behavior of a geosynthetic reinforced retaining wall and bridge abutment on a yielding foundation." Geotexitiles and Geomembranes. 23: 234-260.

Liu, H., 2015. Reinforcement load and compression of reinforced soil mass under surcharge loading. J. Geotech. Geoenvironmental Eng. 141 (6), 04015017.

Saghebfar, M., Abu-Farsakh, M., Ardah, A., Chen, Q., Fernandez, B.A., 2017a. Performance monitoring of geosynthetic reinforced soil integrated bridge system (GRS-IBS) in Louisiana. Geotext. Geomembranes 45 (2), 34-47.

Shannon & Wilson Inc., 2016. GRS Instrumentation I-70 over Smith Road Installation Summary Report.

Smith, I. M. and Griffiths, D. V. (1997). Programming The Finite Element Method. John Wiley & Sons, Third Edition.

Appendix A
Laboratory Tests of Colorado Class I Crushed Rock Backfill

SPECIFIC GRAVITY TEST

Laboratory Experiment # 1

Date of Experiment: 01/19/2015

Abstract

For a purpose of comparison and calculation the other properties of the soil from other test (such as compaction, tri-axial tests), three soil samples passing the No 4 sieve were taken from the CDOT Class I Backfill retaining wall for the Specific Gravity test. The result obtained from the test which **G_s = 2.80** for this soil is accepted.

Introduction and Objective

In soil mechanics, the specific gravity of soil solids is an important parameter and is a factor in many equations involving weight-volume relationships. This experiment was perform to determine the specific gravity (G_S) of the part of soil passing the No.4 sieve taken from CDOT Class I back fill retaining wall. The ASTM D854 would be applied for this test.

Experimental Material and Equipment Used

500 ml Volumetric Flask with stoppers, numbered and calibrated
Thermometer, ranging from 0 to 50˚C, accurate to 0.5˚C
Distilled de-aired water
Drying oven
Evaporating dish
Squeeze Bottle
Funnel
Paper Towels
Ice Cubes

Procedure

1. Prepare around 100 g of representative soil sample per flask being tested.
2. Clean the volumetric flask well and dry it. Fill the flask with de-aired, distilled water up to the 500 ml mark (the bottom of the meniscus should be at this mark), weigh this flask of water and record it, M_1 .
3. Determine the temperature of the water in the flask, T_1 (^oC)
4. Pour half of the water out of the flask, and place the soil in the flask with a funnel. Make sure that all of soil were washed down inside the neck of the flask
5. Boiling the mixture on the oven for about 15-20 minutes, make sure adjust temperature so that the sample does not boil over.
6. Remove from heat, and then place in the cold water bath to reduce the temperature of the soil and water in the flask to the temperature T1.(Check periodically the temperature so that do not let it is not out of T1 ± 1^{o}C.)
7. Add the de-aired, distilled water to the volumetric flask until the bottom of the meniscus touches the 500=ml mark. Dry the outside of the flask and the inside of the neck above the meniscus, then weight this flask plus soil plus water and record the mass M2.
8. Pour the soil and water into an evaporating dish-make sure that no soil left inside the flash, then put it into the oven to dry the soil to a constant weight and record the mass Ws.
9. Calculation Gs = α × (Ms / Mw)

10. At least three Gs values are required, so it may be necessary to repeat the test.
11. Compute the ratio of Gs larger / Gs smaller. This ratio must be less than or equal to 1.06. If this ratio is satisfied, take the average of the Gs values to be the Gs of the soil. If the ratio is greater, repeat the test until the ratio is satisfied.

Laboratory Results:

The results of this laboratory are reasonable. The table below shows the computations for the specific gravity at room temperature, and also adjusts the value with a temperature correction factor.

Item	Test No.		
	1	2	3
Temperature of test, T_1	24	24	23
Temperature correction factor, A	0.9991	0.9991	0.9993
Mass of flask + water filled to mark, M_1 (g)	681.3	645.5	623.5
Mass of flask + soil + water filled to mark, M_2 (g)	745.2	708.8	689.3
Mass of dry soil, Ms (g)	99.2	99.3	101.5
Mass of equal volume of water and soil solids, M_w (g) = (M_1 + M_s) - M_2	35.3	36	35.7
$G_{s(at\ T1^\circ C)}$ = M_s/M_w	2.81	2.76	2.84
$G_{s(at\ 20^\circ C)}$ = $G_{s(at\ T1^\circ C)}$ * A	2.81	2.76	2.84
Average $G_{s(at\ 20^\circ C)}$	2.80		

The factor of the largest and the smallest is 2.84/2.76 = 1.03 → OK

Discussion of Error:

In the process of performing the specific gravity measurement, the procedure to de-air the water by boiling the soil mixture in 15-20 minute was carried out. The source of error can be from this step due to entrapped air that was not removed.

Conclusion:

With the difference between the largest and the smallest is 1.03, the result of Gs is 2.80 could be accepted for a purpose of referring in comparing and valuating other properties of the soil. To obtain exactly the specific gravity of this soil, need to perform more experiments follow the ASTM C127 for determining the specific gravity of the part of soil retained on the No. 4 sieve, and then combine them.

Reference

Braja M. Das. *Soil Mechanics Laboratory Manual, 8th ed.*, Oxford University Press (2013).
Jean-Pierre Bardet. *Experimental Soil Mechanics* , Prentice Hall (1997).

GRADATION ANALYSIS TEST

Dates of Experiment: 09/07/2014

GRADATION ANALYSIS TEST

- Soil Classification Systems
  - ASTM D 422
  - BS1377
  - USCS
  - AASHTO

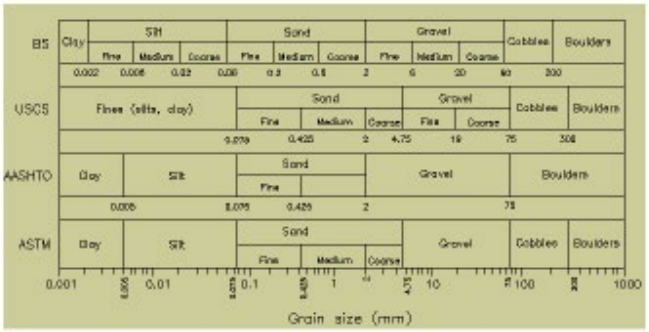

Abstract

The gradation curve of the Colorado Class I Backfill of crushed rocks sample taken from Locky-Matin borrow pit was determined by only using the mechanical sieve analysis due to the small percentage passing the number 200 sieve ($F_{200} = 4.03$ %). This sample is classified as **SW** (well graded sand) according to the USCS, or as **A-1-a** (granular material group) according to the AASHO.

Introduction and Object

A sieve analysis is one of the important first steps in classifying soils. In combination with Atterberg Limits (but not need for this sample because of its graded grain size), soil can be classified in accordance with the Unified Soil Classification System (USCS) or the American Association of State Highway and Transportation Officials (AASHTO). Soils which share a USCS or AASHTO classification have similar mechanical properties, such as strength, permeability, and compressibility. This becomes important in the design process when determining a soil that will meet certain performance specifications.

The ASTMs D421-85, D422-63, and D2487 would be applied for this test.

Experimental Material and Equipment Used

1. A quantity of 700 g oven-dry soil
2. Set of sieves (Sieve numbers 4, 10, 20, 40, 60, 100, and 200);
3. Flat pan;
4. Balance (sensitive to 0.1 g);
5. Brushes (steel bristled, and plastic bristled);
6. Mechanical sieve shaker;

Procedure

1. Obtain 700 g oven-dry soil samples;
2. Clean sieves (use metal brush for the sieve of #4- #10, and plastic brush for the sieve of #20-#200);
3. Weight the mass of each empty sieve and record it;
4. Prepare a stack of sieves. A sieve with larger openings is placed above a sieve with smaller openings. From up to down be sieve numbers: 4, 10, 20, 40, 60, 100, and 200. The pan is last, under the sieve #200;
5. Pour the soil prepare in step 1 into the stack of sieves from the top sieve and place the cover on the top of this sieve;
6. Place the stack of sieves with soil on the sieve shaker and run it for 10 minutes, then stop sieve shaker and remove the stack of sieves;
7. Weigh the amount of soil retained on each sieve and in the bottom pan and record them;

Laboratory Results

The data gotten after operating the sieve shaker were recorded and calculated by the tabular Excel, the results and the grain size distribution curve (the gradation curve) are shown below:

Mass of dry soil sample, W = 694.6 g

Sieve No.	Sieve Opening (mm)	Mass of soil retained on each sieve, W_n (g)	Percent of mass retained on each sieve, R_n	Cumulative percent retained, $\sum R_n$	Percent finer 100 - $\sum R_n$
4	4.75	208.2	29.97	29.97	70.03
10	2	204.1	29.38	59.36	40.64
20	0.85	92.3	13.29	72.65	27.35
40	0.425	50.1	7.21	79.86	20.14
60	0.25	41.9	6.03	85.89	14.11
100	0.15	35.9	5.17	91.06	8.94
200	0.075	34.1	4.91	95.97	4.03
Pan		28.0	4.03	100.00	0.00
	$\sum$ =	694.6 g		The difference = 0	

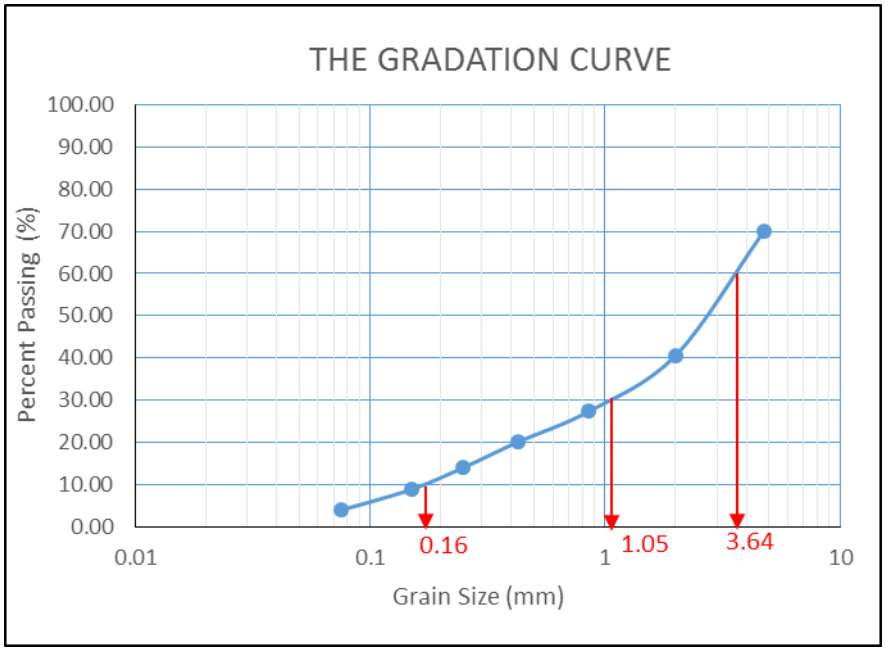

D_{60} = 3.64 mm **D_{30} = 1.05mm** **D_{10} = 0.16 mm**

C_u = 22.75 **C_c = 1.86**

Sources of error

The sources of error for the mechanical sieve analysis essential include the hole in the sieve and may be a significant soil loss during sieving. An objective cause could be a little of soil stuck in opening holes of the sieve above and lead to the soil mass on that sieve is greater than its real mass.

Conclusion

This soil sample would fall under the category of coarse-grained according to the USCS since more than 50% of the sample (R_{200} = 95.97 %) was retained on No.200 sieve. In addition, more than 50 % of the coarse fraction (F_4 = 70.03 %) passed No. 4 sieve, the uniformity coefficient is 22.5 (> 6) and the coefficient of gradation is 1.89 (in the range of 1 – 3), it is classified as a well graded sand **SW.**

According to the AASHTO, this sample would fall under the category of granular material since less than 35% of the sample passed No. 200 sieve (F_{200} = 4.03 %). In addition, the percentage passing No. 10 sieve is less than 50% (F_{10}= 40.64 %), the percentage passing No. 40 sieve is less than 30% (F_{40} = 20.14 %), and the percent passing No. 200 is less than 15% (F_{200} = 4.03 %), it is classified as an **A–1–a.**

Reference

Braja M. Das. *Soil Mechanics Laboratory Manual, 8th ed*., Oxford University Press (2013).
Jean-Pierre Bardet. *Experimental Soil Mechanics* , Prentice Hall (1997).

GRAIN SIZE DISTRIBUTION ANALYSIS - DRY SIEVE MEASUREMENT (ASTM D421, D422, D2487, AND D3282)
LABORATORY DATA SHEET

I. GENERAL INFORMATION

Test by: Ngoan Hoang	Date test: 09/2014
Lab Partner/Organization: Soil Lab, Civil Engineering Department, UC Denver	
Client: Colorado Department of Transportation	Project: Colorado Class I Backfill retaining wall
Boring No: Locky-Martin borrow pit	Recovery depth:
Soil description: Almost crushes rock with a little of fine grain soil, brown color	

II. TEST DETAILS

Sieve shaking method/duration: Automatic Electrical- Mechanical shaker / 10 minutes
Total sample mass before sieving (M_{total}): 694.6 g
Total sample mass after sieving (M_{total}): 694.6 g
Percent soil loss during sieving: 0

III. MEASUREMENT AND CALCULATIONS

Sieve No.	Sieve Opening (mm)	Mass of soil retained on each sieve, $W_{n\,(g)}$	Percent of mass retained on each sieve, R_n	Cumulative percent retained, $\sum R_n$	Percent finer $100 - \sum Rn$
4	4.75	208.2	29.97	29.97	70.03
10	2	204.1	29.38	59.36	40.64
20	0.85	92.3	13.29	72.65	27.35
40	0.425	50.1	7.21	79.86	20.14
60	0.25	41.9	6.03	85.89	14.11
100	0.15	35.9	5.17	91.06	8.94
200	0.075	34.1	4.91	95.97	4.03
Pan		28.0	4.03	100.00	0.00

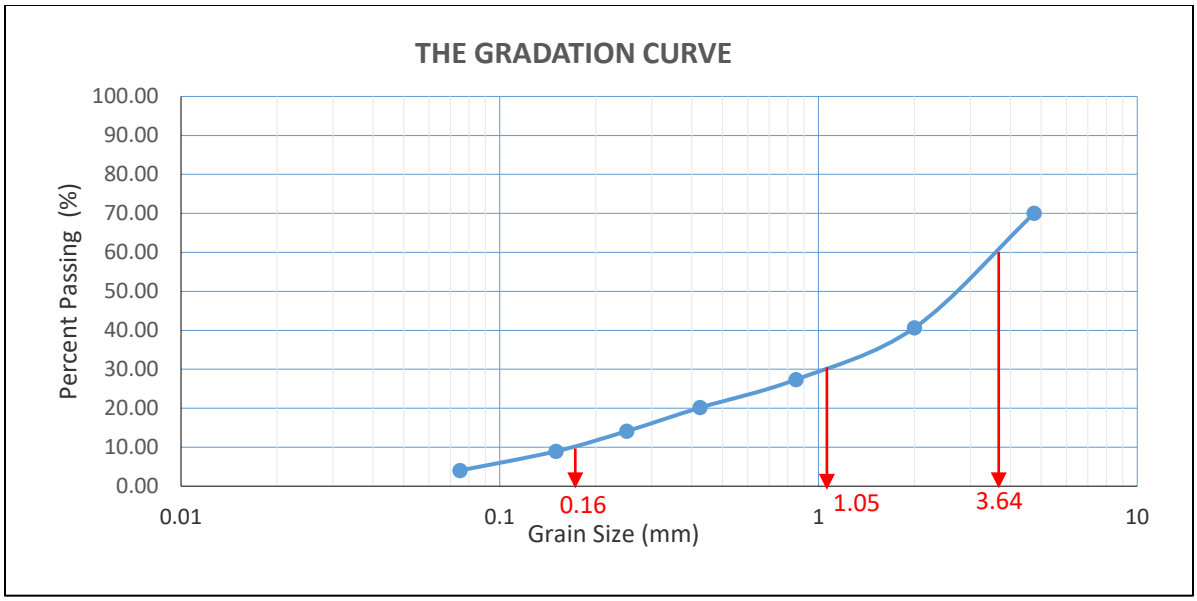

D_{60} = 3.64 mm **D_{30} = 1.05mm** **D_{10} = 0.16 mm**

C_u = 22.75 **C_c = 1.86**

IV. CLASSIFICATION

System	Parameters	Group name	Group symbol
USCS	R_{200} = 95.97 % > 50 %, F_4 = 70.03 % C_u =22.5 > 6, C_c = 1.89 in the range of 1 and 3	Well graded soil	**SW**
AASHTO	F_{200} = 4.03 % < 15 %, F_{10} = 40.64% < 50 %, F_{40} =20.14 % <30 %	Granular soil	**A-1-a**

STANDARD AND MODIFIED PROCTOR COMPACTION TEST

Laboratory Experiment # 3

Date of experiment: 9/2014

STANDARD AND MODIFIED PROCTOR COMPACTION TEST

- ASTM D698, D1557-91 and D5080 are applied
- Soil sample through the #4 US Sieve
- Standard Proctor Rammer: 5.5 lb of weight
- Modified Proctor Rammer: 10 lb of weight

Abstract

Both of two methods of the Proctor Compaction Test (Standard and Modify) are performed to experimentally measure the optimum moisture content and the maximum dry density for the CDOT Class 1 Structural Backfill soil sample. The results obtained from the experiments to be *131.5 lb/ft³* of the maximum dry unit weight with the optimum of *10 %* water content and the maximum dry unit weight of *142 lb/ft³* with the optimum water content of*6.5 %* according to the standard experiment and the modified experiment respectively.

Introduction and Object

The object of this experiment is to define the laboratory maximum dry unit weight and the optimum water content of the soil sample taken from source of the CDOT Class1 Structural Backfill soil. In order to define the soil density by field compaction, both of two basic tests, the standard and modified compaction tests are performed.

The ASTMs: D 698, D 1557-91, and D 5080 would be applied for this test.

Material and Equipment Needed

1. A quantity of 10 lb (4.5 kg mass) of air-dry soil sample
2. Compaction Mold, including base, cylinder, and guider
3. No. 4 US Sieve
4. Graduated Cylinder
5. Standard Proctor Rammer (5.5 lb of weight)
6. Modified Proctor Rammer (10 lb of weight)
7. Balance, sensitive to 0.1g
8. Large flat pan
9. Scoop or trowel
10. Jack, with sample extruder
11. Straight edge
12. Moisture cans
13. Drying oven

Procedure

Procedure processed for the standard and the modified test is only different from the process of the compaction step in which compacting three compacted layers of soil by using the Standard Rammer for the Standard test and five compacted layers of soil by using the Modified Rammer for the Modified test, the other steps are the same. For each of the standard and modified test, the procedure would be completely performed all of steps as follows:

1. Begin by sorting the soil sample through the #4 US Sieve, breaking up any clumps.
2. Obtain a soil sample of 2500 g or more for each test, measure respective water content.

3. Mix the water and soil thoroughly with trowel (or scoop), so that the entire sample is of even moisture content.
4. Determine the weight of the proctor mold + base plate (but not the extension).
5. Begin filling the compaction mold in 3 even layers, or lifts for the standard experiment (or 5 even layers for the modified experiment). Compact each lift with 25 consecutive blows from the proctor test hammer (standard or modified test hammer), evenly distributing the blows by executing a crossing-pattern across the perimeter of the mold. The upper portion of the mold should be attached, it will help guide the compaction hammer, and allow the mold to be overfilled with the sample.
6. After compaction of the last layer, or lift, the upper portion of the mold should be removed, and the sample trimmed flush with the top of the mold.
7. Determine weight of mold + sample.
8. Extract the sample from the mold and take soil samples from the top, middle, and bottom.
9. Place samples into labeled and weighed moisture can and place in the drying oven for at least 24 hours with the temperature of 110 ^{o}C.
10. Repeat steps 2-9, adjusting the amount of water to obtain the appropriate water content for each test point. Perform at least five point tests for each experiment (standard and modify).
11. After samples have completely dried in the oven, obtain the dry weight of the sample + moisture can.

Laboratory Results:

The Standard Proctor Compaction Test was performed with the beginning moisture content of 5 % of soil sample and an increment of 2 % for each test point later. For the Modified Proctor Compaction Test, the beginning moist content is 2 % and an increment of 2%. on each test point later.

Follow the ASTM 5080, for choosing the better optimum moisture content, a plotting of the polynomial quadratic aggression of three points close to the maximum (fitting A with the continuous line) should be plotted beside the cubic polynomial aggression curve (fitting B with the dash line) of all data points for each compaction experiment. Also, zero-aid-void unit weight (with Gs = 2.80) versus moisture content should be plotted on the same graph.

A summary of the results are listed and calculated by tabular form as below:

FOR THE STANDARD PROCTOR COMPACTION TEST

Test	1	2	3	4	5	6	7
1. Weight of mold, W_1 (lb)	9.29	9.29	9.29	9.29	9.29	9.29	9.29
2. Weight of mold + moist soil , W_2 (lb)	13.69	13.84	13.97	14.07	14.04	13.97	13.90
3. Weight of moist soil, $W_2 - W_1$ (lb)	4.41	4.55	4.68	4.79	4.75	4.68	4.61
4. Moist unit weight, $\gamma = [(W_2 - W_1) /0.0333]$ (lb)	132.28	136.64	140.48	143.75	142.58	140.62	138.39
5. Moisture can number	3.00	4.00	5.00	6.00	7.00	8.00	9.00
6. Mass of moisture can, W_3 (g)	15.60	16.10	16.00	15.20	15.10	15.60	15.10
7. Mass of can + moist soil, W_4 (g)	37.80	41.70	42.20	36.20	46.90	46.20	47.20
8. Mass of can + dry soil, W_5 (g)	36.70	40.00	40.10	34.30	43.60	42.60	43.20
9. Moisture content, $w(\%) = [(W_4-W_5)/(W_5-W_3)]*100$	5.21	7.11	8.71	9.95	11.58	13.33	14.23
10. Dry unit weight of compaction γ_d (lb/ft³) $= [\gamma/(1+(w(\%)/100))]$	125.73	127.56	129.22	130.75	127.79	124.07	121.15

FOR THE MODIFIED PROCTOR COMPACTION TEST

Test	1	2	3	4	5	6	7
1. Weight of mold, W_1 (lb)	9.37	9.37	9.37	9.37	9.37	9.37	9.37
2. Weight of mold + moist soil , W_2 (lb)	14.01	14.17	14.37	14.42	14.34	14.20	14.15
3. Weight of moist soil, $W_2 - W_1$ (lb)	4.64	4.80	5.00	5.05	4.97	4.83	4.78
4. Moist unit weight, $\gamma = [(W_2 - W_1) /0.0333]$ (lb)	139.34	144.14	150.15	151.65	149.25	145.05	143.54
5. Moisture can number	1	2	3	4	5	6	7
6. Mass of moisture can, W_3 (g)	12.00	15.40	15.50	15.10	15.40	15.60	15.20
7. Mass of can + moist soil, W_4 (g)	24.60	40.00	42.30	48.90	55.50	52.10	56.00
8. Mass of can + dry soil, W_5 (g)	24.4	39.1	40.8	46.3	51.8	48.3	51.5
9. Moisture content, $w(\%) = [(W_4-W_5)/(W_5-W_3)]*100$	1.61	3.80	5.93	8.33	10.16	11.62	12.40
10. Dry unit weight of compaction γ_d (lb/ft³) $= [\gamma/(1+(w(\%)/100))]$	137.13	138.87	141.75	139.99	135.48	129.94	127.71

The graph of the compaction curves and the zero void curve with G_s = 2. 8 are shown as below:

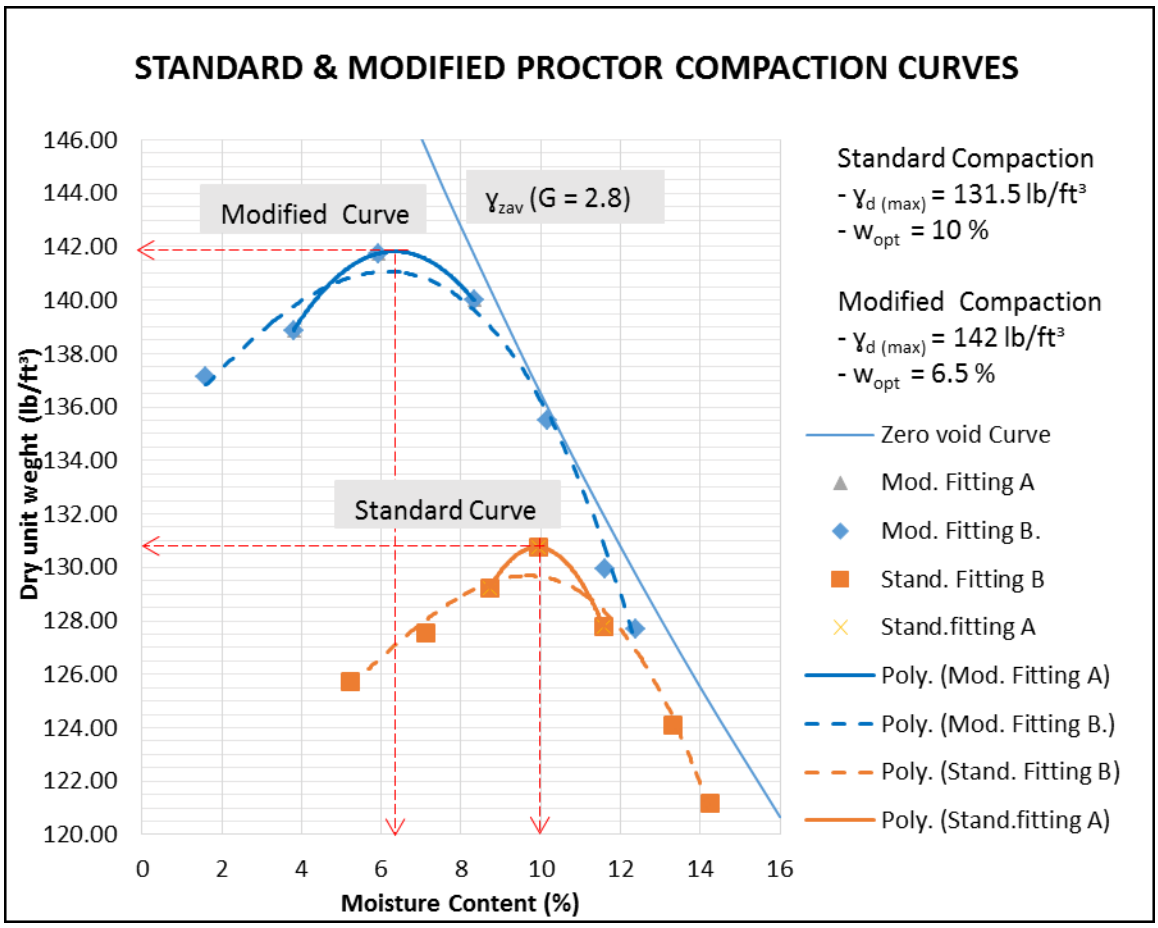

The results from the graph above found the maximum dry unit weight to be *131. 5 lb/ft³* with the optimum moisture content of *10 %* according to the standard experiment and a maximum dry unit weight of *142 lb/ft³* with the optimum moisture content of *6.5 %* according to the modified experiment. The given results are chosen from the fitting A method with the quadratic polynomial aggression curves for the both experiments.

Discussion of Error:

There are two main sources of error in the Proctor Compaction Test follow ASTM D 698 and D 1557. The first arises if the soil sample being tested is not allowed to hydrate for at least 16 hours prior to compaction. If the soil is not allowed to hydrate properly, results can be erroneous and this can lead to a poorly defined compaction curve. The second source of error occurs if new soil is not used for each trial. Crushing, rehydrating, and re-compacting the same sample can cause elevated dry unit weight. This will ultimately lead to a poorly developed compaction curve. This can be avoided by simply using fresh samples for each trial.

Conclusion:

The Proctor compaction test performed to determine the laboratory optimum water content and the dry unit weight of a soil sample. The modified Proctor test gives a higher dry unit weight (140 lb/ft^3) with the lower optimum water content (7%) then the standard Proctor test (134.25 lb/ft^3 dry unit weight and 9% water content). The result from the modified test should be used for defining the density of soil by field compaction.

Appendix B
Wide-Width Tension Test of US4800 Geosynthetic

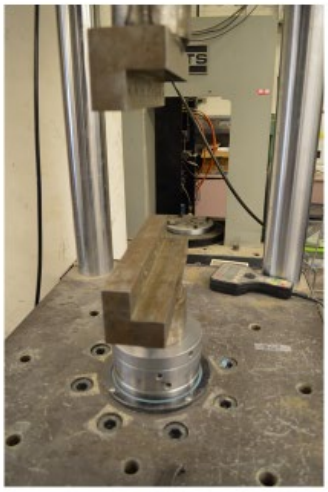

Geosynthetic Clamp

Newly Designed Clamping Technique

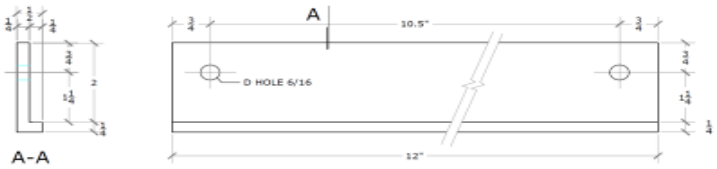

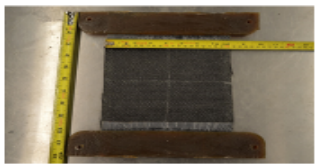

THE GEOTEXTILE FABRIC CLAMP

I1 Exhumed Samples

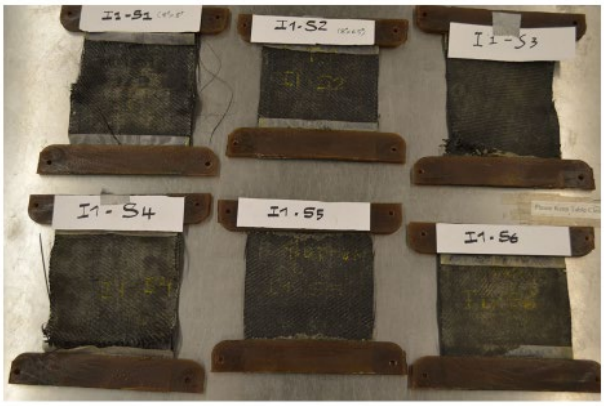

New Samples

I 2 Exhumed Samples

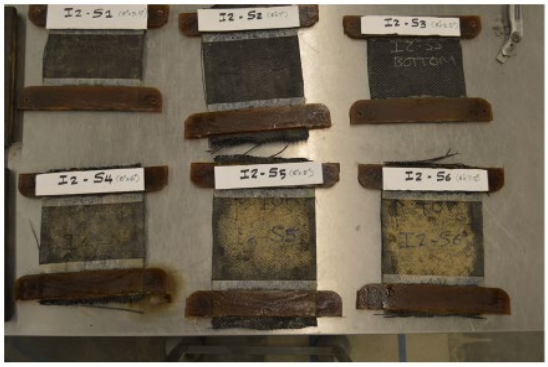

Exhumed Samples

- **I1-S1:** 10 ft back from sheet pile; 7 ft East of I1; 13 in cover; sample from 3 ft-8 in lift
- **I1-S2**: 10 ft back from sheet pile; 10 ft East of I1; sample from 4 ft-8 in lift
- **I1-S3:** 8 ft -8 in full length fabric; 10 ft back; 10 ft East
- **I1-S4**: 9 ft-8 in full length fabric; 10 ft back; 10 ft East
- **I1-S5**: 12 ft full length fabric; 10 ft back; 10 ft West
- **I1-S6**: 12 ft full length fabric; 15 ft back; 7 ft West
- **I2-S1**: 10 ft back from sheet pile; 6 ft West of I2; sample from 3 ft-8 in lift
- **I2-S2**: 10 ft back from sheet pile; 10 ft East of I2; sample from 4 ft-8 in lift of fabric
- **I2-S3:** 8 ft -8 in full length fabric; 10 ft back; 10 ft East
- **I2-S4**: 9 ft-8 in full length fabric; 10 ft back; 10 ft East
- **I2-S5**: 12 ft full length fabric; 10 ft back; 10 ft West
- **I2-S6**: 12 ft full length fabric; 15 ft back; 7 ft West